Operations Research

# ORINCON

CONtrol

An Applied Systems Corporation

Operations Research

# ORINCON

Corp.,
La Jolla, Calif.

## An Applied Systems Corporation

(14) OC-R-76-0564-1

(11) 30 November 1976

(12) 219p.

(6) (9) Final Report,
NAVSTAR/GPS Navigation Analysis
and Algorithm Development Study

Contract No. N00123-76-C-0564    new
(15)

Prepared by

(10) *Charles A. Wolfe*
Charles A. Wolfe
Principal Investigator

Approved by

*Harold W. Sorenson*
Harold W. Sorenson
Program Manager

Submitted to

Naval Electronics Laboratory Center
San Diego, California 92152

392776

2223 Avenida de la Playa, Suite 151        La Jolla, California 92037        (714) 454-3001

# TABLE OF CONTENTS

# TABLE OF CONTENTS (Concluded)

# LIST OF ILLUSTRATIONS

# LIST OF ILLUSTRATIONS (Concluded)

# LIST OF TABLES

## Section 1. - MODELLING

### 1.0 Introduction

This section describes the results of the first part of the NAVSTAR/ GPS Navigation Analysis and Algorithm Development Study. The purpose of this first section is to define the models for use throughout the entirety of the study. The ultimate objective of the study is to determine a set of algorithms which can be used in a NAVSTAR/GPS user navigation system. The criteria for the acceptability of the algorithm will be the accuracy of the position and velocity determination. Since there is no way of getting real data for algorithm verification at this time, it is imperative to establish system and error models. The results of analysis of proposed algorithms is then relative to the models used.

An additional objective of the entire study is that it will be a design aid. Thus it is intended that through analysis of different receiver configurations, an analytic basis for certain design decisions can be established. The final computer program for analysis will not be an interactive computer aided design tool; however, it will provide for inclusion or exclusion of certain receiver options and variability of certain parameters in order to make the analysis useful for making design decisions.

The modelling effort for this task is divided into two parts, System Model and Error Model. The System Model contains the satellite model, user model, control system model, and data stream model. In addition, scenarios are defined for evaluation of the proposed numerical algorithms. The Error Model defines the contributors to the navigation error. This includes errors in the system components, such as receiver and transmitter errors, and error sources exogenous to the System Model, such as atmospheric effects. The distinction between System Model and Error Model is somewhat arbitrary in some instances. How-

1

ever, since the models are not intended to be used separately, this will not cause any difficulty. The emphasis in this report is the form of the models. Specific parameter values may be changed in the course of the study; however, the form of the models should remain constant.

The parts of this report dealing with the system model have been taken from various references (1, 3, 4, 6, 9, 15) and the applicable parts selected for inclusion. A critical look has been taken at each model, but no new models are presented. The error models are taken from various references (7, 10, 11, 12, 14) also along with standard linear models for certain error types. Each error source was examined and the appropriate model chosen according to accepted modelling procedures.

## 1.1 System Model

The System Model must be defined as completely as possible at the outset of the study since the model serves as a set of ground rules. The only major component of the system which will not be modelled is the computational unit. This will have an effect on the algorithms; however, this effect is clearly beyond the scope of this study. The only configuration unknowns in the subsystems which are modelled are in the area of the receiver model. Modelling of various types of user receivers will aid in the development of the design specifications for the receiver. The System Model is divided below into several segments solely for the purpose of exposition.

### 1.1.1 Ephemeris Model

The ephemeris model is concerned with the satellite constellation, the mathematical model for satellite motion, and the information about the satellites which the control system segment supplies to the user.

### 1.1.1.1 Satellite Constellation

The Phase III satellite constellation consists of twenty-four satellites. The constellation will have three planes of satellites in approximately circular twelve-hour orbits. The orbit planes are inclined at approximately $63^\circ$ and spaced so that the ascending nodes of the orbit planes are $120^\circ$ apart. Each orbit plane has eight satellites equally spaced in the orbit. It is intended that between 6 and 11 satellites will be visible from any point on the Earth at all times. On the average there will be eight or nine satellites in view. A complete definition of the Phase III satellite constellation can be found in reference 1.

### 1.1.1.2 Satellite Motion

The satellite motion generation for the System Model will use a simple two-body orbit for each satellite. The positions of each satellite with respect to the Earth could then be computed as a function of time from the six orbital elements (2). The model used by the system for prediction of satellite position uses fourteen elements to achieve the desired navigational accuracy (3). Linear perturbations to this fourteen element model can be expressed by the orbital element model. Therefore to conserve computation in the error analysis, this simpler model can be used.

The nominal GPS orbit configuration calls for circular orbits. For analysis purposes, this simplifies the satellite position and velocity calculations since only four parameters must be specified; the radius of the orbit, orbit inclination, longitude of ascending node, and time of passage of the ascending node. In fact, all of the satellite locations and velocities can be computed by orthogonal transformations of a single satellite position and velocity

$$X_i = T_i X_1 \qquad i = 2, 3, \ldots, 24$$

3

where $X_i$ is the state vector for the $i^{th}$ satellite and $T_i$ is an orthogonal (length preserving) transformation.

### 1.1.1.3 Data Link Information

The control system segment of GPS as a part of its function supplies orbit information to the user. There are two types of orbit data provided. One type is the very accurate set of fourteen parameters which are updated every day, the other type is the Almanac data.

The very precise data consists of fourteen parameters which are to be used in conjunction with the nominal orbit parameters. The satellite is updated once a day with twenty-four sets of this data. Each data set is optimized to fit the predicted orbit accurately over one hour. The data sets should not be considered as true orbit parameters, but rather as coefficients of a numerical fit to the predicted orbit. The parameters take the form of orbital elements and additional information to account for some of the error introduced by effects not considered in the standard two-body orbit (viz. pole wobble, gravitational anomalies, solar pressure, etc.). These corrections are valid only for the instant at which they are computed and tend to degrade with time. Consequently, the control system segment tracks the satellites and updates these parameters on twenty-four hour intervals (3). The most current information available (4) lists the parameters as:

$M_o$ - mean anomaly at reference time

$\Delta n$ - mean motion deviation

$e$ - eccentricity

$\sqrt{A}$ - square root of semi-major axis

4

$\Omega_o$ - right ascension at reference

$i_o$ - inclination at reference

$\omega$ - argument of perigee

$\dot{\Omega}$ - rate of right ascension

$C_{uc}$ - amplitude of the cosine harmonic correction term to the argument of latitude

$C_{us}$ - amplitude of the sine harmonic correction term to the argument of latitude

$C_{rc}$ - amplitude of the cosine harmonic correction term to the orbit radius

$C_{rs}$ - amplitude of the sine harmonic correction term to the orbit radius

$C_{ic}$ - amplitude of the cosine harmonic correction term to the angle of inclination

$C_{is}$ - amplitude of the sine harmonic correction term to the angle of inclination

In addition, the following parameters are provided.

$t_{oe}$ - reference time ephemeris

AODE - age of data (ephemeris)

The algorithm to convert this data to satellite position in ECI is as follows:

$\mu = 3.986008 \times 10^{14} \dfrac{\text{meters}^3}{\text{sec}^2}$    WGS 72 value of the Earth's universal gravitational parameter

$\dot{\Omega}_e = 7.292115147 \times 10^{-5} \dfrac{\text{rad}}{\text{sec}}$    WGS 72 value of the Earth's rotation rate

$A = (\sqrt{A})^2$    semi-major axis

$$n_o = \sqrt{\frac{\mu}{A^3}}$$ computed mean motion

$$t_k = t - t_{oe}*$$ time from epoch

$$n = n_o + \Delta n$$ corrected mean motion

$$M_k = M_o + n t_k$$ mean anomaly

$$M_k = E_k - e \sin E_k$$ Kepler's equation for eccentric anomaly

$$\cos v_k = (\cos E_k - e)/(1 - e \cos E_k)$$
$$\sin v_k = \sqrt{1 - e^2} \sin E_k /(1 - e \cos E_k)$$
true anomaly

$$\Phi_k = v_k + \omega$$ argument of latitude

$$\delta u_k = C_{us} \sin 2\Phi_k + C_{uc} \cos 2\Phi_k$$ argument of latitude correction

$$\delta r_k = C_{rc} \cos 2\Phi_k + C_{rs} \sin 2\Phi_k$$ radius correction

$$\delta i_k = C_{ic} \cos 2\Phi_k + C_{is} \sin 2\Phi_k$$ correction to inclination

second harmonic perturbations

$$u_k = \Phi_k + \delta u_k$$ corrected argument of latitude

$$r_k = A(1 - e \cos E_k) + \delta r_k$$ corrected radius

$$i_k = i_o + \delta i_k$$ corrected inclination

$$x'_i = r_k \cos u_k$$
$$y'_k = r_k \sin u_k$$
position in orbital plane

$$\Omega_k = \Omega_o + (\dot{\Omega} - \dot{\Omega}_e)t_k - \dot{\Omega}_e t_{oe}$$ corrected longitude of ascending node

*t is GPS system time at time of transmission, i.e., GPS time corrected for transit time (range/speed of light)

6

$$x_k = x_k' \cos \Omega_k - y_k' \cos i_k \sin \Omega_k$$

$$y_k = x_k' \sin \Omega_k + y_k' \cos i_k \cos \Omega_k \left. \right\} \quad \text{Earth fixed coordinates}$$

$$z_k = y_k' \sin i_k$$

Tentative scaling and resolution information for each parameter are contained in reference 4.

The data stream from each satellite includes Almanac data for all of the satellites. This data consists of orbital elements, satellite ID and health, and time parameters (4). The Almanac parameters may be used for alert calculations to determine which satellites are "in view", i.e., which may be received. It is not intended that Almanac data be used for precise navigation, but it will be useful for acquisition. Almanac data is updated every six days (4).

## 1.1.2 Time Model

The time model is concerned with the satellite clock and deterministic delays in the downlink. The system model of time (3, 4) has terms in it so that the user can correct the measured time of arrival of the satellite signal for the deterministic part of clock off-sets, biases, satellite electronic delays, relativistic effects, and atmospheric delays.

### 1.1.2.1 Clock Model

The satellite oscillator frequency is set at a nominal value which includes a frequency offset to account for the relativistic effects in the nominal orbit. The control system segment of GPS then monitors each satellite vehicle clock to calibrate deterministic errors in the present value such as offset, frequency bias, and relativistic effects due to off-nominal orbits. The control system then computes three parameters

with which the user may correct the system time.  These are sent as part of the data from the satellite to the user.  The correction parameters are the coefficients of a polynomial correction which the user can apply.  This correction has the form:

$$\Delta t = a_0 + a_1(t_s - t_{oc}) + a_2(t_s - t_{oc})^2$$

so that

$$t = t_s + \Delta t$$

where

$a_0$, $a_1$, $a_2$ are the correction parameters

$t_s$ is the satellite vehicle time

$t_{oc}$ is the satellite vehicle clock epoch time

$t$ is the corrected system time

The coefficients $a_0$, $a_1$, and $a_2$ are computed to fit the predicted clock behavior over small time intervals.  The control system sends new sets of these parameters to the satellite every day.

For $t - t_{oc} <$ 45 min., the approximations provide errors less than .5 nanosecond.  After 45 minutes, these errors of approximation degrade as:

| $t - t_{oc}$ | error |
|---|---|
| 1 hr | 1 ns |
| 2 hr | 8 ns |
| 3 hr | 26 ns |
| 4 hr | 60 ns |

8

This polynomial form of the correction does not provide for a graceful degradation of the relativistic errors. A more graceful degradation of error can be achieved by using the following correction (4):

$$\Delta t = (a_o - a_{0r}) + (a_1 - a_{1r})(t_s - t_{oc}) + (a_2 - a_{2r})(t_s - t_{oc})^2 + \Delta t_r$$

where

$$\Delta t_r = \left(-4.443 \times 10^{-10} \frac{sec}{\sqrt{meter}}\right) e \sqrt{A} \sin E (t)$$

$$a_{0r} = -4.443 \times 10^{-10} \frac{sec}{\sqrt{meter}} e \sqrt{A} \sin E (t_{oc})$$

$$a_{1r} = -4.443 \times 10^{-10} \frac{sec}{\sqrt{meter}} e \sqrt{A} \, n \cos E (t_{oc})/[1 - e \cos E (t_{oc})]$$

$$a_{2r} = 2.2215 \times 10^{-10} \frac{sec}{\sqrt{meter}} e \sqrt{A} \, n^2 \sin E (t_{oc})/[1 - e \cos E (t_{oc})]^2$$

The rationale for this type of correction can be found in reference 14 and in references 18 and 52 of reference 14.

## 1.1.2.2 Atmospheric Model

The atmospheric model is constructed to predict the range error introduced by propagation error due to the atmosphere, specifically the ionospheric and tropospheric delay. Of the two, the tropospheric error has less variation and the range error, $\Delta R$, can be approximated to better than 1 ft at elevations greater than $10^o$ and better than 5 ft at elevations between $5^o$ and $10^o$ by the simple formula (3)

$$\Delta R = K \csc E$$

or (12)

$$\Delta R = K \cdot \frac{1}{\sin E + .026}$$

where

> E, the elevation angle from the user to the satellite is greater than $5^\circ$ and from (3) K is a constant ($\approx$ 4 ft).

The user will use one of these models to compensate for tropospheric range errors.

The ionospheric model must account for seasonal and diurnal variations and latitude dependencies (3). There are two correction schemes available to the user. The first method uses eight parameters which are sent in the data stream. It should be noted that the following model is new and documentation as to its validity is not yet available.

The ionospheric correction time $T_{IONO}$ is calculated by

$$T_{IONO} = \begin{cases} F* \left[ 5. \times 10^{-9} + \left( \sum_{n=0}^{3} \alpha_n \varphi_m^n \right) \left( 1 - \frac{x^2}{2} + \frac{x^4}{24} \right) \right], & |x| < 1.57 \\ & \text{(sec)} \\ F* \quad 5. \times 10^{-9}, & |x| \geq 1.57 \end{cases}$$

where

$$x = \frac{(t - 50400)}{\sum_{n=0}^{3} \beta_n \varphi_m^n}$$

and

$$F = 1. + 16. [.53 - E]^3$$

$\alpha_n$ and $\beta_n$; n = 0, 1, 2, and 3; are the satellite transmitted data words. Other equations that must be solved are

$$t = 4.32 \times 10^4 \lambda_i + \text{GPS time (sec)}; \ t > 86400 \text{ use } t = t - 86400$$

$$\varphi_m = \varphi_i + 0.064 \cos (\lambda_i - 1.617) \text{ (semi-circles)}$$

$$\lambda_i = \lambda_u + \frac{\Psi \sin A}{\cos_i} \text{ (semi-circles)}$$

$$\varphi_i = \begin{cases} \varphi_u + \Psi \cos A \text{ (semi-circles)}, & \varphi_u < .416 \text{ (semi-circles)} \\ \varphi_u & , \varphi_u \geq .416 \text{ (semi-circles)} \end{cases}$$

$$\Psi = \frac{0.0137}{E + 0.11} - 0.022 \text{ (semi-circles)}$$

The terms used in computation of ionospheric delay are as follows:

· Satellite Transmitted Terms

$\alpha_n$ - the coefficients of a cubic equation representing the amplitude of the vertical delay (4 coefficients - 8 bits each)

$\beta_n$ - the coefficients of a cubic equation representing the normalized period of the model. The true period has been divided by $2\pi$. (4 coefficients - 8 bits each)

11

· Receiver Generated Terms

   E - elevation angle between the user and satellite (semi-circles)

   A - azimuth angle between the user and satellite, measured clockwise positive from the true North (semi-circles)

   $\varphi_u$ - user geodetic latitude (semi-circles) WGS-72

   $\lambda_u$ - user geodetic longitude (semi-circles) WGS-72

   GPS time - receiver computed system time

· Computed Terms

   F - obliquity factor (dimensionless)

   t - local time (sec)

   $\varphi_m$ - geomagnetic latitude of the Earth projection of the ionospheric intersection point (mean ionospheric height assumed 350 km) (semi-circles)

   $\lambda_i$ - geodetic longitude of the Earth projection of the ionospheric intersection point (semi-circles)

   $\varphi_i$ - geodetic latitude of the Earth projection of the ionospheric intersection point (semi-circles)

   $\Psi$ - Earth's central angle between user position and Earth projection of ionospheric intersection point. (semi-circles)

The values of $\alpha_0$, $\alpha_1$, $\alpha_2$, and $\alpha_3$; and, $\beta_0$, $\beta_1$, $\beta_2$, and $\beta_3$ are transmitted in Data Block I with 8 bits/coefficient or 64 bits total.

   For a dual frequency receiver, an alternate correction scheme may be used to calculate the user range error. The range error is calculated according to (3)

12

$$\Delta R_1 = \frac{R_1 - R_2}{1 - \left(\dfrac{f_1^2}{f_2^2}\right)}$$

where

$R_1$ is pseudo-range at frequency $f_1$ (denoted $L_1$)

$R_2$ is pseudo-range at frequency $f_2$ (denoted $L_2$)

$\Delta R_1$ is the range error of $R_1$

The dual frequency ionospheric delay correction scheme does not require any external data source. It does require reception of two distinct frequencies, $L_1$ and $L_2$, from the satellite. This correction scheme removes more of the uncertainty due to ionospheric delays.

### 1.1.3 Receiver Model

One of the purposes of this entire study is to aid in the design of the receiver by performing trade-off studies. For this reason, the baseline receiver model has not been established. This section will thus present the alternatives for the trade-off studies and point out other areas of the receiver model which impact the navigation problem. The trade-off areas are 1) single channel or multiple channel receiver, 2) range and range rate or range only data, and 3) whether to demodulate the incoming information stream. Other areas of importance to the navigation problem include the data interface between the receiver and the processor, acquisition time, and the frequency of measurements. The accuracy of the receiver will be discussed in the error model section.

At the present time, there are three candidate receiver configurations. They are 1) dual-frequency multi-channel, 2) single-frequency single channel for P code and C/A, and 3) single-frequency single channel C/A only.

### 1.1.3.1 Receiver Channels

The trade-off in the number of channels is, of course, cost vs. navigational accuracy. In addition, the time to first fix and through put must be considered. The following describe the processing considerations of single-channel and four-channel receivers.

### 1.1.3.1.1 Single Channel Receiver

In order for a single-channel receiver to supply sufficient data for accurate navigation, it must switch between satellites for each new piece of data. This switching involves the acquisition time for each new satellite. This is particularly important in a single fix case where four different satellites must be received before any position computation can be made. If recursive filtering of data is to be done, then each satellite measurement can be incorporated in a sequential fashion as it is received. The acquisition time from one satellite to the next thus becomes an important parameter of the navigation accuracy in the single-channel receiver.

### 1.1.3.1.2 Four-Channel Receiver

This is a special case of a multiple-channel receiver. A four-channel receiver is being considered since this is the minimum needed to get a single fix without having to switch satellites. With four channels of data reception, acquisition time does not effect the accuracy of the navigation algorithms. Even in a recursive filtering mode, some data is available while other satellites are being acquired. With a four-channel receiver, either sequential or batch processing of data may be utilized and should be analyzed.

14

### 1.1.3.2   Measurables

The trade-off to be made in this area is whether or not to make Doppler measurements in addition to time-of-arrival measurements. Making Doppler measurements adds to the complexity of both the hardware and the navigational software. The additional cost will be traded-off against the navigational accuracy obtainable. The Doppler measurements will be particularly useful in reducing platform position and velocity uncertainties when platform accelerations are taking place.

### 1.1.3.3   Data Demodulation

This trade-off concerns whether the ephemeris and clock data will be extracted from the satellite signal. If the data is not demodulated, the nominal values must be used for these parameters. It is possible that some method for updating the nominal values on some infrequent basis can be arranged. Both the hardware and the processing software can be simplified if it is not necessary to demodulate data. The trade-off here is a rather large degradation of navigational accuracy. (Note - It may be possible to reduce the effect of not demodulating data through increased computational complexity. The study of this case is beyond the scope of this study.)

### 1.1.3.4   Receiver Frequencies

The satellites transmit on two separate frequencies denoted $L_1$ and $L_2$. All of the information required for navigation is contained on each frequency. Reception on two frequencies, in addition to two sets of data, allows a more accurate estimation of ionospheric delay errors. The methods for determining ionospheric delay errors for the single and dual frequency have been described above in Section 1.1.2.2.

15

1.1.3.5  Other Parameters

The receiver model also consists of the required interface
between itself and the navigation processor.  It will be necessary to
specify the output formats, resolutions, time delays, frequency of mea-
surements, and acquisition times.  These values can be considered as
parameters of the study.

1.1.4  Reception Model

For the purpose of this study, a simplified reception model will
be used.  It will be assumed that there is sufficient gain in the receiver
and user antenna to receive signals from any satellite which is a fixed
angle $\gamma$ (five degrees in this study) above the horizontal phane.

The effects on satellite visbility due to platform pitch
and roll will be modelled as a decrease in the cone of reception corre-
sponding to the pitch and roll angle.  This is a reasonable model since
pitch and roll periods in other simulations (5) are shorter than probable
acquisition times (6).  Further study will have to be done to see if two
separate parameters are required to characterize the reduction of the
cone of reception.  Two parameters may be required since the require-
ments to re-acquire a signal momentarily lost may be considerably dif-
ferent than the requirements to acquire a new signal.

1.1.5  Integration of Other Sensors

The system model also contains provisions for integrating mea-
surements from three other sensors into the navigation algorithm.  These
sensors are the EM log, gyrocompass, and Omega receiver.  The sys-
tem and error models for these are taken from reference 7.  The refer-
ence goes into considerable detail in the development of these models.

16

It also cites the primary references for the models to be used in this study. These sensors are actually external to the NAVSTAR/GPS system. Their inclusion is to evaluate the accuracy improvement obtainable from the relatively minimal cost of the integration of these data sources. It may also be possible to use the GPS data to calibrate the other sensors for times when GPS is not available.

### 1.1.5.1 EM Log

The EM log is an instrument which measures a ship's speed along its longitudinal axis. The measured speed is with respect to the water so that ocean currents become a source of error.

### 1.1.5.2 Gyrocompass

The gyrocompass is an instrument aboard ship which indicates the ships heading. This heading information then combined with the EM log data gives the ship's velocity. The pitch and roll information can be used to modify the set of possible satellites which can be tracked.

### 1.1.5.3 Omega Receiver

Omega is a land-based worldwide coverage hyperbolic radio navigation system. The Omega receiver receives signals from the transmitting stations and determines the user position. The basic measurable is a phase difference from two transmitting stations. The system model consists of four Omega transmitters so that three independent lines of position are available.

### 1.1.6 Scenarios

The following scenarios have been selected for use in the analysis

of the navigation algorithms.   These scenarios were chosen at random
and not contrived to emphasize any particular point.   The scenarios are
intended to be two typical cases.   They are depicted in Figures 1-1 and 1-2.

### Test Scenarios

#1  Ship initially at $45^{\circ}$N $160^{\circ}$W travelling due south at 10 kts

at t = 30 secs. accelerate to 30 kts at rate of .5 kts/sec

at t = 72 secs turn starboard to $360^{\circ}$ at $1^{\circ}$/sec and decelerate to
15 kts at .25 kts/sec

at t = 260 secs turn port to $300^{\circ}$ at $3^{\circ}$/sec followed by an additional
turn to port of $30^{\circ}$ at .5$^{\circ}$/sec

at t = 350 secs decelerate to stop at .1 kts/sec

at t = 530 secs accelerate at .05 kts/sec and turn port at accelerat-
ing rate of .01$^{\circ}$/sec$^2$ for 100 secs.   Maintain turn rate at
$1^{\circ}$/sec.   Change acceleration to .2 kts/sec for 40 secs.
Maintain velocity and heading for 40 seconds.

**Total run:  710 secs**

#2  Aircraft initially at $32^{\circ}$N $120^{\circ}$W travelling West at 600 kts.
Altitude 38,000 ft

at t = 0 secs accelerate at 2 kts/sec for 5 min
at t = 300 secs turn to port at $5^{\circ}$/sec for 36 secs.
at t = 360 secs turn port at .5$^{\circ}$/sec for 120 secs
End at t = 600 secs

18

Δ LATITUDE (DEGREES)

t=0

t=30 secs

t=530 secs          t=340 secs

t=260 secs

t=72 secs

t=710 secs

Δ LONGITUDE (DEGREES)

-0.028 -0.026 -0.024 -0.022 -0.020 -0.018 -0.016 -0.014 -0.012 -0.010 -0.008 -0.006 -0.004 -0.002 0.

TIME

TIME
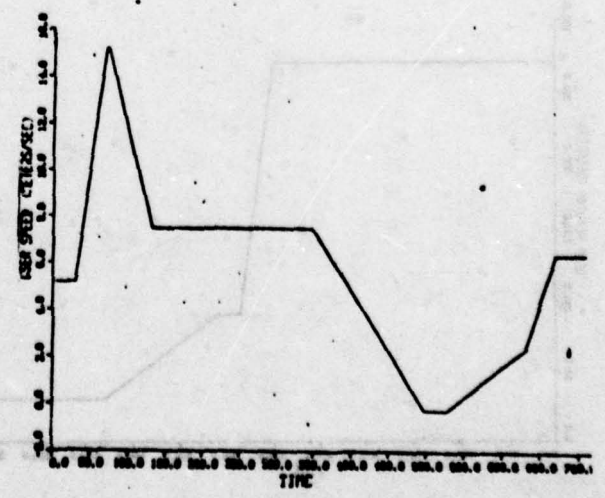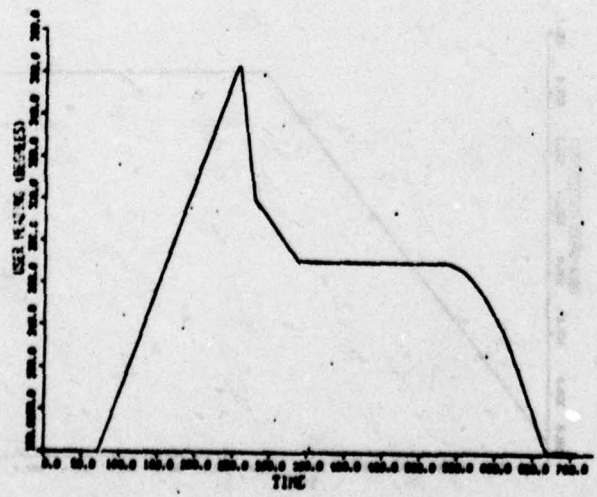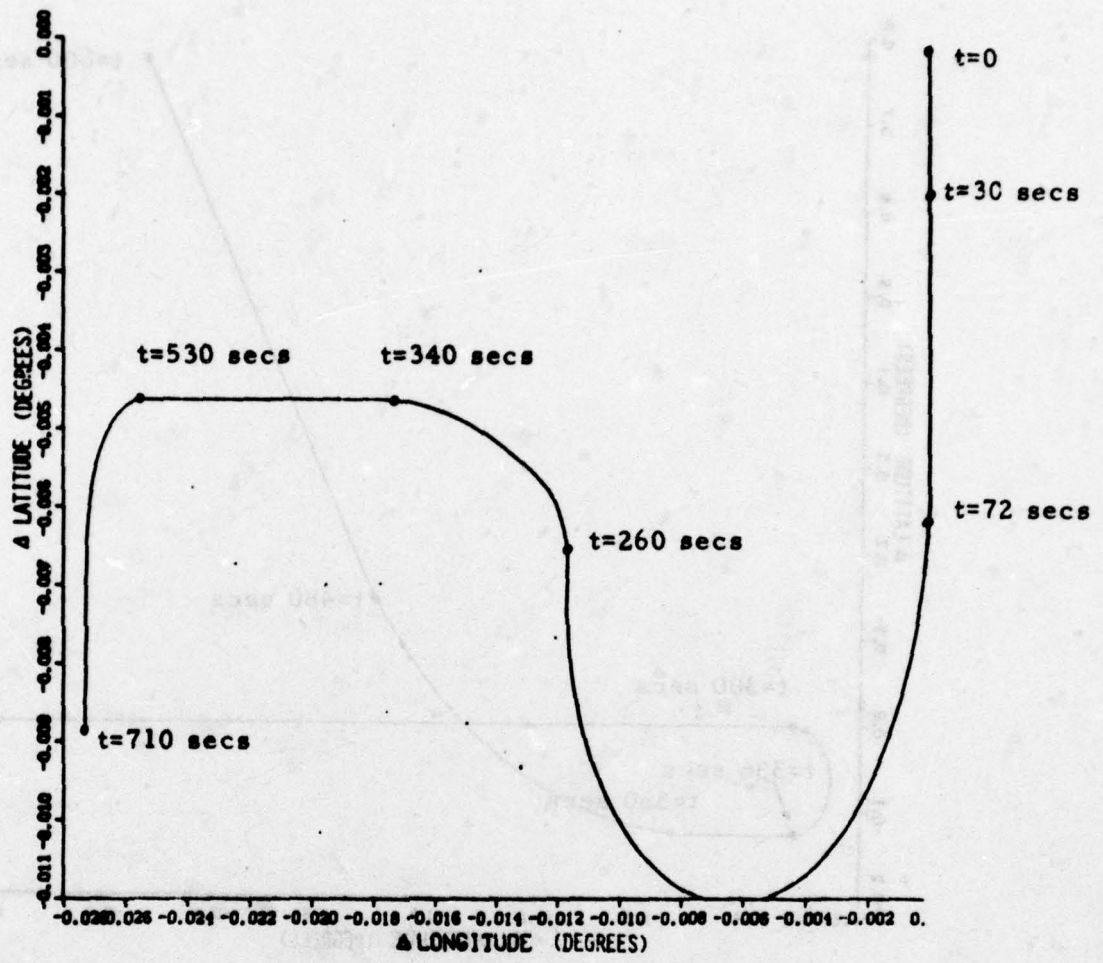
**FIGURE 1.1 SHIP SCENARIO**

19
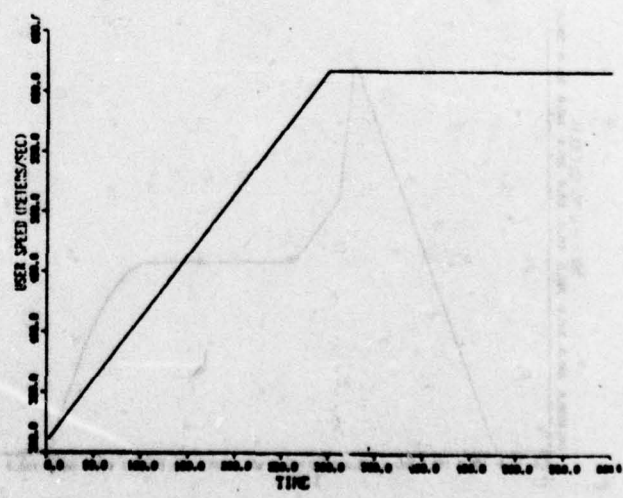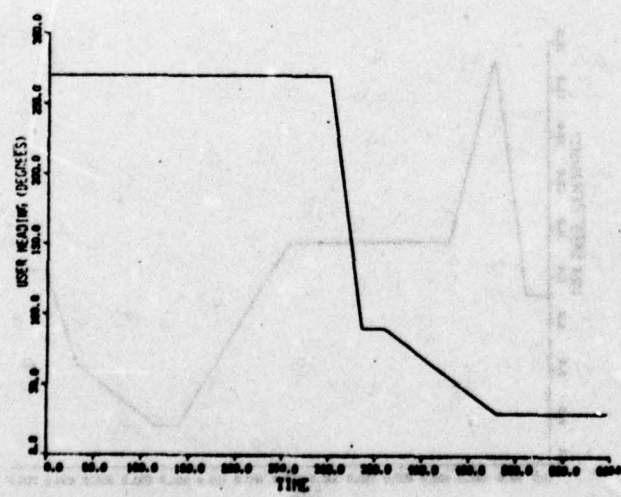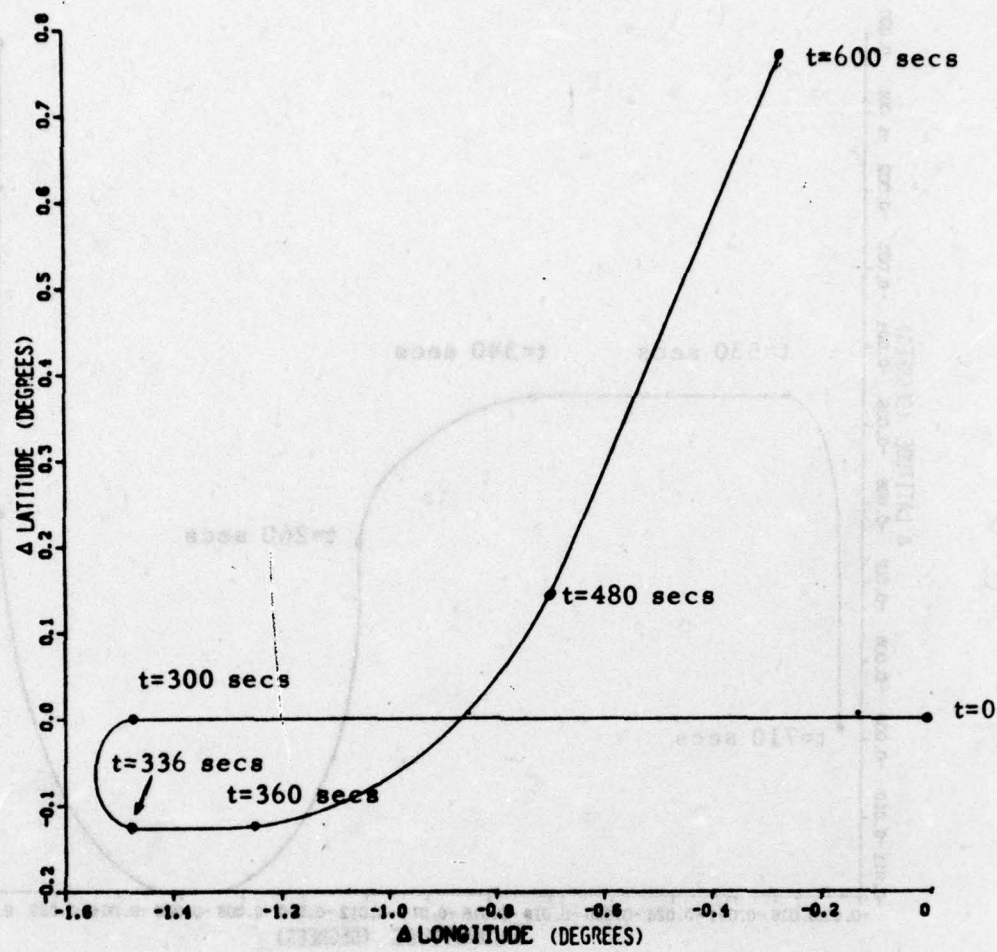
**FIGURE 1.2 AIRCRAFT SCENARIO**

20

## 1.2 Error Model

The error model is a model of those effects which tend to degrade the accuracy of the NAVSTAR/GPS navigation mechanization. To make a meaningful evaluation of any proposed navigation algorithm, it is important to have a realistic error model containing all of the significant error sources. However, in a system as complex as the NAVSTAR/GPS navigation system, this groundrule would demand an error model consisting of hundreds of states. The error model outlined below will attempt to simplify most of the individual error models to keep the total number of states down while maintaining the integrity of the error model. Each reduced state error model will be justified within the report or the references cited.

Much of the analytic work which uses this error model takes the form of linearized covariance analysis. For this reason it is desirable to not only make the error models simple, but to pose as many of them as possible as linear models; i.e., error models whose behavior is described by linear differential or difference equations. Models of this form are then easily adapted to methods of linear analysis.

### 1.2.1 Ephemeris Error Model

A complete error model for satellite position and velocity uncertainties is a large order system containing many high-order gravity harmonic errors. This type of model is used and is necessary for accurate satellite position determination and prediction over long time intervals. When residual errors to accurate position predictions are considered, the effects of the high-order gravity harmonics are negligible. This justifies the use of the two-body orbit equations, utilizing just six states per satellite, for propagating satellite position errors. These six states

21

can be propagated from initial conditions by a state transition matrix calculated in closed form (8).

Propagating six states per satellite for up to eleven visible satellites is still a large number of states. Further reduction in the number of states is thus desirable. One way of doing this is to assume that the position uncertainty is constant rather than growing with time. Since the growth is very small, choosing the maximum user equivalent range error as the constant uncertainty along each axis will give a realistic though somewhat pessimistic model for the ephemeris. Furthermore, assume that the errors are given initially in the principal axes, so that the initial error covariance matrix is diagonal. This can be expressed by

$$E[\Delta X] = \begin{bmatrix} 0 \\ 0 \\ 0 \end{bmatrix} ; E[\Delta X \ \Delta X^T] = \begin{bmatrix} \sigma^2 & 0 & 0 \\ 0 & \sigma^2 & 0 \\ 0 & 0 & \sigma^2 \end{bmatrix}$$

where

$\Delta X$ is the satellite position error vector

$\sigma$ is the user equivalent range error for Phase III specified in Reference 9, p. 8.

Another source of error in the ephemeris model arises numerically. This error is the difference between the control segment predicted satellite position and the position computed by the user from the received data. In reference (15), it is shown that this error source can be made negligible by scaling of data and careful algorithm design.

22

## 1.2.2 Time Error Model

As in the system time model, the time error model consists of a satellite clock error model and an atmospheric delay error model. In addition a user clock error model must be considered. The time error model, like the ephemeris error model, is concerned with the modelling of the residual errors between actual time and the system model of time (Section 1.1.2). Now the errors in time and ephemeris are correlated inherently by the methods which the control system segment uses to estimate the system model parameters (3). Ignoring such correlations may give somewhat optimistic results, however determination of such correlations would require extensive simulation of the control system segment estimation techniques. This is clearly not within the scope of the present study.

### 1.2.2.1 Satellite Clock Error Model

The residual time error consists of two parts, the error in the predicted correction parameters and the random part. The errors in the correction parameters, which represent bias error, frequency error, and frequency rate error, are used to determine initial conditions for the dynamic error model of the satellite clock. The type of error model required for the random part can be determined from the curves of the Allan variance* (10) for the clock. For the Phase III system, Cesium beam clocks will be used in the satellites. These clocks will be updated every day so that the error model is based on the twenty-four hour variance. The Allan variance of the typical Cesium beam clock data indicates the fractional frequency error can be modelled as a white noise (i.e.,

---

*The Allan variance is the variance of the fractional frequency error as a function of the sampling interval $\tau$. See reference 10 for details.

23

Flicker noise and integrated white noise are not important for times less than one day).  The satellite clock error model is thus

$$\begin{pmatrix} \dot{x}_{1n} \\ \dot{x}_{2n} \end{pmatrix} = \begin{pmatrix} 0 & 1 \\ 0 & 0 \end{pmatrix} \begin{pmatrix} x_{1n} \\ x_{2n} \end{pmatrix} + \begin{pmatrix} \sigma \\ 0 \end{pmatrix} u(t)$$

where

$x_{1n}$ is the time error of the $n^{th}$ satellite clock

$x_{2n}$ is the frequency bias error of the $n^{th}$ satellite clock

$\sigma$ is PSD magnitude (typically for Cesium Beam $\sigma = 10^{-11}$ $sec/sec^{1/2}$)

$u(t)$ is white noise with unity PSD

and

$x_{1n}(0)$ is the error in $a_o$

$x_{2n}(0)$ is the error in $a_1$

## 1.2.2.2 User Clock Error Model

The user clock error model is based on data for typical crystal oscillators.  The Allan variance for crystal oscillator clocks indicates that the error model over the times of interest consists of a fractional frequency error model with white noise, flicker noise, and integrated white noise.  Following the procedures in reference 10, a clock model for the user which also includes a frequency offset and an aging coefficient is given by the following seven-state description.

$$
\begin{bmatrix} \dot{x}_1 \\ \dot{x}_2 \\ \dot{x}_3 \\ \dot{x}_4 \\ \dot{x}_5 \\ \dot{x}_6 \\ \dot{x}_7 \end{bmatrix} = \begin{bmatrix} -\omega_a & 0 & 0 & 0 & 0 & 0 & 0 \\ \alpha(\alpha-1)\omega_a & -\alpha^2\omega_a & 0 & 0 & 0 & 0 & 0 \\ \alpha^2(\alpha-1)\omega_a & \alpha^3(\alpha-1)\omega_a & -\alpha^4\omega_a & 0 & 0 & 0 & 0 \\ \dfrac{\omega_1-\omega_o}{\alpha^3} & \dfrac{\omega_1-\omega_o}{\alpha^2} & \dfrac{\omega_1-\omega_o}{\alpha} & -\omega_o & 0 & 0 & 0 \\ 0 & 0 & 0 & 0 & 0 & 1 & 0 \\ 0 & 0 & 0 & 0 & 0 & 0 & 0 \\ \dfrac{\beta}{\alpha^3} & \dfrac{\beta}{\alpha^2} & \dfrac{\beta}{\alpha} & \beta & 1 & 0 & 0 \end{bmatrix} \begin{bmatrix} x_1 \\ x_2 \\ x_3 \\ x_4 \\ x_5 \\ x_6 \\ x_7 \end{bmatrix}
$$

$$
+ \begin{bmatrix} (\alpha-1)\omega_a \\ \alpha(\alpha-1)\omega_a \\ \alpha^2(\alpha-1)\omega_a \\ \dfrac{\omega_1-\omega_o}{\alpha^3} \\ 0 \\ 0 \\ \dfrac{\beta}{\alpha^3} \end{bmatrix} u(t)
$$

**where**

u(t) is white noise with unity PSD

$$\alpha = (\omega_2/\omega_1)^{1/2\,n}$$

n is the order of the flicker noise model (3 in this case)

$$\omega_a = \omega_1(\alpha)^{1/2}$$

25

$$\beta = \alpha^n 10^{M/20}$$

$M$ = gain at $\omega_2$ in dB (for crystal clocks $\approx$ -220)

$$\omega_o = \frac{\sqrt{3}}{\tau_3}$$

$$\omega_1 = \frac{6 \ln 2}{\pi \tau_2}$$

$$\omega_2 = \frac{\pi}{2 \tau_1 \ln 2}$$

$\tau_1$, $\tau_2$, $\tau_3$ are parameters of the Allan variance curve (10)

Typical values for a crystal oscillator are $\tau_1 = .5$ sec,

$\tau_2 = 80$ sec, $\tau_3 = 5 \times 10^4$ sec

The state $x_7$ is the user clock error in seconds. The parameters $\tau_1$, $\tau_2$, $\tau_3$, and M will depend on the particular oscillator type chosen for the user frequency standard.

### 1.2.2.3 Atmospheric Delay Error Model

The atmospheric delay error model consists of a residual error model for both ionospheric and tropospheric delays. The largest uncertainties are the ionospheric model when a single frequency is used. The ionospheric error model discussed here is the residual model for the single frequency case. The dual frequency correction will be considered to have negligible residual time error.

The tropospheric error model is an uncertainty in the correction constant K (see Section 1.1.2.2 above). The time error in the

26

incoming signal is a zero mean random constant $\Delta K$ times the cosecant of the elevation angle. The variance of $\Delta K$ is approximately .1K (3). This error source is independent of the other time models.

The ionospheric residual error model (see references 11 and 14) is modelled as a Gauss-Markov error source which is correlated in both time and distance. The covariance of two measurements at two different times and two different places will be modelled as (12)

$$\sigma^2_{R_1 R_2} = \Delta R_1 \Delta R_2 \eta_t(\Delta t)\eta_p(\Delta p)$$

where

$\Delta R_1, \Delta R_2$ are the prediction residuals

$$\Delta R_i = \epsilon \, csc[\sqrt{E_i^2 + (18^{o})^2}]$$

$\epsilon$ is the RMS correction error

$E_i$ is the elevation angle for the $i^{th}$ measurement in degrees

$\Delta t$ is the time difference between measurements

$\Delta p$ is distance between the ionospheric "pierce points" of the measurements (The pierce point is the point at which the transmitted signal intersects the ionosphere. The ionosphere here is assumed to be a thin shell 350 km above the surface of the Earth)

For the simulations in this study, the functions $\eta_t$ and $\eta_p$ can be approximated over the range of interest from the data in reference 12. (The model given in references 12 and 14 have two time constants, but for times in the selected scenarios, one is sufficient. )

27

$$\eta_t(\tau) = e^{-\tau/6.7 \text{ hr}}$$

$$\eta_p(\rho) = e^{-\rho/2500 \text{ km}}$$

In order to model this covariance in a linear system model, the distance correlation will be changed to a time function. This can be done since the "pierce point" of the 350 km altitude ionosphere shell moves with a constant velocity when the satellite orbits are circular. Thus replacing $\rho$ with $\dot{\rho} \cdot \tau$, when $\dot{\rho}$ is constant, transforms the spatial correlation into a time function. Combining $\eta_t$ and $\eta_p$ then yields a Gauss-Markov model with a modified time constant. So

$$\sigma^2_{R_1 R_2} = \Delta R_1 \Delta R_2 \, e^{-\tau/6.7 \text{ hr}} \cdot e^{-\tau \cdot \dot{\rho}/2500 \text{ km}}$$

$$= \Delta R_1 \Delta R_2 \, e^{-\tau \left( \frac{1}{6.7 \text{ hr}} + \frac{\dot{\rho}}{2500 \text{km}} \right)}$$

$$\approx \Delta R_1 \Delta R_2 \, e^{-\tau/1.17 \text{ hr}}$$

where $\dot{\rho} \approx 2\pi \cdot (6378 \text{ km} + 350 \text{ km})/24 \text{ hr} \approx 1761 \text{ km/hr}$. 24 hr is the apparent period of the satellite with respect to an Earth fixed coordinate frame. In addition, $\dot{\rho}$ can be modified to account for user motion.

The ionospheric delay error for each satellite can be modelled as above. In addition, a cross-correlation of the ionospheric delay error between the various satellites can be computed using the original formula above.

## 1.2.3 Receiver Measurement Error Model

The exact form of the receiver is as yet unresolved. The error model of the measured data is for one channel of both time of arrival measurements (for pseudo-range or range difference) and Doppler mea-

28

surements (for pseudo range rate). The Doppler errors are not independent for the case of multi-channel reception. The multi-channel error model can be put together from copies of the single-channel model with the correlations noted and accounted for.

## 1.2.3.1 TOA (Time of Arrival) Measurement Error Model

The primary error in the TOA measurement is the user clock error which has been described in Sec. 1.2.2.2. In addition to this is a uniformly distributed random error corresponding to the measurement resolution. This may result from the clock resolution or the finite word length of the time data. The mean error will be different for the case where the data is rounded rather than truncated. Let $\delta t_{res}$ denote the resolution error, then

$$E(\delta t_{res}) = \begin{cases} 0 \text{ for rounded error} \\ .5 \Delta t_{res} \text{ for truncated error} \end{cases}$$

$$E(\delta t_{res}^2) = \frac{\Delta t_{res}^2}{12}$$

where $\Delta t_{res}$ is the smallest unit of time resolvable. If the resolution is very fine, other measurement errors will limit how small the TOA errors may become. In either case a random measurement error will be included.

## 1.2.3.2 Doppler Measurement Error Model

Ideally a Doppler measurement is an instantaneous determination of frequency. Practically, this is not possible so a count of frequency over a short time is done. This can be represented as

29

$$N = \int_{t_0}^{t_1} (\omega_{Ref} - \omega_S)\, dt$$

where

N is the Doppler count

$\omega_{Ref}$ is the reference frequency $\omega_{Ref} = \omega_R + \omega_o$

$\omega_R$ is the receiver's estimate of the transmitted signal frequency

$\omega_o$ is an offset frequency so that N is always $> 0$

$\omega_S$ is the received frequency $\omega_S = \omega_T + \omega_D$

$\omega_T$ is the transmitted frequency

$\omega_D$ is the Doppler shift frequency

Now if the time period $t_1 - t_0 = \delta t$ is short compared to the dominant dynamics of the system; i.e., the user and the satellite, the Doppler frequency can be assumed constant over $\delta t$ and

$$\omega_D = \frac{\omega_T}{C} \dot{\rho}$$

where $\dot{\rho}$ is the assumed constant range rate between the user and the transmitting satellite, $\dot{\rho} = \bar{V} \cdot u$ . $\bar{V}$ is the relative velocity and u is the unit line-of-sight (LOS) vector, and C is the speed of light.

The Doppler count equation can then be integrated to get N

30

$$N = (\omega_R + \omega_o - \omega_T)\delta t - \frac{\omega_T}{C}\dot{\rho}\,\delta t$$

The error equation for $\Delta N$, the Doppler count residual is

$$\Delta N = \Delta\delta t\,\omega_T(1 + \frac{\dot{\rho}}{C}) - \delta t\Delta\omega_T(1 + \frac{\dot{\rho}}{C}) - \frac{\omega_T\delta t}{C}\Delta\dot{\rho}$$

since $\dot{\rho} \ll C$, this reduces to

$$\Delta N = \Delta\delta t\,\omega_T - \delta t\Delta\omega_T - \frac{\omega_T}{C}\delta t\Delta\dot{\rho}$$

    The above equation has assumed that time $\delta t$ and the frequency $(\omega_R + \omega_o)$ are derived from the same oscillator so that the product $(\omega_R + \omega_o)\delta t$ is error free.

    The term $\Delta\dot{\rho}$ is a function of uncertainties in user position, user velocity, satellite position, and satellite velocity. Of these, the satellite contributions are negligible since the ephemeris data gives extremely accurate delta range information. Expanding $\Delta\dot{\rho}$ in terms of the user states yields (see Ref. 7 for details)

$$\Delta\dot{\rho} = \left[\frac{(\dot{X}_u - \dot{X}_s)}{\rho} - \frac{(X_u - X_s)}{\rho^2}\dot{\rho}\right]\Delta X_u + \left[\frac{(\dot{Y}_u - \dot{Y}_s)}{\rho} - \frac{(Y_u - Y_s)}{\rho^2}\dot{\rho}\right]\Delta Y_u$$

$$+ \left[\frac{(\dot{Z}_u - \dot{Z}_s)}{\rho} - \frac{(Z_u - Z_s)}{\rho^2}\dot{\rho}\right]\Delta Z_n + \left(\frac{X_u - X_s}{\rho}\right)\Delta\dot{X}_u$$

$$+ \left(\frac{Y_u - Y_s}{\rho}\right)\Delta\dot{Y}_u + \left(\frac{Z_u - Z_s}{\rho}\right)\Delta\dot{Z}_u$$

where

u has been assumed to be $[(X_u - X_s), (Y_u - Y_s), (Z_u - Z_s)] \cdot \frac{1}{||\rho||}$

$\rho$ is the user to satellite range

$X_u$, $Y_u$, $Z_u$ are the user coordinates

$X_s$, $Y_s$, $Z_s$ are the transmitting satellite coordinates

Not included in the above model are the refractive errors. The refractive errors occur because the transmitting satellite is outside the atmosphere. It is shown in reference 13 that the Doppler shift due to the transmitter and the receiver velocities are dependent on the velocity of light in their respective media. Ignoring this leads to a negligible error since the light velocity difference is of the order of .03%. The other refraction error is a change in the direction of the incoming signal from the calculated line of sight. Arguments similar to those in Ref. 13 show that this error is negligible in the GPS geometry.

Additionally, there is a truncation or round-off error similar to the TOA error above.

### 1.2.4 Other Sensors

The error models for the EM log, gyrocompass and Omega are taken from Ref. 7.

### 1.2.4.1 EM Log Error Model

The state space error model for the EM log is

$$\begin{pmatrix} \dot{x}_1 \\ \dot{x}_2 \end{pmatrix} = \begin{pmatrix} 0 & 0 \\ 0 & -.00185 \end{pmatrix} \begin{pmatrix} x_1 \\ x_2 \end{pmatrix} + \begin{pmatrix} .193 & 0 \\ 0 & .0257 \end{pmatrix} \begin{pmatrix} u_1 \\ u_2 \end{pmatrix}$$

where $x_1$ represents a random walk error state and $x_2$ represents a Gauss-Markov error source with correlation time = .15 hrs and RMS value = .422 fps ; $u_1$ and $u_2$ are white noise with unity PSD; $E[x_1^2(0)]$ = 71.23 fps$^2$; $E[x_2^2(0)]$ = .178 fps$^2$.

The output model is

$$y = x_1 + x_2 + \sigma u_3$$

where

$\sigma$ = .472 fps measurement noise (1$\sigma$)

$u_3$ is white noise with unity PSD

### 1.2.4.2 Gyrocompass

The state space error model for the gyrocompass is

$$\begin{pmatrix} \dot{x}_1 \\ \dot{x}_2 \end{pmatrix} = \begin{pmatrix} 0 & 0 \\ 0 & -7.25 \times 10^{-4} \end{pmatrix} \begin{pmatrix} x_1 \\ x_2 \end{pmatrix} + \begin{pmatrix} 1.68 \times 10^{-3} & 0 \\ 0 & .0133 \end{pmatrix} \begin{pmatrix} u_1 \\ u_2 \end{pmatrix}$$

where

$x_1$ is a random walk bias state .013$^{\circ}/\sqrt{\text{sec}}$(1$\sigma$)

$x_2$ is a Gauss-Markov error with correlation time = 23 min and RMS value = .35$^{\circ}$

$u_1$ and $u_2$ are white noises with unity PSD

33

$$E[x_1^2(0)] = 0 \quad E[x_2^2(0)] = .1225 \text{ deg}^2$$

**The output is modelled as**

$$y = x_1 + x_2 + \sigma u_3$$

where

$$\sigma = \begin{cases} .15 \text{ deg} & 1\sigma \text{ no maneuvers} \\ .52 \text{ deg} & 1\sigma \text{ during maneuvers} \end{cases}$$

$u_3$ is white noise with unity PSD

### 1.2.4.3 Omega Error Model

The details of the derivation of the Omega error model can be found in Ref. 7. The state space equations for the phase error for each station are:

$$\begin{bmatrix} \dot{x}_1 \\ \dot{x}_2 \\ \dot{x}_3 \\ \dot{x}_4 \end{bmatrix} = \begin{bmatrix} 0 & 0 & 0 & 0 \\ 0 & -\beta & 0 & 0 \\ 0 & 0 & 0 & 1 \\ 0 & 0 & -\omega^2 & 0 \end{bmatrix} \begin{bmatrix} x_1 \\ x_2 \\ x_3 \\ x_4 \end{bmatrix} + \begin{bmatrix} 0 \\ \sigma \\ 0 \\ 0 \end{bmatrix} u(t)$$

where

$x_1$ is a bias state

$x_2$ is a Gauss-Markov error

34

$x_3$, $x_4$ form a sinusoidal (periodic) error with period $\omega$

$$\beta = (1/3600)\sec^{-1}$$

$$\omega = (2\pi/12)\ hr^{-1}$$

$$\sigma^2 = .00277\ \text{centicycles}^2/\sec^2\ *$$

$$E[x_1^2(0)] = 8.5\ \text{centicycles}^2$$

$$E[x_2^2(0)] = 5.\ \text{centicycles}^2$$

u(t) is a white noise with unity PSD

$$E[x_3^2(0)] = 5.\ \text{centicycles}^2$$

$$E[x_4^2(0)] = 1.05 \times 10^{-7}\ \text{centicycles}^2$$

Converting this phase error into equivalent position error of the user is a function of the user location. Details of the calculation may be found in reference 7.

### 1.2.5 Platform Error Model

To account for random motions and accelations of the user, the position, velocity and acceleration states will be modelled as random walks. The magnitudes of the random walk driving noise variances will vary according to the type of platform and the scenario.

*A centicycle is 1/100 of a cycle.

## Section 2. - SINGLE FIX ALGORITHM

### 2.0 Introduction

This section is concerned with the problem of determining an accurate estimate of a user location, i.e., a navigational fix, using the minimum amount of data required for the fix. This first step in the development of the NAVSTAR/GPS navigation algorithm is called the single fix algorithm. In some system configurations, the initial fix may be made simply by entry of present position derived from other navigation aid sources such as inertial navigation systems, star fixes, Omega, etc., or from known initial conditions. The single fix algorithm is, however, needed to establish initial conditions for some system configurations. Additionally it may be used to make the NAVSTAR/GPS system autonomous even if other data sources are available and it may be used in some pseudo-measurement mechanizations (e.g. the $\alpha - \beta$ filter in section 3).

The single-fix algorithm as presented in this report consists of two distinct parts. The first part is the selection of the available satellites to use for the navigation fix. The second part is the actual position determination using the time of arrival data from the selected satellites. The single-fix algorithms may be mechanized for either position only or position plus user clock bias. The body of the report is concerned with the latter case. The mechanization for the position only algorithm is discussed in Appendix 2 of Reference 16.

Processing of the measurables for the single-fix algorithm falls into two categories, batch and sequential processing. This section is concerned with iterative techniques for batch processing of data. Sequential processing mechanizations fall more naturally in the domain of recursive filtering algorithms. As such these techniques will be

studied in subsequent sections of this report as part of the start-up pro-
cedures for the recursive filtering algorithms. Recursive filters which
can be initialized from relatively crude initial conditions may be thought
of as having a built-in single-fix capability. In this sense a separate
single-fix algorithm as described herein may not be needed to initialize
all of the candidate recursive filters. This does not, however, preclude
the use for other purposes.

This section is organized in four subsections corresponding to
four areas of the single-fix algorithm development and analysis. Section
2. 1 describes the candidate alert algorithms, one from the GDE proposal (3)
and one proposed maximum volume using a known principle for approximate
minimization of GDOP. Section 2. 2 developes the algorithms for solving
the set of non-linear equations to determine position. Section 2. 3 describes
the techniques used to evaluate the algorithms developed in Section 2. 2.
The results from the studies of Sections 2. 1-2. 3 are given in Section 2. 4.
All of the computer programs used in the analyses are given in Appendix 1
of Reference 16.

## 2. 1    Alert Algorithm for Single-fix

The measure of a good alert algorithm is the value of GDOP (6)
for the satellites which it selects. The nature of GDOP does not allow
for any exact methods of GDOP minimization short of an exhaustive
enumeration of all possibilities. With from six to eleven satellites
visible at any point in time, an exhaustive enumeration may take too
much computation time. For this reason, two approximate GDOP mini-
mizations are also being considered as candidates for the alert calcula-
tions. The first technique is the one developed by GDE for its proposal (3).
The second technique is based on an approximate maximization of the
tetrahedron enclosed by four satellites. The form of the GDOP calcula-
tions used will be described in Section 2. 3.

37

## 2.1.1 GDE Alert Algorithm (3, p. 1-39 to 1-41)

This algorithm gives criteria for the selection of the four satellites to be used. The minimizations/maximizations to be performed involve only dot products of vectors and so are simple and fast computationally. This method proceeds as follows:

Satellite No. 1 selection: Choose the satellite which is closest to the zenith. This is found by maximizing the dot product of the unit vector to the user with the unit vector from the user to the satellites.

$1^{st}$ Satellite No. = i such that $\underline{U}_i \cdot \underline{U}_u \geq \underline{U}_j \cdot \underline{U}_u$

where

$\underline{U}_u$ is the ECI unit vector to the user

$\underline{U}_k$ is the unit vector along the line of sight from the user to the $k^{th}$ satellite ( k=i, j)

j varies over the visible satellites

Satellite No. 2 selection: The second satellite is chosen as the satellite among those visible which is closest to the horizon but not in the same orbit plane as the first selected satellite.

$2^{nd}$ Satellite No. = i such that

1) $\underline{U}_i \cdot \underline{U}_u \leq \underline{U}_j \cdot \underline{U}_u$ with j varying over the visible satellites
2) i is not in the same orbit plane as the first selected satellite.

Satellite No. 3 selection: The third satellite is selected as the one among the visible satellites which is closest to being orthogonal to both the first and second satellites selected.

$3^{rd}$ Satellite No. = i such that

$$\left| \underline{U}_i \cdot (\underline{U}_1 \times \underline{U}_2) \right| \geq \left| \underline{U}_i \cdot (\underline{U}_1 \times \underline{U}_2) \right|$$

where

j varies over the visible satellite and $\underline{U}_1$ is the unit vector from the user to the satellite chosen as Satellite No. 1 and $\underline{U}_2$ is the unit vector from the user to the satellite chosen as Satellite No. 2.

Satellite No. 4 selection: This satellite is chosen as the one which is closest to the vector sum of the first three.

4$^{th}$ Satellite No. = i such that

$$\underline{U}_i \cdot (\underline{U}_1 + \underline{U}_2 + \underline{U}_3) \geq \underline{U}_j \cdot (\underline{U}_1 + \underline{U}_2 + \underline{U}_3)$$

j varies over the visible satellites

where

$U_3$ is the unit vector from the user to the satellite chosen as Satellite No. 3.

It should be noted that the reference contains some obvious errors which have been corrected in this summary. The above described algorithm is the one which was used for purposes of comparison.

## 2.1.2 Maximum Volume Alert Algorithm

The maximum volume alert algorithm is based on the observation that the satellite constellation which maximizes the volume of the tetrahedron with vertices at the selected satellites (see Figure 2.1) also approximately minimizes GDOP. The maximization of the volume is done in an approximate fashion. The steps outlined below will lead to a local rather than global maximum. This is done to keep the amount of computation down. The procedure is as follows:

1$^{st}$ Satellite No. = i such that $\underline{U}_i \cdot \underline{U}_u \geq \underline{U}_j \cdot U_u$

where

j varies over the visible satellites.

Satellites No. 2, 3, and 4 selection: These satellites are chosen as a group by iterating once through all of the remaining satellites. The procedure is as follows.

A) Pick three visible satellites and compute the tetrahedral volume (see Figure "Hexahedron of satellite and user".

B) Pick another visible satellite, if there are no more, then procedure is finished.

C) Compute the volume of the tetrahedrons with the new satellite successively replacing satellites No. 2, 3, and 4. Pick the configuration with the largest volume and label those included satellites as the new No. 2, 3, and 4. (Go to Step B).

This algorithm for finding the best satellites creates a monotonically decreasing GDOP. This procedure converges to a local minimum and it is certainly dependent on the order of the satellites chosen. In the analysis section, the order taken is arbitrary so that the analysis represents a lower bound on the ability of the technique to choose a good constellation (i.e., an upper bound for an achievable GDOP).

The volume computation is a simple calculation. The volume may be computed using the scalar triple product.

$$V = V_I$$

$$= (1/16) \left| a_{12} \cdot (a_{13} \times a_{14}) \right|$$
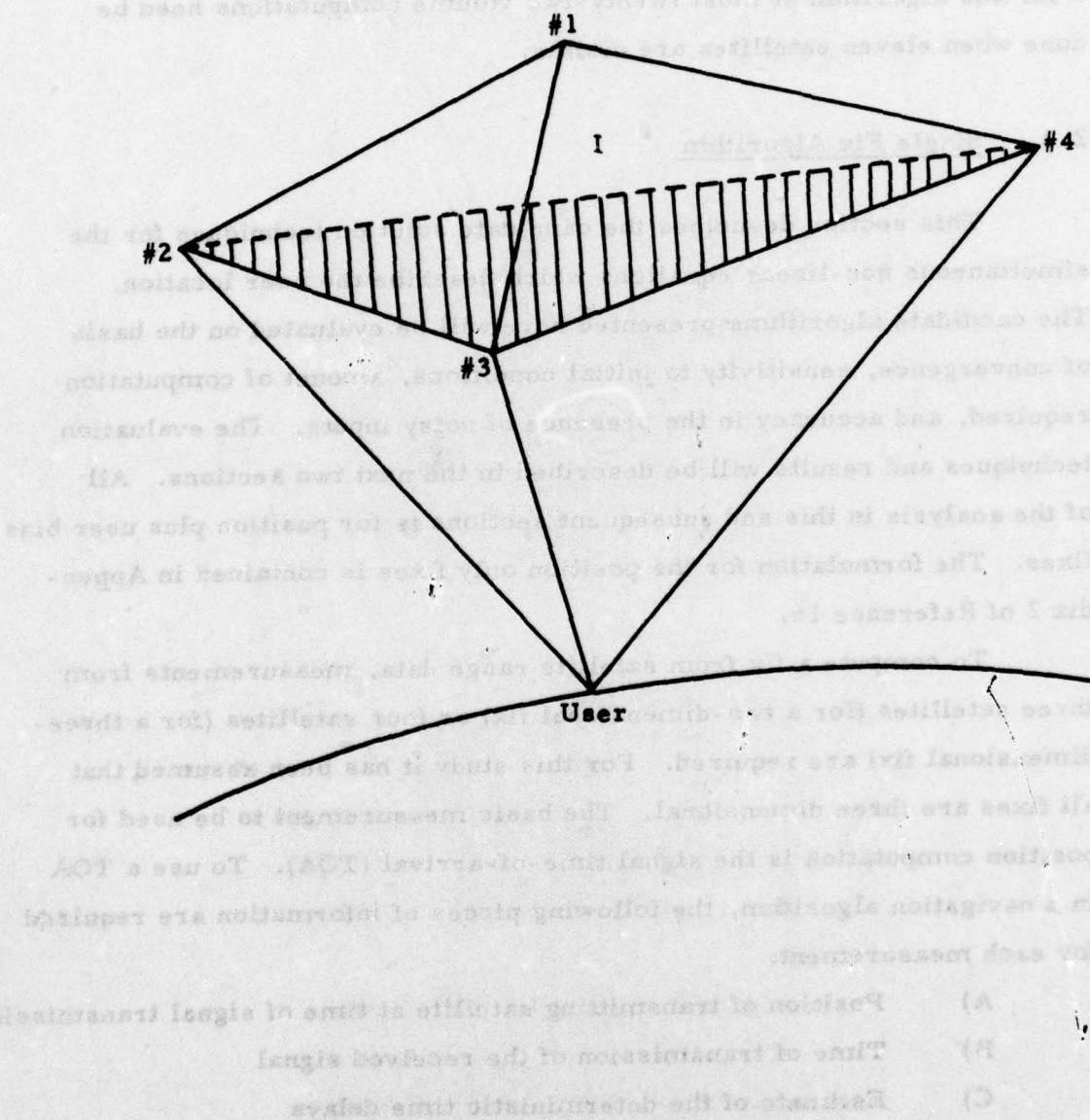
Figure 2.1. Hexahedron of satellite and user.

where

> $V_I$ is the volume of the tetrahedron labeled I (See Figure 2.1)
>
> $a_{1j}$ is the vector from Satellite No. 1 to Satellite No. j.
>
> $|\ |$ indicates absolute value

With this algorithm at most twenty-two volume computations need be done when eleven satellites are visible.

## 2.2 Single Fix Algorithm

This section describes the candidate solution techniques for the simultaneous non-linear equations which describe the user location. The candidate algorithms presented here will be evaluated on the basis of convergence, sensitivity to initial conditions, amount of computation required, and accuracy in the presence of noisy inputs. The evaluation techniques and results will be described in the next two sections. All of the analysis in this and subsequent sections is for position plus user bias fixes. The formulation for the position only fixes is contained in Appendix 2 of Reference 16.

To compute a fix from satellite range data, measurements from three satellites (for a two-dimensional fix) or four satellites (for a three-dimensional fix) are required. For this study it has been assumed that all fixes are three dimensional. The basic measurement to be used for position computation is the signal time-of-arrival (TOA). To use a TOA in a navigation algorithm, the following pieces of information are required for each measurement:

A) Position of transmitting satellite at time of signal transmission

B) Time of transmission of the received signal

C) Estimate of the deterministic time delays

Figure 2.1. Hexahedron of satellite and user.

42

With this information, the user may use the TOA's from selected satellites to determine its position. The equations to be solved can be developed as follows:

The measured time of arrival from satellite i, $AT_i$, is given by

$$AT_i = (1/c) \parallel \underline{S}_i - \underline{X} \parallel + T_i + t_i + b + w$$

where

$\underline{S}_i$ is the position of the ith satellite at the time of transmission

$\underline{X}$ is the user position

$T_i$ is the transmission time

$t_i$ is the deterministic delay

$b$ is the user bias (clock and electronic delay)

$w$ is the measurement error due to receiver error, random atmospheric delays, ephemeris errors, satellite electronic random delays, etc.

$c$ is the speed of light

When a set of AT have been measured, a position fix can be obtained. Two cases must be considered for collecting sets of data. The two cases correspond to the single channel and four channel receiver configurations. In the first case there will be motion of the user platform between measurements; in the second case, there is no motion. The user motion in the first case will lead to some error unless an external velocity determination is available.

The set of measurements leads to the simultaneous non-linear equations. The candidate solution techniques are presented below. They are all iterative techniques.

## 2.2.1 Newton-Raphson Method

The Newton-Raphson method is a well known procedure for solving sets of simultaneous non-linear equations (17). The system of equations to be solved here is:

$$f_1(\underline{X}, b) = (1/c) \| \underline{S}_1 - \underline{X} \| + b + (T_1 - AT_1) = 0$$

$$f_2(\underline{X}, b) = (1/c) \| \underline{S}_2 - \underline{X} \| + b + (T_2 - AT_2) = 0$$

$$f_3(\underline{X}, b) = (1/c) \| \underline{S}_3 - \underline{X} \| + b + (T_3 - AT_3) = 0$$

$$f_4(\underline{X}, b) = (1/c) \| \underline{S}_4 - \underline{X} \| + b + (T_4 - AT_4) = 0$$

Note that if there is a bias in the system such that all of the AT are off by a fixed constant increment, this looks like a user bias b. The user and system biases are inseparable and only the sum may be estimated for navigational purposes. Lumping the two biases into b creates no problem. The above set of equations will be used throughout this section as the set of equations to be solved.

The Newton-Raphson method proceeds from one estimate to the next according to

$$x_{n+1} = x_n + k_n$$

$$y_{n+1} = y_n + l_n$$

$$z_{n+1} = z_n + m_n$$

$$b_{n+1} = b_n + p_n$$

where

$x_i$, $y_i$, $z_i$ are the user's position estimate at the end of the $i^{th}$ iteration and $b_i$ is the estimate of the user bias at the $i^{th}$ iteration.

44

The increments $k_n$, $l_n$, $m_n$, and $p_n$ are the solutions to the following set of linear equations.

$$
\begin{bmatrix}
\nabla f_1^T (x_n, y_n, z_n, b_n) \\
\nabla f_2^T (x_n, y_n, z_n, b_n) \\
\nabla f_3^T (x_n, y_n, z_n, b_n) \\
\nabla f_4^T (x_n, y_n, z_n, b_n)
\end{bmatrix}
\begin{bmatrix}
k_n \\
l_n \\
m_n
\end{bmatrix}
+
$$

$$
\begin{bmatrix}
\dfrac{\partial}{\partial b} f_1 (x_n, y_n, z_n, b_n) \\
\dfrac{\partial}{\partial b} f_2 (x_n, y_n, z_n, b_n) \\
\dfrac{\partial}{\partial b} f_3 (x_n, y_n, z_n, b_n) \\
\dfrac{\partial}{\partial b} f_4 (x_n, y_n, z_n, b_n)
\end{bmatrix}
p_n
+
$$

$$
\begin{bmatrix}
f_1 (x_n, y_n, z_n, b_n) \\
f_2 (x_n, y_n, z_n, b_n) \\
f_3 (x_n, y_n, z_n, b_n) \\
f_4 (x_n, y_n, z_n, b_n)
\end{bmatrix}
= 0
$$

**where**

$\nabla$ denotes the gradient of the function evaluated at the point indicated by the argument.

These equations can be solved by a Gaussian elimination scheme. No matrix inversion is required. Other than add, subtract, multiply, and divide, the only computational operation required is a square root. In the GPS geometry, the Newton-Raphson method converges very well with large initial condition errors.

## 2.2.2 Non-linear Gauss-Seidel Iteration

The basic Gauss-Seidel iteration philosophy is easily applied to sets of non-linear equations. The simplicity of the iteration procedure makes this algorithm a candidate for use in the single-fix computation.

The Gauss-Seidel approach to sets of simultaneous non-linear equation is as follows:

Let $f_i(x_1, x_2, \ldots, x_n) = 0$   $i = \frac{1}{2}, 2, \ldots, n$ be a set of simultaneous non-linear equations. During the $k^{th}$ iteration, the update of $x_i$ comes from the $i^{th}$ equation by solving for $x_i$ in

$$f_i (x_1^{(k)}, x_2^{(k)}, \ldots, x_i^{(k)}, x_{i+1}^{(k-1)}, \ldots, x_n^{(k-1)}) = 0$$

where the superscript (j) denotes the value of the variable from the $j^{th}$ iteration.

For this problem, the iteration is obtained from the set of equations for the navigation problem (see Section 3.1). The $k^{th}$ iteration is given by:

$$x = x_{s1} \pm ((AT_1 - T_1 - b_{k-1})c)^2 - (y_{s1} - y_{k-1})^2 - (z_{s1} - z_{k-1})^2)^{1/2}$$

$$y_k = y_{s2} \pm ((AT_1 - T_1 - b_{k-1})c)^2 - (x_{s2} - x_k)^2 - (z_{s2} - z_{k-1})^2)^{1/2}$$

$$z_k = z_{s3} \pm ((AT_3 - T_3 - b_{k-1})c)^2 - (x_{s3} - x_k)^2 - (y_{s3} - y_k)^2)^{1/2}$$

$$b_k = AT_4 - T_4 - 1/c((x_{s4} - x_k)^2 + (y_{s4} - y_k)^2 + (z_{s4} - z_k)^2)^{1/2}$$

where $x_{si}$, $y_{si}$, and $z_{si}$ are the ECI coordinates of the $i^{th}$ satellite being used.

This technique is particularly simple since there are no simultaneous equations to solve. There is, however, some additional logic to resolve the sign in the first three equations.

### 2.2.3 Successive Linearizations of Measurement Matrix

This method is similar to the one in (18) except that the same data will be used in the iteration instead of new data points. Because of this, there will actually be two simultaneous iterations in progress. Some efficient means for calculating initial conditions for the iteration must be developed. The basic equations for this method are the linearized perturbed measurement equations, i.e.,

$$\Delta T_T^{(i)} = \frac{\partial f_i(\underline{X}, b)}{\partial x}\bigg|_{x=x_n} \Delta x$$

$$+ \frac{\partial f_i(\underline{X}, b)}{\partial y}\bigg|_{y=y_n} \Delta y + \frac{\partial f_i(\underline{X}, b)}{\partial z}\bigg|_{z=z_n} \Delta z$$

$$+ \frac{\partial f_i(\underline{X}, b)}{\partial b}\bigg|_{b=b_n} \Delta b \quad , \quad i = 1, 2, 3, 4$$

47

where $\Delta T_T^{(i)}$ refers to transit time of the satellite signal from satellite i. This can be expressed as

$$[\Delta T_T] = F(\underline{X}_n, b_n)[\Delta \underline{X}, \Delta b]^T$$

Then

$$[\Delta \underline{X}, \Delta b]^T = F^{-1}(\underline{X}_n, b_n)[\Delta T_T]$$

where $[\Delta \underline{X}, \Delta b]$ is the update vector.

Given the initial conditions of the iteration viz. $[\underline{X}_o, b_o]$ and $F^{-1}(\underline{X}_o, b_o)$ the iteration proceeds as follows.

1. Compute vector $[\Delta T_T]$ where

$$[\Delta T_T] = AT_i - T_i - [(1/c)\|\underline{S}_i - \underline{X}_n\|_n + b]$$

2. Compute F

3. Compute new $F^{-1}$

$$F_n^{-1} = F_{n-1}^{-1}(2I - F\,F_{n-1}^{-1}) \text{ where I is the identity}$$

4. Compute $[\Delta \underline{X}_n, b_n]$

$$[\Delta \underline{X}_n, \Delta b_n]^T = F_n^{-1}[\Delta T_T]$$

5. Compute $[\underline{X}_n, b_n]$

$$[\underline{X}_n, b_n] = [\underline{X}_{n-1}, b_{n-1}] + [\Delta \underline{X}_n, \Delta b_n]$$

6. Check convergence criteria and end iteration or go to 1.

48

## 2.3    Algorithm Analysis

Three areas of algorithm analysis are addressed in this section.
The first is the analysis of the two candidate alert algorithms.  The cri-
teria for selection of one algorithm over the other include lower average
GDOP, computational complexity, and length of time to do the computa-
tion.   The second area of analysis is the convergence of the numerical
techniques presented in Sections 2.2.1-2.2.3.  The analysis will attempt
to determine regions of convergence for each algorithm.  The third area
of analysis is the effect of noisy measurements on the single fix algorithms.
The possible effects are accuracy of the resulting fix and a possible change
in the convergence properties.  The analysis techniques are described in
this section with the results in Section 2.4.

### 2.3.1   Alert Algorithm Analysis

The relative measure of how accurately position may be deter-
mined using noisy measurements from different satellite constellations
is called GDOP (Geometric Dillution of Precision).  This measure is
a static quantity which is valid only for a single set of measurements.
It represents an error multiplication factor relating the uncertainty in
the measured TOA to the resulting least squares position determination.
A complete derivation of GDOP can be found in Reference (6).  The fol-
lowing formula for computing GDOP is derived in Reference (6).

$$\text{GDOP} = (\text{Trace } (F^T F)^{-1})^{1/2}$$

where

F is the matrix of partial derivatives  (see Section 2.2.3 above)
evaluated at the user's actual location.

49

The analysis of the alert algorithms uses the satellites in their nominal orbits.

To help determine which alert algorithm is to be used, an average GDOP value over a grid will be computed using each alert algorithm. The grid selected takes advantage of the symmetries of the problem, so that only one-sixth of the Earth is considered. The grid* is every $10^{\circ}$ in latitude from the equator to the North Pole, every $10^{\circ}$ in longitude for a total of $120^{\circ}$, and in time, every 15 minutes for one and a half hours. The average value will be computed for the GDE alert and the Max. Volume alert. The optimum achievable GDOP for a given constellation can be computed through an exhaustive search.

## 2.3.2 <u>Single Fix Convergence Analysis</u>

Each of the single-fix algorithm solution techniques has been programmed for checkout purposes. To check the convergence of the algorithms, several sets of initial conditions were used with varying error magnitudes. The convergence checks were also made over varying geometric conditions, i.e., different user locations and different times to include the changing satellite positions.

## 2.3.3 <u>Effects of Noisy Measurements</u>

Since the measurements obtained by any GPS receiver are noisy, that is the measured time is not an exact indication of the signal transit time, the single-fix algorithms should be checked for accuracy and convergence in the presence of noise. For the analysis of the single-fix algorithm, the measurement noise will be modelled as a Gaussian

---

*The grid consists of 654 points.

50

distributed random variable added to the simulated signal transit time. The noise can be assumed to be zero mean with variance specified by the phase III specification (6). The theoretical lower limit on the navigational error variance is the measurement noise variance times the GDOP factor squared. This limit will be reached if the numerical algorithms do not introduce errors which are comparable in magnitude to this basic limitation.

To investigate the effects of noisy measurements, a Monte Carlo type checkout will be done. The procedure will be to select a user location, then simulate the measureables. The simulated measurables are given by

$$T_i = \| \underline{S}_i - \underline{X} \| + b + w$$

where

$\underline{S}_i$ is the simulated actual location of the $i^{th}$ satellite

$\underline{X}$ is the simulated actual location of the user

b is the simulated actual bias

w is a random number which is Gaussian distributed with zero mean and variance equal to phase III specification for system error variance. w is generated by subroutine GAUSS.

At each user location, about a hundred fixes will be made with simulated measurables as above. The error will then be computed as:

$$\zeta_{RMS} = ( \frac{1}{N} \sum_{i=1}^{N} \| \underline{X} - \underline{X}_i \| )^{1/2}$$

51

where

N is the number of fixes using simulated noisy data

$\underline{X}$ is the simulated actual user location

$\underline{X}_i$ is the computed fix using the $i^{th}$ set of noise measurables

$\zeta_{RMS}$ is the root mean square error

The variance of the noise will also be increased to account for inaccuracies in the receiver measurement. Good single fix algorithms should not be sensitive to the magnitude of the noise as long as the magnitude is not unreasonable. Results of this analysis are in section 2.4.

## 2.4 Results of the Analyses

In this section, the numerical results of the analyses described in Sections 2.3.1-2.3.3. All of the computer programs to obtain the numerical results are given in Appendix 1 of Reference (16).

## 2.4.1 Alert Algorithm Results

The results of computing the average GDOP using each of the alert algorithms with a $5^{\circ}$ elevation horizon described in Section 2.1 is given in Table 2.4.1. The average was taken over the space-time grid described in Section 2.3.1.

Table 2.4.1 Alert Algorithm Comparison Results

| Algorithm | GDE Proposal Alg | Maximum Volume | Optimum Configuration |
|-----------|------------------|----------------|-----------------------|
| Average GDOP | 47.6* | 2.84 | 2.73 |
| Max Deviation | 3088* | 1.67 | ---- |

*Excluding singular points of algorithm

A more detailed look at the GDOP analysis is presented in the histograms of Figures 2.2 - 2.4. Using the grid described in Section 2.3.1, Figure 2.2 presents a histogram of the GDOP deviations of the GDE proposal alert algorithm constellation selection from the optimal constellation selected by exhaustive enumeration. Figure 2.3 does the same for the maximum volume algorithm. The distribution of the GDOP for the optimally selected constellations is presented in Figure 2.4. The histograms show that the GDE proposal algorithm selects poor constellations (i.e., GDOP deviation > 7) in what is felt to be an unacceptably large percentage of the cases. In addition, the GDE proposal algorithm produced some constellations for which GDOP did not exist, (i.e., GDOP = $\infty$). This situation may result since the satellites are in nominal orbits with perfect symmetry. Although in practice this condition probably would not arise, its possibility is a shortcoming of the algorithm.

To compare the computation time of the Maximum Volume algorithm with the optimum selection based on volume maximization, the number of volume computations should be noted. For the Maximum Volume algorithm the number is $3*(N - 4) + 1$ where N is the total number of visible satellites. For the optimum exhaustive enumeration, the number can be computed from the binomial coefficient. Table 2.4.2 compares the numbers for the minimum number of satellites visible, 6, the typical values, 8 and 9, and the maximum number 11. The amount of logic and hence the amount of computation per satellite set required for the two mechanizations is not significantly different.

53
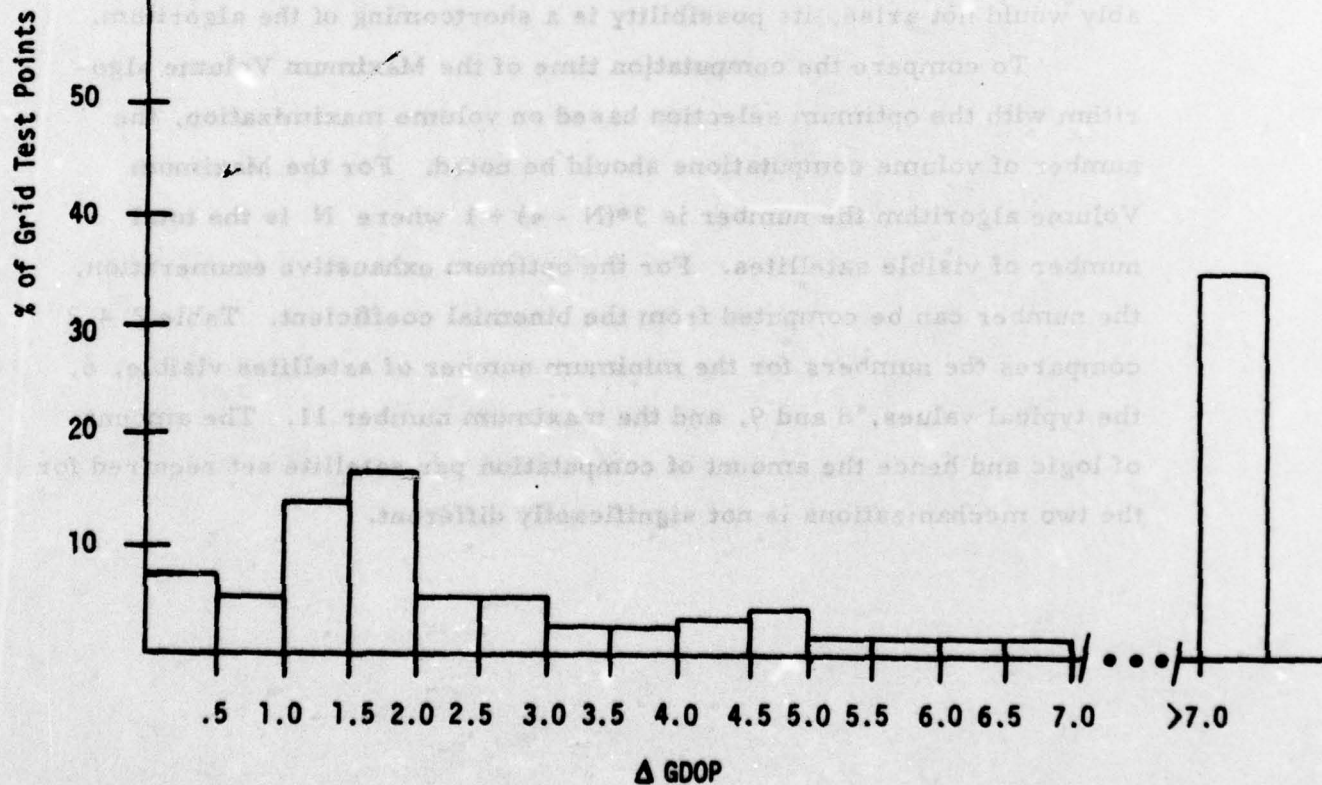
**Figure 2.2  Histogram of GDOP Deviations for GDE Proposal Algorithm.**

54
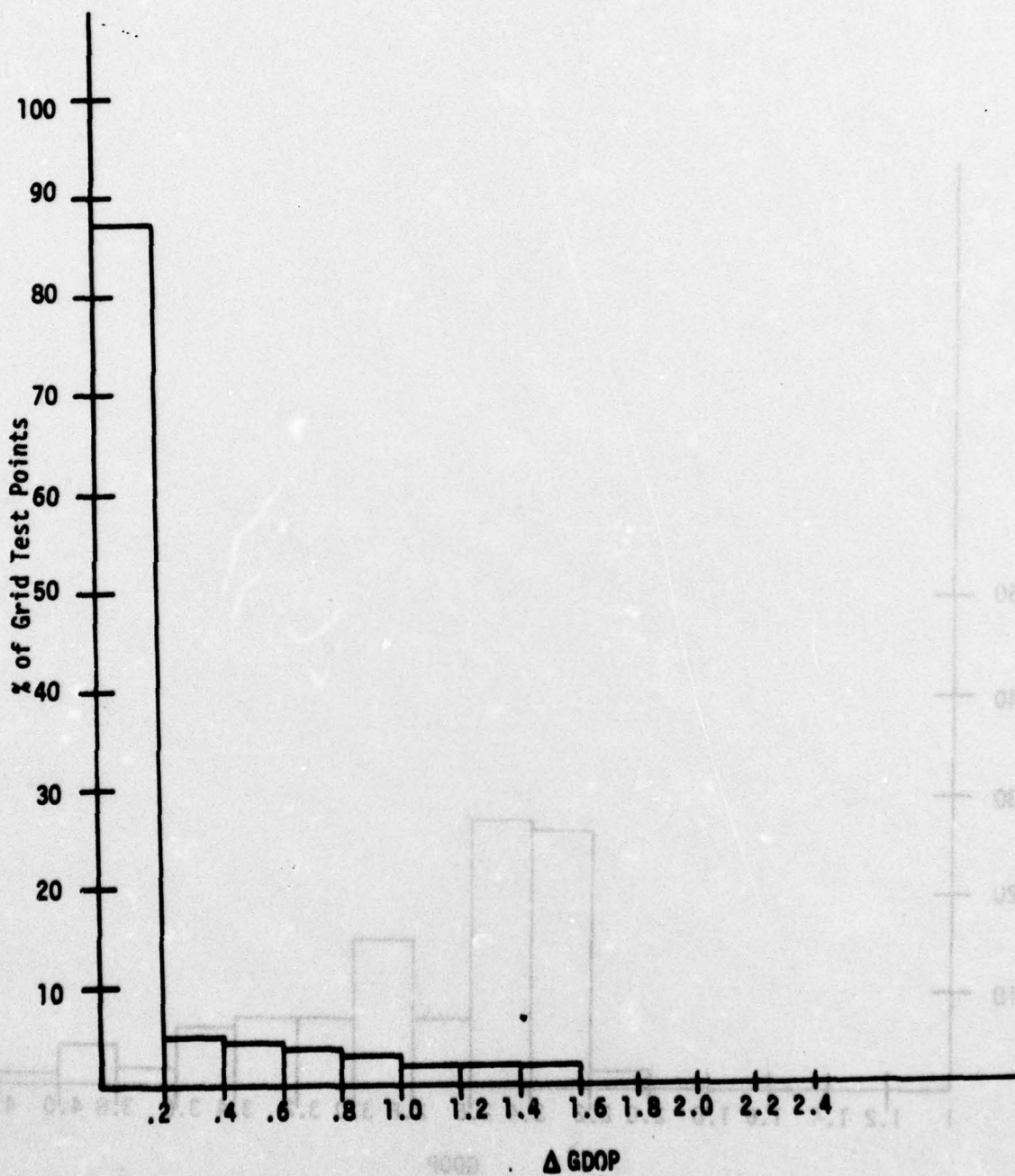
Figure 2.3   Histogram of GDOP Deviations for Maximum Volume Algorithm.
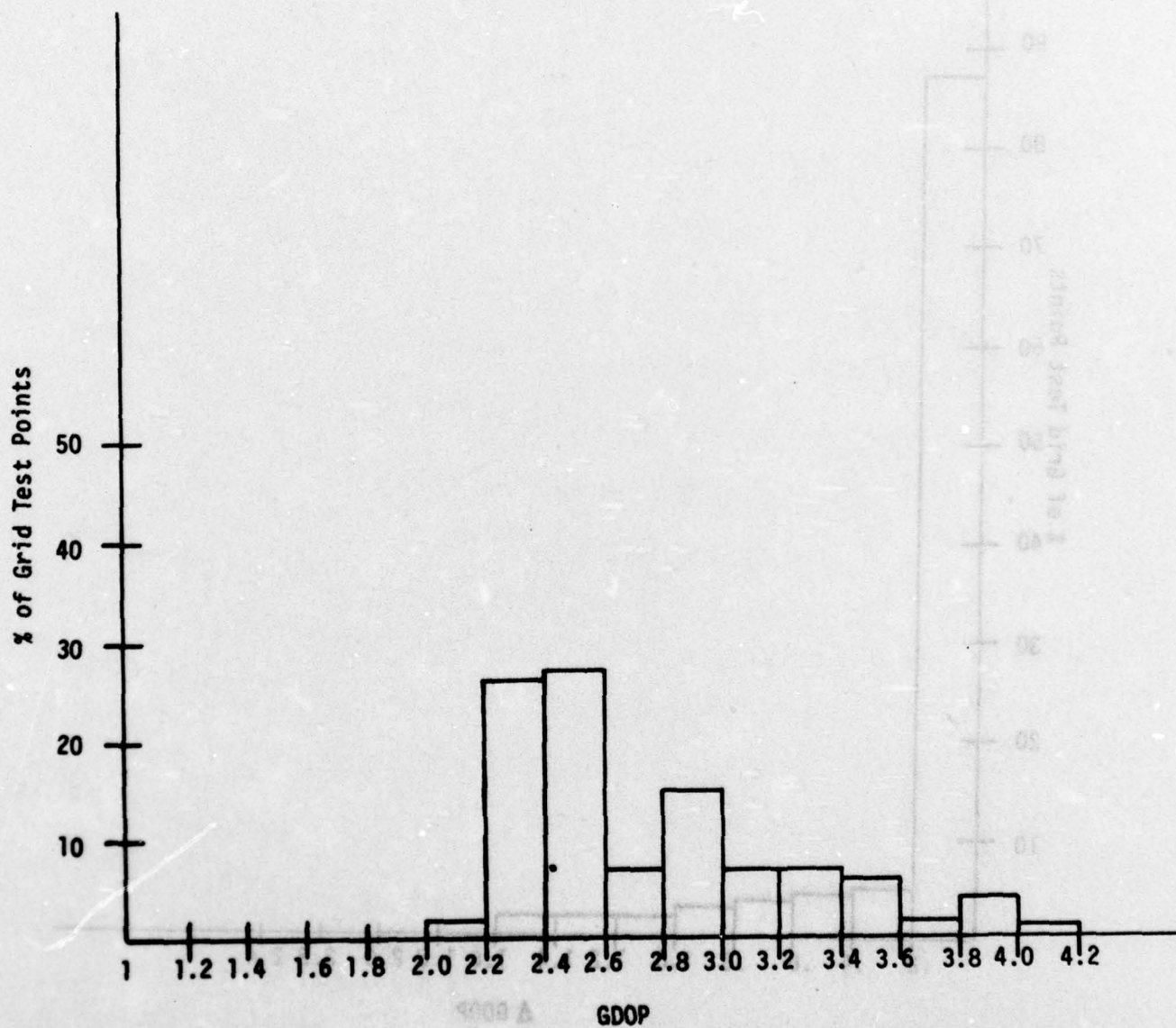
Figure 2.4   Histogram of Optimal GDOP Distribution.

**Table 2.4.2   Volume Computations Comparison**

| No. of Visible Satellites | Volume Computations Maximum Volume Algorithm | Volume Computations Optimum |
|:---:|:---:|:---:|
| 6 | 7 | 15 |
| 8 | 13 | 70 |
| 9 | 16 | 126 |
| 11 | 22 | 330 |

### 2.4.2   Convergence Analysis Results

The convergence of the three single fix algorithms was checked for several user locations and initial conditions.   Early in the analysis it was apparent that the non-linear Gauss-Seidel iteration was not well suited for the single fix algorithm.   The convergence was found to be very sensitive to initial conditions, so the method was not considered for further analyses.

The computer program written to run convergence test cases is called ITERTEST.   The program is documented in Appendix 1 of Reference (16).   This is the same program which will be used to study the effects of noisy measurements.   The convergence checks are made by setting the noise variance to zero and the number of iterations to one.

Table 2.4.3, Convergence Analysis Sample Results, contains some sample results.   The initial conditions for the iterations were chosen to correspond to an octant of uncertainty.   The center of the Earth was chosen in an attempt to arrive at a universally acceptable starting point.

57

Table 2.4.3   Convergence Analysis Sample Results.

| Run | User Location (Lat. Long.) | Iteration Initial Condition (in Lat. Long. or Center of Earth Indication) | Converged? | | | |
|---|---|---|---|---|---|---|
| | | | NR Iteration | | Meas. Matrix Iteration | |
| | | | Yes | No | Yes | No |
| 1 | 45°N 160°W | Center of Earth | | X | X | |
| 2 | 45°N 160°W | 0°N 180°W | | X | X | |
| 3 | 45°N 160°W | 90°N | X | | X | |
| 4 | 45°N 160°W | 0°N 90°W | | X | X | |
| 5 | 32°N 120°W | Center of Earth | X | | X | |
| 6 | 32°N 120°W | 90°N | X | | X | |
| 7 | 32°N 120°W | 0°N 120°W | | X | X | |
| 8 | 32°N 120°W | 0°N 90°W | X | | X | |
| 9 | 89°S 20°W | Center of Earth | X | | X | |
| 10 | 89°S 20°W | 90°S | X | | X | |
| 11 | 89°S 20°W | 0°N 0°W | X | | X | |
| 12 | 89°S 20°W | 0°N 90°W | | X | X | |

## 2.4.3  Noisy Measurement Analysis Results

The Newton-Raphson iteration and the successive linearization
iteration methods were analyzed with noisy inputs.  The analysis was
done with main program ITERTEST.  Results are presented in Table
2.4.4,  Measurement Noise Analysis Sample Runs.  Initial conditions
were chosen to correspond to cases where the iterations both converged.

If there is no error or negligible error introduced, the RMS
errors will be GDOP times the input noise sigma.  For the purpose of
this analysis, only one hundred iterations were done to save computer
costs.  The true error is within twenty-five percent of the indicated
error at a ninety percent confidence level when one hundred samples
are used.  ($\chi^2$ test)

Table 2.4.4  Measurement Noise Analysis Sample Runs
(100 Monte Carlo Solutions per Run)

| Input Noise Sigma (meters) | Constellation PDOP [6] | User Location (Lat. Long.) | Iteration Initial Condition (in Lat. Long. or Center of Earth Indication) | RMS Position Error (meters) | |
|---|---|---|---|---|---|
| | | | | NR Iteration | Meas. Matrix Iteration |
| 6 | 2.28 | 45°N 160°W | 90°N | 13.6 | 13.6 |
| 6 | 2.28 | 45°N 160°W* | 90°N | 12.4 | 12.4 |
| 6 | 3.78 | 32°N 120°W | 90°N | 24.2 | 24.2 |
| 6 | 3.78 | 32°N 97$\frac{1}{2}$°W | 90°N | 22.2 | 22.2 |
| 6 | 3.64 | 89°S 20°W | Earth Center | 19.5 | 19.5 |
| 60 | 3.64 | 89°S 20°W | Earth Center | 197 | 197 |
| 600 | 3.64 | 89°S 20°W | Earth Center | 2360 | 2360 |

## 2.5 Conclusions and Recommendations.

The following conclusions and recommendations have been drawn as a result of this portion of the study.

A.  The GDE proposal alert algorithm is not acceptable. It is recommended that an algorithm based on volume maximixation be used. Depending on how much time can be allocated to this task either the approximate or the exhaustive algorithm should be used.

B.  The convergence of the iterative algorithm is not affected by noisy inputs. Furthermore, they appear to converge with a close approximation to the accuracy of a least squares solution.

C.  If it is desirable to have a single-fix algorithm which converges from an initial condition of an octant of the Earth uncertainty, the successive linearizations of the measurement matrix method (sec. 2.2.3) should be used with initial conditions of the center of the Earth.

## Section 3. - FILTER DEVELOPMENT

### 3.0    Introduction

The purpose of this section is to present the results of the filter algorithm development task of the study. There were two objectives in this task. The first was to establish the optimum filter for the NAVSTAR/ GPS receiver based on the models in Section 1. The second objective was to outline the form of several candidate sub-optimum filters. The details of the sub-optimum filters are not established until the end of the covariance analysis section.

The optimum filter will include all of the significant error sources identified in the modeling section of this report. This will lead to a filter with a very large number of states, in fact too large to be considered for actual implementation in an operational receiver. The purpose of establishing this optimum filter is to set a bound on the obtainable accuracy. In addition, this optimum filter will become the reference system for use in the covariance analysis of the next section.

Several sub-optimum filters will be presented which vary greatly in both complexity and computational burden. Each of the filters is recursive in nature to take advantage of the large amount of data available. For the purpose of this section, only the form of the various filters can be considered. Determination of the state vectors can only be done through sensitivity analysis. Thus an evaluation of both accuracy and computational burden will be presented in a subsequent section.

The problem of actual operational mechanization for a given filter will not be discussed here. By this it is meant that for the purpose of this report, for example, no distinction will be made between a standard or square root formulation for the Kalman filter. No mention will be made of sequential vs. batch processing except in the cases where the nature of the filter demands one type or the other.

## 3.1 Optimum Filter/Reference System

This section will describe in detail the optimum filter. The description will include a summary of the Kalman filter equations and a complete description of the models used. The model description is a compendium of the models in Section 1. It serves a definite purpose of its own since this is the first time that all of the models are brought together and the interrelationships shown. For an understanding of the individual models, it is required to consult Section 1.

The filters to be described in this and following sections are based on linearized equations. The state equations for the filters can be expressed by linear relationships. The measurements are, however, highly nonlinear functions of both time and user location. Thus in order to apply the results from linear system theory to the estimation problem at hand, the measurement equations must be linearized about some point. In an actual operational system, this point can only be the current best estimate of the user location. The procedure for the filter implementation is as follows:

1) Using the current best estimate of the state (either from initial conditions or the value extrapolated from the previous estimate) and the nonlinear measurement equations, compute the expected values of the measureables.

$$\hat{\underline{z}}_k = \underline{h} \, (\varphi_{k, \, k-1} \hat{\underline{x}}_{k-1}, \, t)$$

2) Difference this expected measureable from the actual measured value. This resulting value is the measureable for the linearized (or error state) equation

$$\underline{\Delta z}_k = \underline{z}_k - \hat{\underline{z}}_k$$

62

3) Use the difference computed above as the measurement in the
linearized filter equations to estimate the error states, i. e. the
difference between the true value and the current estimate.

$$\hat{\underline{x}}_k = K_k \, \underline{\Delta z}_k$$

4) Add the estimated error states to the current estimate, $\hat{\underline{X}}_k^s$, to
produce a new best estimate. This is sometimes referred to as
resetting the state.

$$\hat{\underline{X}}_k^s = \varphi_{k, k-1} \, \hat{\underline{X}}_{k-1}^s + \hat{\underline{x}}_k$$

The linear systems descriptions which follow are the system
equations for the errors of the best estimate. This system is called
the error system.

### 3.1.1 Optimum Filter Equations [19]

The optimum filter equations are optimum in the sense that they
provide the minimum variance estimate for a linear system. The opti-
mum (or Kalman) filter equations can be written for either continuous or
discrete systems. The nature of the data from the NAVSTAR/GPS re-
ceiver dictates a discrete-time measurement and estimate update. On
the other hand, the system has a continuous time system description from
which a transition matrix may be computed. The system model will be
presented as a continuous system for purposes of exposition. The filter
equations will be presented in this and subsequent sections as discrete
time systems where the transition matrices are computed using the con-
tinuous time representation given.

The linearized differential equation for the reference system is

63

identical to the error system given by

$$\dot{\underline{x}} = F\underline{x} + G\underline{u} \qquad (3.1)$$

where

$\underline{x}$ is the error system state vector

$F$ is the reference system matrix

$G$ is the reference system input distribution

$\underline{u}$ is a vector of independent gaussian white noise

inputs each with unity PSD.

The vector $\underline{x}$ has dimension n and $\underline{u}$ has dimension m. The matrices $F$ and $G$ are dimensioned conformably. The linearized observation process is

$$\Delta \underline{z}_k = H_k \underline{x}_k + \underline{v}_k = \underline{z}_k - \hat{\underline{z}}_k \qquad (3.2)$$

where

$\hat{\underline{z}}_k$ is the vector of predicted observations

$\underline{z}_k$ is the vector of actual observations

$\Delta \underline{z}_k$ is the vector of observations for the error system

$H_k$ is the error system measurement matrix

$\underline{v}_k$ is a vector of independent gaussian white noise

measurement errors.

In addition $\underline{z}$ and $\underline{v}$ have dimension r with $H$ dimensioned conformably. The usual assumptions on the random processes are made and given by

$$E[\underline{u}(t)] = E[\underline{v}(t)] = 0$$

$$E[\underline{u}(t)\underline{u}^T(\tau)] = I\delta(t-\tau)$$

$$E[\underline{v}(t)\underline{v}^T(\tau)] = R(t)\delta(t-\tau) \qquad (3.3)$$

$$E[\underline{u}(t)\underline{v}^T(\tau)] = 0$$

64

$$E[\underline{x}(t_0)\underline{u}^T(t)] = E[\underline{x}(t_0)\underline{v}^T(t)] = 0 \qquad t \geq t_0$$

$$E[\underline{x}(t_0)\underline{x}^T(t_0)] = P(t_0) \geq 0.$$

The state transition matrix $\varphi$ for the constant coefficient reference system of Eq. (1) is defined by

$$\dot{\phi}(t) = F\varphi(t) \tag{3.4}$$

or solving for the time invariant case

$$\varphi(t) = \exp(Ft) \tag{3.5}$$

With these definitions, the Kalman filter equations for the minimum variance estimate $\hat{\underline{x}}$ of the error system state vector $\underline{x}$ at the $k^{th}$ measurement time are

$$\hat{\underline{x}}_k = K_k \underline{\Delta z}_k = K_k(\underline{z}_k - \hat{\underline{z}}_k) \tag{3.6a}$$

and

$$P'_k = \varphi_{k,k-1} P_{k-1} \varphi^T_{k,k-1} + Q_k \tag{3.6b}$$

$$K_k = P'_k H^T_k [H_k P'_k H^T_k + R_k]^{-1} \tag{3.6c}$$

$$P_k = [I - K_k H_k] P'_k [- K_k H_k]^T + K_k R_k K^T_k \tag{3.6d}$$

$$Q_k = \int_0^{\Delta t} \varphi(\Delta t - \tau) G G^T \varphi^T (\Delta t - \tau) d\tau \tag{3.6e}$$

where $\Delta t$ is the time between measurements $k$ and $k - 1$.

### 3.1.2 Reference System Model

At this point of the report, the complete state vector and measurement equations are defined only for the optimum filter/reference system.

The description to be presented here will clarify the relationships of the various models presented in Section 1.

Table 3.1 contains the reference system states used in the optimum filter. Only four satellites are contained in the state vector at any point in time. This has been done to reduce computer costs. The four satellites contained in the state vector are those which are currently being tracked by the receiver. As the set of satellite changes, appropriate changes must be made to the reference system/optimum filter covariance matrix. This is analytically justified since covariance values associated with un-tracked satellites do not affect other system states either in the time propagation or in the update. The only case where a problem would arise is if a satellite which is being tracked is replaced for a short time and then reacquired. Should this situation arise, the state vector size will have to be increased unless it is determined that ignoring the correlation introduces negligible error.

The reference system F matrix and G matrix [see Eq. (3.1)] are a sparse matrices. Because of this, displaying only the non-zero elements is more enlightening. The non-zero elements of F are given in Table 3.2. In Table 3.2, the parameters in the value column are taken from Section 1. The values are listed below for the typical models given in Section 1. The values in Table 3.2, are parameterized for ease in changing when new information is available. The definitions and values are as follows:

$$\alpha = (\omega_2/\omega_1)^{1/6}$$

$$\omega_a = \omega_1(\alpha)^{1/2}$$

$$\beta = \alpha^3 \cdot 10^{+M/20}$$

$$M = \text{gain at } \omega_2 \text{ in dB (for crystal clocks} \approx -220 \text{ [24])}$$

66

## Table 3.1

### Reference System State Vector

| No. | Symbol | Definition |
|---|---|---|
| 1 | $\Delta x$ | position error component x in ECI |
| 2 | $\Delta y$ | position error component y in ECI |
| 3 | $\Delta z$ | position error component z in ECI |
| 4 | $\Delta \dot{x}$ | velocity error component x in ECI |
| 5 | $\Delta \dot{y}$ | velocity error component y in ECI |
| 6 | $\Delta \dot{z}$ | velocity error component z in ECI |
| 7 | $\Delta \ddot{x}$ | acceleration error component x in ECI |
| 8 | $\Delta \ddot{y}$ | acceleration error component y in ECI |
| 9 | $\Delta \ddot{z}$ | acceleration error component z in ECI |
| 10 | $C_1$ | |
| 11 | $C_2$ | |
| 12 | $C_3$ | Noise model for user clock |
| 13 | $C_4$ | |
| 14 | $C_5$ | frequency offset for user clock |
| 15 | $C_6$ | aging coefficient for user clock time error |
| 16 | $C_7$ | Time error |
| 17 | $\tau_{T_1}$ | Tropospheric delay uncertainty |
| 18 | $\Delta s_x^1$ | position error component x in ECI of tracked satellite 1 |
| 19 | $\Delta s_y^1$ | position error component ? in ECI of tracked satellite 1 |
| 20 | $\Delta s_z^1$ | position error component z in ECI of tracked satellite 1 |
| 21 | $\tau_{s_1}^1$ | Time error of tracked satellite 1 |
| 22 | $\tau_{s_2}^1$ | Time rate error of tracked satellite 1 |
| 23 | $\tau_i^1$ | Ionospheric residual error along LOS to satellite 1 |
| 24-29 | | same as 18-23 for tracked satellite 2 |
| 30-35 | | same as 18-23 for tracked satellite 3 |
| 36-41 | | same as 18-23 for tracked satellite 4 |
| 42 | $X_{EM1}$ | EM-log random walk error |
| 43 | $X_{EM2}$ | EM-log G-Markov error |

67

## Table 3. 1 (cont'd)

### Reference System State Vector

| No. | Symbol | Definition |
|-----|--------|------------|
| 44 | $X_{GC_1}$ | GC random walk error |
| 45 | $X_{GC_2}$ | GC G-Markov Error |
| 46 | $x_{O1}^1$ | OMEGA bias for received station 1 |
| 47 | $x_{O2}^1$ | OMEGA G-Markov error for received station 1 |
| 48 | $x_{O3}^1$ | } OMEGA periodic error for received station 1 |
| 49 | $x_{O4}^1$ | |
| 50-53 | | same as 46-49 for received OMEGA 2 |
| 54-57 | | same as 46-49 for received OMEGA 3 |
| 58-61 | | same as 46-49 for received OMEGA 4 |

68

## Table 3.2
### Reference System  F-matrix

| Row | Col | Value[*] | Units |
|-----|-----|----------|-------|
| 1 | 4 | 1. | |
| 2 | 5 | 1. | |
| 3 | 6 | 1. | |
| 4 | 7 | 1. | |
| 5 | 8 | 1. | |
| 6 | 9 | 1. | |
| 10 | 10 | $-\omega_a$ | $sec^{-1}$ |
| 11 | 10 | $\alpha(\alpha - 1)\omega_a$ | $sec^{-1}$ |
| 11 | 11 | $-\alpha^2 \omega_a$ | $sec^{-1}$ |
| 12 | 10 | $\alpha^2(\alpha - 1)\omega_a$ | $sec^{-1}$ |
| 12 | 11 | $\alpha^3(\alpha - 1)\omega_a$ | $sec^{-1}$ |
| 12 | 12 | $-\alpha^4 \omega_a$ | $sec^{-1}$ |
| 13 | 10 | $(\omega_1 - \omega_0)/\alpha^3$ | $sec^{-1}$ |
| 13 | 11 | $(\omega_1 - \omega_0)/\alpha^2$ | $sec^{-1}$ |
| 13 | 12 | $(\omega_1 - \omega_0)/\alpha$ | $sec^{-1}$ |
| 13 | 13 | $-\omega_0$ | $sec^{-1}$ |
| 14 | 15 | 1. | |
| 16 | 10 | $\beta/\alpha^3$ | |
| 16 | 11 | $\beta/\alpha^2$ | |
| 16 | 12 | $\beta/\alpha$ | |
| .16 | 13 | $\beta$ | |
| 16 | 14 | 1. | |
| 21 | 22 | 1. | |
| 23 | 23 | $-1./\tau_i$ | $sec^{-1}$ |
| 27 | 28 | 1. | |
| 29 | 29 | $-1./\tau_i$ | $sec^{-1}$ |
| 33 | 34 | 1. | |

[*]See text for variable definitions.

## Table 3.2 (cont'd)

## Reference System F-matrix

| Row | Col | Value[*] | Units |
|---|---|---|---|
| 35 | 35 | $-1./\tau_i$ | $sec^{-1}$ |
| 39 | 40 | $1.$ | |
| 41 | 41 | $-1./\tau_i$ | $sec^{-1}$ |
| 43 | 43 | $-1./\tau_{EM}$ | $sec^{-1}$ |
| 45 | 45 | $-1./\tau_{GC}$ | $sec^{-1}$ |
| 47 | 47 | $-1./\tau_{OM}$ | $sec^{-1}$ |
| 48 | 49 | $1.$ | |
| 49 | 48 | $-\omega_{OM}^2$ | $sec^{-2}$ |
| 51 | 51 | $-1./\tau_{OM}$ | $sec^{-1}$ |
| 52 | 52 | $1.$ | |
| 53 | 52 | $-\omega_{OM}^2$ | $sec^{-2}$ |
| 55 | 55 | $-1./\tau_{OM}$ | $sec^{-1}$ |
| 56 | 57 | $1.$ | |
| 57 | 56 | $-\omega_{OM}^2$ | $sec^{-2}$ |
| 59 | 59 | $-1./\tau_{OM}$ | $sec^{-1}$ |
| 60 | 61 | $1.$ | |
| 61 | 60 | $-\omega_{OM}^2$ | $sec^{-2}$ |

[*]See text for variable definitions.

$$\omega_0 = \sqrt{3}/\tau_3$$

$$\omega_1 = 6 \ln 2/(\pi \cdot \tau_2)$$

$$\omega_2 = \pi/(2 \tau_1 \ln 2)$$

$\tau_1, \tau_2, \tau_3$ are breakpoints of the Allan variance curve

$\tau_1 = .5$ sec (typical crystal clock [24])

$\tau_2 = 80$ sec (typical crystal clock [24])

$\tau_3 = 50000$ sec (typical crystal clock [24])

$\tau_i = 1.17$ hr.

$\tau_{EM} = .15$ hr.

$\tau_{GC} = 23$ min.

$\tau_{OM} = 1$ hr.

$\omega_{OM} = (2\pi/12)$ hr$^{-1}$

In the reference system state vector, states 42 through 61 will be used only when the Gyrocompass, EM-log, and OMEGA are being measured. In the bulk of the NAVSTAR/GPS analysis, only the first forty-one states will be propagated. This again is done to conserve computer costs.

To complete specification of equation (3.1), the matrix G must be defined. However, certain of the models are specified only in terms

71

of covariance propagation. For these models it is easier to define the product $G G^T$. The non-zero elements of $G G^T$ are listed in Table 3.3. To get a particular formulation of Eq. (3.1), any of the non-unique square roots of $G G^T$ may be used. The easiest determined square root is probably the one obtained using a Cholesky decomposition [20]. Some of the values in Table 3.4 are in terms of parameters. Some of them are defined above, the remainder are as follows:

$\sigma_{posi}$, $\sigma_{veli}$, $\sigma_{acci}$  $i = x, y, z$  are PSD values for random
walk models

$\sigma_{CLK}$ is the PSD for the satellite clock fractional frequency
error $\approx 10^{-11}$

$\sigma_{ri}$  $i = 1, 2, 3, 4$  is the prediction residual for the ionospheric
error

$$\sigma_{Ri} = \sigma \csc [ \sqrt{E_i^2 + (18^o)^2} ]$$

$E_i$ is the elevation angle to the $i^{th}$ satellite
$\sigma$ is the RMS correction error ($\approx 8 - 17$ ft)[23]

$R_i$  $i = 1, 2, 3, 4$  ionospheric pierce points of $i^{th}$ line of
sight vector

$D$ ionospheric distance constant $\approx 2500$ km

The model for the correlated ionospheric error is discussed more fully in Appendix

The final specification of the reference system is the measurement equation. This equation relates the state vector elements to the measured quantities or measurables. In terms of the state vector of

72

## Table 3.3
## Reference System $G\,G^T$
### (Upper Triangle of Symmetric Matrix)

| Row | Col | Value* | Units |
|-----|-----|--------|-------|
| 1 | 1 | $\sigma^2_{pos\,x}$ | $meter^2/sec$ |
| 2 | 2 | $\sigma^2_{pos\,y}$ | $meter^2/sec$ |
| 3 | 3 | $\sigma^2_{pos\,z}$ | $meter^2/sec$ |
| 4 | 4 | $\sigma^2_{vel\,x}$ | $meter^2/sec^3$ |
| 5 | 5 | $\sigma^2_{vel\,y}$ | $meter^2/sec^3$ |
| 6 | 6 | $\sigma^2_{vel\,z}$ | $meter^2/sec^3$ |
| 7 | 7 | $\sigma^2_{acc\,x}$ | $meter^2/sec^5$ |
| 8 | 8 | $\sigma^2_{acc\,y}$ | $meter^2/sec^5$ |
| 9 | 9 | $\sigma^2_{acc\,z}$ | $meter^2/sec^5$ |
| 10 | 10 | $\omega_a^2(\alpha - 1)^2$ | $sec^{-2}$ |
| 10 | 11 | $\omega_a^2\alpha(\alpha - 1)^2$ | $sec^{-2}$ |
| 10 | 12 | $\omega_a^2\alpha^2(\alpha - 1)^2$ | $sec^{-2}$ |
| 10 | 13 | $(\alpha - 1)\omega_a(\omega_1 - \omega_0)/\alpha^3$ | $sec^{-2}$ |
| 10 | 16 | $(\alpha - 1)\omega_a\beta/\alpha^3$ | $sec^{-1}$ |
| 11 | 11 | $\omega_a^2\alpha^2(\alpha - 1)^2$ | $sec^{-2}$ |
| 11 | 12 | $\omega_a^2\alpha^3(\alpha - 1)^2$ | $sec^{-2}$ |
| 11 | 13 | $\omega_a(\alpha - 1)(\omega_1 - \omega_0)/\alpha^2$ | $sec^{-2}$ |
| 11 | 16 | $\omega_a(\alpha - 1)\beta/\alpha^2$ | $sec^{-1}$ |
| 12 | 12 | $\omega_a^2(\alpha - 1)^2\alpha^4$ | $sec^{-2}$ |

*See text for variable definitions.

73

Table 3.3 (cont'd)

## Reference System $G\,G^T$
### (Upper Triangle of Symmetric Matrix)

| Row | Col | Value* | Units |
|-----|-----|--------|-------|
| 12 | 13 | $\omega_a(\alpha - 1)(\omega_1 - \omega_0)/\alpha$ | $\text{sec}^{-2}$ |
| 12 | 16 | $\omega_a(\alpha - 1)\beta/\alpha$ | $\text{sec}^{-1}$ |
| 13 | 13 | $(\omega_1 - \omega_0)^2/\alpha^6$ | $\text{sec}^{-2}$ |
| 13 | 16 | $(\omega_1 - \omega_0)\beta/\alpha^6$ | $\text{sec}^{-1}$ |
| 16 | 16 | $\beta^2/\alpha^6$ | |
| 21 | 21 | $\sigma_{CLK}^2$ | $\text{sec}^2/\text{sec}$ |
| 23 | 23 | $\sigma_{R1}^2 \cdot 2/\tau_i$ | $\text{sec}^2/\text{sec}$ |
| 23 | 29 | $\sigma_{R1}\sigma_{R2} \cdot 2 \cdot \exp(-|R_1 - R_2|/D)/\tau_i$ | $\text{sec}^2/\text{sec}$ |
| 23 | 35 | $\sigma_{R1}\sigma_{R3} \cdot 2 \cdot \exp(-|R_1 - R_3|/D)/\tau_i$ | $\text{sec}^2/\text{sec}$ |
| 23 | 41 | $\sigma_{R1}\sigma_{R4} \cdot 2 \cdot \exp(-|R_1 - R_4|/D)/\tau_i$ | $\text{sec}^2/\text{sec}$ |
| 27 | 27 | $\sigma_{CLK}^2$ | $\text{sec}^2/\text{sec}$ |
| 29 | 29 | $\sigma_{R2}^2 \cdot 2/\tau_i$ | $\text{sec}^2/\text{sec}$ |
| 29 | 35 | $\sigma_{R2}\sigma_{R3} \cdot 2 \cdot \exp(-|R_2 - R_3|/D)/\tau_i$ | $\text{sec}^2/\text{sec}$ |
| 29 | 41 | $\sigma_{R2}\sigma_{R4} \cdot 2 \cdot \exp(-|R_2 - R_4|/D)/\tau_i$ | $\text{sec}^2/\text{sec}$ |
| 33 | 33 | $\sigma_{CLK}^2$ | $\text{sec}^2/\text{sec}$ |
| 35 | 35 | $\sigma_{R3}^2 \cdot 2/\tau_i$ | $\text{sec}^2/\text{sec}$ |
| 35 | 41 | $\sigma_{R3}\sigma_{R4} \cdot 2 \cdot \exp(-|R_3 - R_4|/D)/\tau_i$ | $\text{sec}^2/\text{sec}$ |
| 39 | 39 | $\sigma_{CLK}^2$ | $\text{sec}^2/\text{sec}$ |
| 41 | 41 | $\sigma_{R4}^2 \cdot 2/\tau_i$ | $\text{sec}^2/\text{sec}$ |
| 42 | 42 | .03722 | $\text{fps}^2/\text{sec}$ |

*See text for variable definitions.

## Table 3.3 (cont'd)
## Reference System $G\,G^T$
### (Upper Triangle of Symmetric Matrix)

| Row | Col | Value[*] | Units |
|-----|-----|----------|-------|
| 43 | 43 | $6.6 \times 10^{-4}$ | $fps^2/sec$ |
| 44 | 44 | $.282 \times 10^{-5}$ | $deg^2/sec$ |
| 45 | 45 | $1.775 \times 10^{-4}$ | $deg^2/sec$ |
| 47 | 47 | .00277 | $centicycle^2/sec$ |
| 51 | 51 | .00277 | $centicycle^2/sec$ |
| 55 | 55 | .00277 | $centicycle^2/sec$ |
| 59 | 59 | .00277 | $centicycle^2/sec$ |

[*]See text for variable definitions.

error states as presented here, the measured quantity is the difference between the actual measured quantity and the expected measurable based on current estimates. This means that the measurement equation can be linearized about the current estimate. The non-zero elements of the measurement matrix H are presented in Table 3.4. The measurement matrix elements described there are for the most general case being considered where there are thirteen measured quantities. Rows 1-4 are concerned with time-of-arrival measurements, rows 5-8 are concerned with doppler measurements, row 9 is concerned with EM-log measurements, row 10 is concerned with gyrocompass measurements, rows 11-13 are concerned with OMEGA station pair measurements. Any subset of these measurements may be used in a specific scenario. For most cases only the first four or eight measurables will be considered. A more detailed explanation of the measurement equations follows the symbol defintions.

The measurement matrix is a truly time varying matrix which is also dependent on the scenario. For this reason most of the elements are defined in terms of variables. The following are the definitions of the variables from Table 3. 4 and the equations following the definitions.

$$u_x^i, u_y^i, u_z^i \quad i = 1, 2, 3, 4 \quad \text{are the x, y, and z components}$$
of the unit vector from the user to the $i^{th}$ tracked satellite

$$k_j^i = \left( \frac{v_j^i}{\rho^i} + \frac{u_j^i}{\rho^i} \dot{\rho}^i \right) \left( \frac{-\omega_T dt}{c} \right) \quad i = 1, 2, 3, 4 \quad j = x, y, z$$

$\rho^i$ = distance from user to the $i^{th}$ tracked satellite

$v_j^i$ = $j^{th}$ component of the relative velocity of the user with respect to the $i^{th}$ tracked satellite

76

## Table 3.4
### Reference System Measurement Matrix

| Row | Col | Value* | Units |
|-----|-----|--------|-------|
| 1 | 1 | $u_x^1(\frac{1}{c})$ | sec/meter |
| 1 | 2 | $u_y^1(\frac{1}{c})$ | sec/meter |
| 1 | 3 | $u_z^1(\frac{1}{c})$ | sec/meter |
| 1 | 16 | 1. | |
| 1 | 17 | 1. | |
| 1 | 18 | $u_x^1(\frac{1}{c})$ | sec/meter |
| 1 | 19 | $u_y^1(\frac{1}{c})$ | sec/meter |
| 1 | 20 | $u_z^1(\frac{1}{c})$ | sec/meter |
| 1 | 21 | 1. | |
| 1 | 23 | 1. | |
| 2 | 1 | $u_x^2(\frac{1}{c})$ | sec/meter |
| 2 | 2 | $u_y^2(\frac{1}{c})$ | sec/meter |
| 2 | 3 | $u_z^2(\frac{1}{c})$ | sec/meter |
| 2 | 16 | 1. | |

*See text for variable definitions.

77

## Table 3.4 (cont'd)
### Reference System Measurement Matrix

| Row | Col | Value[*] | Units |
|---|---|---|---|
| 2 | 17 | $1.$ | |
| 2 | 24 | $u_x^2(\frac{1}{c})$ | sec/meter |
| 2 | 25 | $u_y^2(\frac{1}{c})$ | sec/meter |
| 2 | 26 | $u_z^2(\frac{1}{c})$ | sec/meter |
| 2 | 27 | $1.$ | |
| 2 | 29 | $1.$ | |
| 3 | 1 | $u_x^3(\frac{1}{c})$ | sec/meter |
| 3 | 2 | $u_y^3(\frac{1}{c})$ | sec/meter |
| 3 | 3 | $u_z^3(\frac{1}{c})$ | sec/meter |
| 3 | 16 | $1.$ | |
| 3 | 17 | $1.$ | |
| 3 | 30 | $u_x^3(\frac{1}{c})$ | sec/meter |
| 3 | 31 | $u_y^3(\frac{1}{c})$ | sec/meter |
| 3 | 32 | $u_z^3(\frac{1}{c})$ | sec/meter |

[*]See text for variable definitions.

## Table 3. 4 (cont'd)
## Reference System Measurement Matrix

| Row | Col | Value* | Units |
|-----|-----|--------|-------|
| 3 | 33 | $1.$ | |
| 3 | 35 | $1.$ | |
| 4 | 1 | $u_x^4 \left(\dfrac{1}{c}\right)$ | sec/meter |
| 4 | 2 | $u_y^4 \left(\dfrac{1}{c}\right)$ | sec/meter |
| 4 | 3 | $u_z^4 \left(\dfrac{1}{c}\right)$ | sec/meter |
| 4 | 16 | $1.$ | |
| 4 | 17 | $1.$ | |
| 4 | 36 | $u_x^4 \left(\dfrac{1}{c}\right)$ | sec/meter |
| 4 | 37 | $u_y^4 \left(\dfrac{1}{c}\right)$ | sec/meter |
| 4 | 38 | $u_z^4 \left(\dfrac{1}{c}\right)$ | sec/meter |
| 4 | 39 | $1.$ | |
| 4 | 41 | $1.$ | |
| 5 | 1 | $k_x^1$ | counts/meter |
| 5 | 2 | $k_y^1$ | counts/meter |

*See text for variable definitions.

## Table 3.4 (cont'd)
## Reference System Measurement Matrix

| Row | Col | Value[*] | Units |
|-----|-----|----------|-------|
| 5 | 3 | $k_z^1$ | counts/meter |
| 5 | 4 | $u_x^1 \cdot \omega_T dt(\frac{1}{c})$ | counts/(meter/sec) |
| 5 | 5 | $u_y^1 \cdot \omega_T dt(\frac{1}{c})$ | counts/(meter/sec) |
| 5 | 6 | $u_z^1 \cdot \omega_T dt(\frac{1}{c})$ | counts/(meter/sec) |
| 5 | 10 | $dt\,\omega_T\,\beta/\alpha^3$ | counts/sec |
| 5 | 11 | $dt\,\omega_T\,\beta/\alpha^2$ | counts/sec |
| 5 | 12 | $dt\,\omega_T\,\beta/\alpha$ | counts/sec |
| 5 | 13 | $dt\,\omega_T\,\beta$ | counts/sec |
| 5 | 14 | $dt\,\omega_T$ | counts/sec |
| 5 | 22 | $-dt\,\omega_T$ | counts/sec |
| 6 | 1 | $k_x^2$ | counts/meter |
| 6 | 2 | $k_y^2$ | counts/meter |
| 6 | 3 | $k_z^2$ | counts/meter |

[*]See text for variable definitions.

80

## Table 3. 4 (cont'd)

### Reference System Measurement Matrix

| Row | Col | Value[*] | Units |
|-----|-----|----------|-------|
| 6 | 4 | $u_x^2 \cdot \omega dt \left(\frac{1}{c}\right)$ | counts/(meter/sec) |
| 6 | 5 | $u_y^2 \cdot \omega dt \left(\frac{1}{c}\right)$ | counts/(meter/sec) |
| 6 | 6 | $u_z^2 \cdot \omega dt \left(\frac{1}{c}\right)$ | counts/(meter/sec) |
| 6 | 10 | $dt\, \omega_T \beta /\alpha^3$ | counts/sec |
| 6 | 11 | $dt\, \omega_T \beta /\alpha^2$ | counts/sec |
| 6 | 12 | $dt\, \omega_T \beta /\alpha$ | counts/sec |
| 6 | 13 | $dt\, \omega_T \beta$ | counts/sec |
| 6 | 14 | $dt\, \omega_T$ | counts/sec |
| 6 | 28 | $-dt\, \omega_T$ | counts/sec |
| 7 | 1 | $k_x^3$ | counts/meter |
| 7 | 2 | $k_y^3$ | counts/meter |
| 7 | 3 | $k_z^3$ | counts/meter |
| 7 | 4 | $u_x^3 \cdot \omega_T\, dt \left(\frac{1}{c}\right)$ | counts/(meter/sec) |
| 7 | 5 | $u_y^3 \cdot \omega_T\, dt \left(\frac{1}{c}\right)$ | counts/(meter/sec) |

[*]See text for variable definition.

81

Table 3. 4 (cont'd)

## Reference System Measurement Matrix

| Row | Col | Value* | Units |
|-----|-----|--------|-------|
| 7 | 6 | $u_z^3 \cdot \omega_T \, dt \, (\frac{1}{c})$ | counts/sec |
| 7 | 10 | $dt \, \omega_T \beta / \alpha^3$ | counts/sec |
| 7 | 11 | $dt \, \omega_T \beta / \alpha^2$ | counts/sec |
| 7 | 12 | $dt \, \omega_T \beta / \alpha$ | counts/sec |
| 7 | 13 | $dt \, \omega_T \beta$ | counts/sec |
| 7 | 14 | $dt \, \omega_T$ | counts/sec |
| 7 | 34 | $-dt \, \omega_T$ | counts/sec |
| 8 | 1 | $k_x^4$ | counts/meter |
| 8 | 2 | $k_y^4$ | counts/meter |
| 8 | 3 | $k_z^4$ | counts/meter |
| 8 | 4 | $u_x^4 \cdot \omega_T \, dt \, (\frac{1}{c})$ | counts/(meter/sec) |
| 8 | 5 | $u_x^4 \cdot \omega_T \, dt \, (\frac{1}{c})$ | counts/(meter/sec) |
| 8 | 6 | $u_z^4 \cdot \omega_T \, dt \, (\frac{1}{c})$ | counts/(meter/sec) |
| 8 | 10 | $dt \, \omega_T \, \beta / \alpha^3$ | counts/sec |

*See text for variable definition.

82

## Table 3.4 (cont'd)
### Reference System Measurement Matrix

| Row | Col | Value[*] | Units |
|-----|-----|---------|-------|
| 8 | 11 | $dt\ \omega_T\beta/\alpha^2$ | counts/sec |
| 8 | 12 | $dt\ \omega_T\beta/\alpha$ | counts/sec |
| 8 | 13 | $dt\ \omega_T\beta$ | counts/sec |
| 8 | 14 | $dt\ \omega_T$ | counts/sec |
| 8 | 40 | $-dt\ \omega_T$ | counts/sec |
| 9 | 4 | $H_x$ | |
| 9 | 5 | $H_y$ | |
| 9 | 6 | $H_z$ | |
| 9 | 42 | 1. | |
| 9 | 43 | 1. | |
| 10 | 4 | $H_x^+/|v|$ | sec/meter |
| 10 | 5 | $H_y^+/|v|$ | sec/meter |
| 10 | 6 | $H_z^+/|v|$ | sec/meter |
| 10 | 44 | 1. | |

[*]See text for variable definition.

83

## Table 3. 4 (cont'd)

### Reference System Measurement Matrix

| Row | Col | Value[*] | Units |
|---|---|---|---|
| 10 | 45 | 1. | |
| 11 | 1 | $g_{11}$ | meter$^{-1}$ |
| 11 | 2 | $g_{12}$ | meter$^{-1}$ |
| 11 | 3 | $g_{13}$ | meter$^{-1}$ |
| 11 | 46 | 1. | |
| 11 | 47 | 1. | |
| 11 | 48 | 1. | |
| 11 | 50 | -1. | |
| 11 | 51 | -1. | |
| 11 | 52 | -1. | |
| 12 | 1 | $g_{21}$ | meter$^{-1}$ |
| 12 | 2 | $g_{22}$ | meter$^{-1}$ |
| 12 | 3 | $g_{23}$ | meter$^{-1}$ |
| 12 | 46 | 1. | |

[*]See text for variable definition.

**Table 3. 4 (cont'd)**
**Reference System Measurement Matrix**

| Row | Col | Value* | Units |
|-----|-----|--------|-------|
| 12 | 47 | 1. | |
| 12 | 48 | 1. | |
| 12 | 54 | -1. | |
| 12 | 55 | -1. | |
| 12 | 56 | -1. | |
| 13 | 1 | $g_{31}$ | meters$^{-1}$ |
| 13 | 2 | $g_{32}$ | meters$^{-1}$ |
| 13 | 3 | $g_{33}$ | meters$^{-1}$ |
| 13 | 54 | 1. | |
| 13 | 55 | 1. | |
| 13 | 56 | 1. | |
| 13 | 58 | -1. | |
| 13 | 59 | -1. | |
| 13 | 60 | -1. | |

*See text for variable definition.

$\dot{\rho}^i$ = range rate from the satellite to the user

dt is the Doppler integration time

$\omega_T$ is the satellite transmitter frequency

c is the speed of light

$H_x$, $H_y$, $H_z$ are the x, y, and z components in ECI of the vector along the heading of the user

$H_x^+$, $H_y^+$, $H_z^+$ are the x, y, and z components in ECI of the vector in the plane tangent to the Earth at the user's location and orthogonal to the heading vector

$|v|$ is the magnitude of the user velocity $\omega$. r. t. the Earth

$g_{ij}$  i = 1, 2, 3 ; j = 1, 2, 3 are elements of $\mathcal{G}$ where

$$\mathcal{G} = \begin{bmatrix} 1 & -1 & 0 & 0 \\ 1 & 0 & -1 & 0 \\ 0 & 0 & 1 & -1 \end{bmatrix} \begin{bmatrix} \dfrac{\partial \varphi_A}{\partial L} & \dfrac{\partial \varphi_A}{\partial \lambda} \\[2mm] \dfrac{\partial \varphi_B}{\partial L} & \dfrac{\partial \varphi_B}{\partial \lambda} \\[2mm] \dfrac{\partial \varphi_C}{\partial L} & \dfrac{\partial \varphi_C}{\partial \lambda} \\[2mm] \dfrac{\partial \varphi_D}{\partial L} & \dfrac{\partial \varphi_D}{\partial \lambda} \end{bmatrix} \begin{bmatrix} \dfrac{\partial L}{\partial x} & \dfrac{\partial L}{\partial y} & \dfrac{\partial L}{\partial z} \\[2mm] \dfrac{\partial \lambda}{\partial x} & \dfrac{\partial \lambda}{\partial y} & \dfrac{\partial \lambda}{\partial z} \end{bmatrix}$$

with the partial derivatives evaluated at the present user location and from [7]

$$\frac{\partial \varphi_i}{\partial L} = .9974 \frac{R_0 f}{C} \left[ \frac{\sin L_R \cos L_i \cos(\lambda_R - \lambda_i) - \cos L_R \sin L_i}{(1 - U_i^2)^{1/2}} \right]$$

$$\frac{\partial \varphi_i}{\partial \lambda} = .9974 \frac{R_0 f}{C} \left[ \frac{\cos L_R \cos L_i \sin (\lambda_R - \lambda_i)}{(1 - U_i^2)^{1/2}} \right]$$

$R_0$ = radius of the Earth

$L_R, \lambda_R$ are latitude and longitude resp. of the user

$L_i, \lambda_i$   i = A, B, C, D   are the latitude and longitude resp. of the OMEGA transmitter

$U_i = \sin L_R \sin L_i + \cos L_R \cos L_i (\cos \lambda_R - \cos \lambda_i)$

f  is the frequency

$\frac{\partial L}{\partial x}, \frac{\partial L}{\partial y}, \frac{\partial L}{\partial z}, \frac{\partial \lambda}{\partial x}, \frac{\partial \lambda}{\partial y}, \frac{\partial \lambda}{\partial z}$  can be computed from the relations

for an ellipsoid of revolution.

$$x = R_e \frac{\cos L_R \sin (\omega t + \lambda_R)}{(1 - \epsilon^2 \sin^2 L_R)^{1/2}}$$

$$y = R_e \frac{\cos L_R \cos (\omega t + \lambda_R)}{(1 - \epsilon^2 \sin^2 L_R)^{1/2}}$$

$$z = R_e \frac{(1 - \epsilon^2) \sin L_R}{(1 - \epsilon^2 \sin^2 L_R)^{1/2}}$$

$\epsilon = 1/298.25$

The modeling section presents the error model dynamics for each of the reference system states. The following will show how each of the measurables depends on these system states. The measurables are of five different types. They are: (1) TOA (time-of-arrival), (2) doppler, (3) EM-log derived velocity, (4) gyrocompass heading, and (5) OMEGA phase errors. The equation for each measurable type is presented below with a brief explanation.

The measurement equations presented are all linearized about a nominal or estimated value. Thus the equations presented are the measurement equations of the deviations of each quantity from its expected or computed value.

(1) <u>TOA Measurements</u>. (Rows 1-4) The equation relating the difference in the measured TOA and the predicted TOA (i. e., $\Delta$TOA) to the error state variable is given by

$$\Delta\text{TOA}_i = \frac{u_x^i}{c}\,\Delta x + \frac{u_y^i}{c}\,\Delta y + \frac{u_z^i}{c}\,\Delta z + c_7 + \tau_T$$

$$+ \frac{u_x^i}{c}\,\Delta s_x^i + \frac{u_y^i}{c}\,\Delta s_y^i + \frac{u_z^i}{c}\,\Delta s_z^i + \tau_{s1}^i + \tau_i + \sigma v_1^i$$

where i indicates the quantities are related to the $i^{th}$ tracked satellite and $\sigma v_1^i$ is the receiver measurement error (i = 1, 2, 3, 4).

It can be seen from this equation that the TOA error is a function of both time and position error states of the user and the transmitting satellite. Additionally it is a function of the atmospheric errors along the transmission path.

(2) <u>Doppler Measurements</u>. (Rows 5-8) The equation relating the difference between predicted and measured doppler counts (frequency integrated over dt) to the error state variables can be derived from the relation given in Section 1.

88

$$\Delta N^i = \Delta dt\, \omega_T - dt\, \Delta \omega_T^i - \frac{\omega_T}{c} dt\, \Delta \dot{\rho}^i + \sigma_{DOP} v_2^i$$

The doppler count error comes from three basic sources, the $dt$ error which is a function of user clock parameters, the $\omega_T$ error which is a function of satellite clock parameters, and the $\dot{\rho}$ error which is a function of user position and velocity errors. Each of these can be identified in terms of the reference system states.

The error in the integration time is equal to first order to the user clock rate error times the nominal integration time $dt$.

$$\Delta dt = dt \left( \frac{\beta}{\alpha^3} c_1 + \frac{\beta}{\alpha^2} c_2 + \frac{\beta}{\alpha} c_3 + \beta c_4 + c_5 \right)$$

Similarly the transmitted frequency error is to first order equal to the satellite clock rate error times the nominal transmitted frequency.

$$\Delta \omega_T^i = \tau_{s2}^i \omega_T$$

The range rate error is given in Section 1 in terms of user position and velocity errors. Using the notation above

$$\Delta \dot{\rho} = \frac{c}{\omega_T dt} \left( k_x^i \Delta x + k_y^i \Delta y + k_z^i \Delta z \right) - u_x \Delta \dot{x} - u_y \Delta \dot{y} - u_z \Delta \dot{z}$$

The measurement error represented by $\sigma_{DOP} v_2^i$ is a truncation error since only full counts are measured. The full equation is

$$\Delta N^i = dt\, \omega_T \left( \frac{\beta}{\alpha^3} c_1 + \frac{\beta}{\alpha^2} c_2 + \frac{\beta}{\alpha} c_3 + \beta c_4 + c_5 \right) - dt\, \omega_T \tau_{s2}^i$$

$$+ \frac{\omega_T}{c} dt \left( u_x \Delta \dot{x} + u_y \Delta \dot{y} + u_z \Delta \dot{z} \right) - k_x^i \Delta x - k_y^i \Delta y$$

$$- k_z^i \Delta z + \sigma_{DOP} v_2^i$$

89

(3) <u>EM log velocity.</u> (Row 9) The EM log velocity is measured along the ships heading axis. The difference between the predicted and measured velocity is dependent upon the velocity error projected on the ships heading vector and the EM log errors. The EM log error measurement is given in terms of the reference system states:

$$\Delta s = H_x \Delta \dot{x} + H_y \Delta \dot{y} + H_z \Delta \dot{z} + x_{EM1} + x_{EM2} + \sigma v_3$$

(4) <u>Gyrocompass derived heading.</u> (Row 10) The difference between the gyrocompass derived heading and the predicted velocity vector (in the absence of ocean currents) can be expressed in terms of the reference system error states. Figure 1 shows the relationship between the predicted velocity unit vector and the measured heading. To first order the heading error can be represented by

$$\Delta H = H_x^+ \frac{\Delta \dot{x}}{|v|} + H_y^+ \frac{\Delta \dot{y}}{|v|} + H_z^+ \frac{\Delta \dot{z}}{|v|} + x_{GC1} + x_{GC2} + \sigma v_4$$

$$= \text{Measured Heading - Predicted Heading} = H_p - H_m$$



$$H_m = \frac{v}{|v|} \qquad \Delta H = \left( \frac{\Delta \dot{x}}{|v|}, \frac{\Delta \dot{y}}{|v|}, \frac{\Delta \dot{z}}{|v|} \right) \cdot H^+$$

$$H_p = \frac{\hat{v}}{|v|}$$

**Figure 3.1**

90
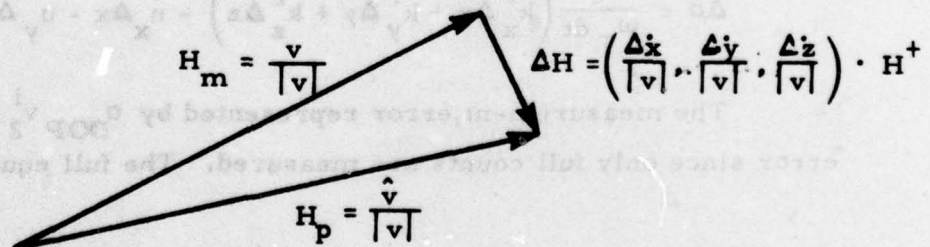
(5) **OMEGA phase errors.** (Rows 11-13) The OMEGA phase difference between the predicted and measured values are a function of the OMEGA phase errors and the user location error states.

$$\Delta\varphi_{KJ} = \frac{\partial\varphi_{KJ}}{\partial x}\Delta x + \frac{\partial\varphi_{KJ}}{\partial y}\Delta y + \frac{\partial\varphi_{KJ}}{\partial z}\Delta z + x_{01}^{K} - x_{01}^{J} + x_{02}^{K} - x_{02}^{J}$$

$$+ x_{03}^{K} - x_{03}^{J}$$

$$\frac{\partial\varphi_{KJ}}{\partial x} = \frac{\partial\varphi_{KJ}}{\partial L}\frac{\partial L}{\partial x} + \frac{\partial\varphi_{KJ}}{\partial\lambda}\frac{\partial\lambda}{\partial x}$$

$$\varphi_{KJ} = \varphi_{K} - \varphi_{J}$$

where

$$K = A \text{ with } J = B, C$$

and

$$K = C \text{ with } J = D$$

The remaining definition needed for the filter relations of (3.6) is the R matrix. This is the measurement noise covariance matrix. The purpose of this measurement matrix is to simulate receiver measurement errors including truncation effects. Table V gives the non-zero elements of R. As is apparent, all of the measurement errors are uncorrelated with the exception of the OMEGA phase difference measurement errors. As above in the measurement matrix definition, it should be noted here that not all of the measurement states and hence not all of the measurement error covariance terms are required in each simulation. Typical values for the parameters in Table 3.5 are:

91

$$\sigma_{TOA} = \frac{1}{4} \text{ chip} \approx \frac{1}{4} \cdot \frac{1}{10.23 \times 10^6} \approx 24.5 \text{ ns}$$

$$\sigma_{DOP} \approx .29 \text{ counts} \quad \text{(uniformly distributed truncation error)}$$

$$\sigma_{EM} = .193 \text{ fps } [1]$$

$$\sigma_{GC} = .15 \text{ degree } [1]$$

$$\sigma_{OM} = .01 \text{ cycle } [1]$$

$$
R_{OM} = 
\begin{bmatrix}
1 & -1 & 0 & 0 \\
1 & 0 & -1 & 0 \\
0 & 0 & 1 & -1
\end{bmatrix}
\begin{bmatrix}
\sigma^2_{OM} & 0 & 0 & 0 \\
0 & \sigma^2_{OM} & 0 & 0 \\
0 & 0 & \sigma^2_{OM} & 0 \\
0 & 0 & 0 & \sigma^2_{OM}
\end{bmatrix}
\begin{bmatrix}
1 & 1 & 0 \\
-1 & 0 & 0 \\
0 & -1 & 1 \\
0 & 0 & -1
\end{bmatrix}
$$

Table 3.5

## Reference System Measurement Noise Covariance

| Row | Col | Value* | Units |
|---|---|---|---|
| 1 | 1 | $\sigma^2_{TOA}$ | $\text{sec}^2$ |
| 2 | 2 | $\sigma^2_{TOA}$ | $\text{sec}^2$ |
| 3 | 3 | $\sigma^2_{TOA}$ | $\text{sec}^2$ |
| 4 | 4 | $\sigma^2_{TOA}$ | $\text{sec}^2$ |
| 5 | 5 | $\sigma^2_{DOP}$ | $\text{counts}^2$ |
| 6 | 6 | $\sigma^2_{DOP}$ | $\text{counts}^2$ |
| 7 | 7 | $\sigma^2_{DOP}$ | $\text{counts}^2$ |
| 8 | 8 | $\sigma^2_{DOP}$ | $\text{counts}^2$ |
| 9 | 9 | $\sigma^2_{EM}$ | $\text{fps}^2$ |
| 10 | 10 | $\sigma^2_{GC}$ | $\text{deg}^2$ |
| 11 | 11 | $2\sigma^2_{OM}$ | |
| 11 | 12 | $\sigma^2_{OM}$ | |
| 12 | 11 | $\sigma^2_{OM}$ | |
| 12 | 12 | $2\sigma^2_{OM}$ | |
| 12 | 13 | $-\sigma^2_{OM}$ | |
| 13 | 12 | $-\sigma^2_{OM}$ | |
| 13 | 13 | $2\sigma^2_{OM}$ | |

*See text for typical parameter values.

93

## 3.2    Suboptimal Filters

In this section, several suboptimal filter candidates will be described. Only the general form of the filters will be described since the exact state vector can be chosen only after sensitivity analyses. Consequently, any conclusions about advantages in computational burden must be reserved until after an appropriate state vector is chosen for the filter.

### 3.2.1    Kalman Suboptimum Filters

The form of the Kalman suboptimum filter is exactly the same as the Kalman optimum filter, i.e., it is governed by the equations given in Section 2.1. The primary difference is the number of states in the state vector. In addition, some of the models for a given state may be different than the model for the same state in the optimum filter. This is often done when it is desirable for the model to attempt to accomodate a variety of errors in a suboptimum fashion rather than concentrating on a particular error. This type of filter has proven very successful in a large number of cases. The number of states required and which state models to incorporate are determined by sensitivity analyses and experience.

### 3.2.2    Fixed/Scheduled Gain Suboptimum Filters

This suboptimum filter considerably reduces the number of operations required at each measurement time by eliminating the gain calculation from Eq. (3.6). The amount of computation in the extrapolation phase is also reduced since a covariance is no longer needed. The equations required are:

$$\hat{\underline{x}}_k = \varphi_{k,k-1}\hat{\underline{x}}_{k-1} + K_k[z_k - H_k\varphi_{k,k-1}\hat{\underline{x}}_{k-1}]$$

94

and defining equations for $K(k)$.

$K(k)$ may be a single fixed matrix of gains or it may be a set of gain matrices from which the appropriate matrix is chosen by some pre-determined criteria or by some external signal (e.g., a maneuver detector). A common method for selecting the gain values is to solve the steady state Riccati equation for the covariance P.

$$FP + PF^T - PHR^{-1}H^TP + GG^T = 0 \qquad (3.7)$$

and then use the P obtained to calculate K

$$K = PH^T[HPH^T + R]^{-1}$$

Note to do this some nominal geometry must be selected. The value of $GG^T$ may also be adjusted to improve the performance of the filter.

The reduction in the amount of computation is naturally accompanied by degraded performance and a possible requirement for additional states to meet minimum performance requirements.

### 3.3    Fading Memory Filters [21]

This filter is a modification to the Kalman suboptimum filter in Section 3.1. The basic idea is to fade out information based on past measurements and weigh the most recent measurements more. This is an attempt to overcome effects of the mismodelling which is called a divergence phenomenon. This is said to occur when the estimate of the state becomes inconsistent with the error covariance predicted by the filter equations.

The fading memory filter is a simple modification to the filter equations in Eq. (3.6). The change is to Eq. (3.6c) which becomes

95

$$P'_k = \varphi_{k,k-1} P_{k-1} \varphi^T_{k,k-1} (e^{\beta \Delta \tau}) + Q_k$$

where $\beta > 0$.

It is hoped that this rather minor modification to the suboptimum filter in Section 3.2.1 will make a noticeable improvement in performance.

## 3.4 $\alpha - \beta$ Filter [22]

This is a simple filter which has proven successful in some applications. This filter would apply in the case where TOA measurements only are made. The state vector would then consist of position and time estimates and rates of each. The basic assumption of the $\alpha$-$\beta$ filter for multivariable systems is that the measurements and the dynamics of the sets of a variables and its associated rates are independent and do not interact. The simplest form of the $\alpha$-$\beta$ filter would use constant values for $\alpha$ and $\beta$. Other methods for choosing $\alpha$ and $\beta$ may also be considered.

Let $s$ represent a generic state and $r$ its rate. In the navigation problem $s$ might represent each of the coordinates and the clock bias while $r$ represents the corresponding rates. The $\alpha$-$\beta$ filter can then be described by the following equations:

$$s^+(k) = s^-(k) + \alpha(k)[y(k) - s^-(k)]$$

$$r^+(k) = r^-(k) + \beta(k)[(y(k) - s^-(k))/T]$$

where

$s^+$, $r^+$ represent updated values and $s^-$, $r^-$ represent

the extrapolated values and T is the time between updates

96

$$s^-(k) = s^+(k-1) + T r^+(k-1)$$

$$r^-(k) = r^+(k-1)$$

$y(k)$ is the state measurement at time $k$

One method for choosing "optimal $\alpha$-$\beta$ gains" is to use the Kalman filter equations for the two state systems of the state variable and its rate where only a measurement of the state is available [22]. The formulations are shown to be equivalent in Ref. [22]. In the multivariable case, gains for each of the coordinate components of the state are computed ignoring the correlations. Then one set of gains will serve for each of the three coordinates plus one set for the user bias.

In using an $\alpha$-$\beta$ filter in the NAVSTAR/GPS system, it will be required to generate pseudo-measurements since the measurables are time of arrivals and not positions. Thus in addition to the $\alpha$-$\beta$ filter, an algorithm, such as a single-fix, must be implemented to generate the pseudo-measurements.

By their nature, $\alpha$-$\beta$ filters do not perform well when the rate variables change rapidly. It is in the period of acceleration that this type of filter must be examined most carefully. Perhaps increased plant noise or a fading memory mechanization will make the filter less sensitive to changing velocities.

## Section 4. - COVARIANCE ANALYSIS

### 4.0    Introduction

The purpose of this section is to describe the covariance analysis task of the NAVSTAR/GPS Navigation Analysis and Algorithm Development Study.   This description includes a summary presentation of covariance analysis, a discussion of the particular application to the candidate algorithms described in Section 3, and the results of the analysis runs completed to date.

The objective of covariance analysis is to establish the expected navigation accuracy of the filtering algorithms selected as candidates for use in the operational system.   The accuracy can be established only with respect to the reference model and the assumed statistics of the error sources.   Many of the factors affecting accuracy, such as user to satellite geometry, receiver configuration, satellite selection algorithm, update rates, etc., cannot be modelled in the format required for covariance analysis.   For this reason, each covariance analysis run has associated with it a scenario which consists of a particular choice from all possible combinations of these factors.   Covariance analysis cannot tell the entire story of accuracy except with respect to the reference system and a particular scenario.   It does, however, give a good indication of the expected error variance when several scenarios are analyzed.

### 4.1    Covariance Analysis

This section describes in a summary fashion the problem to be solved by covariance analysis and the technique of solution.   The method of solution described herein has been implemented in a general

covariance analysis program CANOMIS (Covariance ANalysis Of Multisensor Integrated Systems). The results presented in subsequent sections are the result of applying CANOMIS to the specific problem of GPS navigation.

### 4.1.1 The Problem

All of the candidate filters in Section 3 use weighting matrices or gains when incorporating new data. The gains are computed based on such things as the assumed estimation error covariance, the assumed measurement noise covariance, the assumed input noise covariance, and assumed system dynamics and measurement process. In general, each of the assumed values may be incorrect at least in part. Additionally, it is necessary to ignore certain known error sources to reduce the computational burden in actual operational mechanizations. The purpose of covariance analysis is to determine the expected error arising from each of these sources. For purposes of discussion, these error sources may be classified into the following categories:

(1)  an incomplete state vector,

(2)  incorrect system matrices,

(3)  incorrect initial state statistics,

(4)  incorrect statistics for the white noise processes,

(5)  nonwhite noise in the plant and/or measurements.

These errors in the modelling can lead to the so-called "divergence problem" which, loosely speaking, occurs when the actual errors between the true states and the estimated states become inconsistent with the assumed filter covariance. The greatest concern is of course when the errors become much larger than indicated by the filter covariance. Two versions of this divergence phenomenon may

be distinguished. "True" divergence is said to occur when the covariance of the actual error becomes unbounded as the length of the data span increases. "Apparent" divergence occurs when the actual error covariance matrix remains bounded, but is much larger in some sense than the filter error covariance. In each case the estimate of the true state is unreliable so that the behavior of the estimator is unsatisfactory. Of less concern, but a problem nonetheless, is the situation in which the actual estimation error is substantially less than indicated by the filter covariance. While the estimator may provide acceptable estimates, the lack of knowledge of the covariance can inhibit actions based on the response of the estimator.

To discuss the problem in more detail, consider the following linear systems, each of which describes the errors about some point.

$$\dot{\underline{x}}_F = F_F \underline{x}_F + G_F \underline{u}_F$$

$$\underline{z}_F = H_F \underline{x}_F + \underline{v}_F \tag{4.1}$$

$$\dot{\underline{x}}_s = F_s \underline{x}_s + G_s \underline{u}_s$$

$$\underline{z}_s = H_s \underline{x}_s + \underline{v}_s \tag{4.2}$$

where

$\underline{x}_F$ is the filter state vector, dimensioned $n_F$

$F_F$ is the filter plant matrix

$G_F$ is the filter input distribution matrix

$\underline{u}_F$ is the filter plant noise vector (unity PSD white noise)

$\underline{z}_F$    is the filter observation vector

$H_F$    is the filter measurement matrix

$\underline{v}_F$    is the filter measurement noise vector

$\underline{x}_s$    is the reference error system state vector, dimensioned $n_s$

$F_s$    is the reference error system plant matrix

$G_s$    is the reference error system input distribution matrix

$\underline{u}_s$    is the reference error system plant noise vector (unity PSD white noise)

$\underline{z}_s$    is the reference error system observation vector

$H_s$    is the reference error system measurement matrix

$\underline{v}_s$    is the reference error system measurement noise vector

The system in equation (4.1) is the system used to generate the gains to be used in recursive filtering of the data. Section 3 concerned itself with the problem of defining the relationships used to generate these gains. Now the techniques for determining the accuracy obtainable with each of the gain computation methods will be presented. The results to be presented are of course scenario dependent. The technique of covariance analysis determines directly a statistical accuracy and thus eliminates the need for extensive Monte Carlo simulation.

4.1.2 Solution Technique

The desired output of the covariance analysis is the 1-$\sigma$ error of the filter estimates and the sensitivity of each estimated state to

101

selected reference system error sources. This information is
embodied in the estimate error covariance matrix P.

$$P = E[(\underline{x}_s - \underline{x}_F^*)(\underline{x}_s - \underline{x}_F^*)^T] \qquad (4.3)$$

where

$\underline{x}_F^*$ is the filter state vector augmented with zeros to make the subtraction well defined, i.e.,

$$\underline{x}_F^* = \begin{bmatrix} \underline{x}_F \\ 0 \end{bmatrix} \text{ and } 0 \text{ is a } (n_s - n_F) \text{ zero vector.}$$

The solution technique is to generate the matrix P as a func-
tion of time. To do this, the equations for P must be available and
can be developed as follows. First, to simplify the notation, define
a new vector $\underline{x}_s^*$

$$\underline{x}_s^* = \underline{x}_s - \underline{x}_F^* = \underline{x}_s - \begin{bmatrix} x_F \\ 0 \end{bmatrix} \qquad (4.4)$$

In the most general case, the dynamics of the new state vector
$\underline{x}_s^*$ is different from both $\underline{x}_s$ and $\underline{x}_F$ since the difference is being
propagated. However, in all of the filters proposed in Section 3, only
kinematic relations are considered so that it is safe to assume that
$F_F$ in (4.1) is a subblock of $F_s$ in (4.2) and thus $\underline{x}_s^*$ has dynamics
described by (4.2). More explicitly

$$\dot{\underline{x}}_s^* = \dot{\underline{x}}_s - \dot{\underline{x}}_F^* = F_s \underline{x}_s - \begin{bmatrix} F_F & 0 \\ \hline 0 & 0 \end{bmatrix} \begin{bmatrix} x_F \\ \hline 0 \end{bmatrix} + G_s u_s$$

$$= F_s \underline{x}_s^* + G_s u_s \qquad (4.5)$$

102

Note that $G_F u_F$ does not appear since it is an artificial quantity used only in the filter gain generation and estimate extrapolation assumes zero-mean noise.

In addition to the dynamics described by equation (4.5), there is a measurement done at discrete times. At the time of a measurement $\underline{x}_s^*$ is replaced by

$$\underline{x}_s^* = \underline{x}_s - \left( \begin{bmatrix} \underline{x}_F \\ \text{---} \\ 0 \end{bmatrix} + \begin{bmatrix} K\underline{z}_s \\ \text{----} \\ 0 \end{bmatrix} \right) \tag{4.6}$$

where

    $K$   is the gain matrix

    $\underline{z}_s$   is the vector of observations from the reference error system $\underline{z}_s = H_s \underline{x}_s + \underline{v}_s$

The equations to define $P$ are now available. Using equations (4.3), (4.4), (4.5), and (4.6) the following are obtained.

**(a)**    **Extrapolation**

$$P'_k = \varphi_{k, k-1} P_{k-1} \varphi_{k, k-1}^T + Q_k \tag{4.7}$$

where

$$Q_k = \int_0^{\Delta t} \varphi(\Delta t - \tau) G_s G_s^T \varphi^T(\Delta t - \tau) \, d\tau$$

$\varphi_{k, k-1}$ is the state transition matrix for (4.2)

103

**(b) Estimation**

$$P_k = \left\{ I - \begin{bmatrix} K\,H_s \\ \text{----} \\ 0 \end{bmatrix} \right\} P_k' \left\{ I - \begin{bmatrix} K\,H_s \\ \text{----} \\ 0 \end{bmatrix} \right\}^T \tag{4.8}$$

$$+ \begin{bmatrix} K \\ -- \\ 0 \end{bmatrix} R_s \begin{bmatrix} K \\ -- \\ 0 \end{bmatrix}^T$$

where

$R_s$ is the measurement error covariance

$$R_s = E[v_s v_s^T]$$

and the partitions are conformable with the defined vector $\underline{x}_s^*$

ORINCON's covariance analysis program CANOMIS propagates these equations as a special case of the more general problem. This is done by setting logical input variables (see CANOMIS description).

### 4.1.3  Analysis of Results

All of the covariance analysis is being done in inertial coordinates. Therefore the individual axis components have no particular relation to the navigation coordinates. A more meaningful output is the root sum square (RSS) error. This is the usual Euclidean Norm of the 1-$\sigma$ errors along the component axes. All of the position and velocity results presented will be in terms of the RSS quantities.

In addition to results considering all error sources, it is desirable to isolate the effects of certain individual error sources. In this

way an error budget can be made which quantifies the sources of error. Also note that the error covariance equations (4.7) and (4.8) are linear, therefore it makes sense to define sensitivities to the various error contributions, i.e., the variance of each of the navigation variables $\sigma_j^2$ $j = 1, 2, \ldots, m$ may be written as a sum of say $r$ input error variances times a sensitivity for each.

$$\sigma_i^2 = \sum_{i=1}^{n} \sigma_j^2 \, \alpha_{ji} \qquad j = 1, 2, \ldots, m \qquad i = 1, 2, \ldots, r \qquad (4.9)$$

where

$\sigma_i$ is a generic error source such as white noise PSD, initial condition variances, etc.

$\alpha_{ji}$ is the sensitivity of the $j^{th}$ variance to the $i^{th}$ input variance.

These sensitivity coefficients are useful in that through their use, error budgets can be updated without extensive simulation. The method for determining these sensitivities is generally to run the covariance analysis with all of the error sources set to zero with the exception of the one of interest. For a certain class of error source, the sensitivity is derivable from the covariance matrix of the complete error system [see Appendix A].

### 4.1.4 Analysis Scenario

The usefulness of covariance analysis lies in its ability to provide statistical information over an ensemble of errors. To extend this philosophy to the scenarios, an approximate method of analysis was used. In this method, a step change of acceleration variance was introduced into the reference system. This was done to simulate the

105

effects of an ensemble of acceleration changes and to determine the
expected navigation error. The approximation comes in due to the
fact that the linearization of the measurement process must be made
about the nominal or zero acceleration trajectory. For short periods
of time, this error is not large and the results are still valid for com-
parison results.

The values of the reference system parameters used in the
covariance analyses are listed in Table 4.1. Table 4.2 contains the
initial covariance matrix values for the reference system. These
values were used in all of the covariance analysis computer runs
except as noted.

## 4.1.5 Results of Covariance Analysis

In this study, covariance analysis was used not only to analyze
the performance of suboptimal filters, but as a design tool. The
filter development became an evolutionary process with the covariance
analysis providing the data for decisions on the filter development.
The primary emphasis in the filter development was the unaided ship
receiver. By unaided, it is meant that no external velocity or accelera-
tion information is provided. It was assumed, however, that in all
cases pitch and roll information was available from gyros.

The candidate filters contained only kinematically related states
involving position velocity, acceleration, and clock states. The states
also had plant noise added to adjust the gains. Table 4.3 is a matrix
indicating which states are contained in each of the filters for which
extensive analysis was performed. Table 4.4 gives the plant noise
1-$\sigma$ values. The filter measurement matrices are the submatrices
of the reference system measurement matrix corresponding to the
included states.

106

## Table 4.1.  Reference System Parameter Values

| Parameter | | Value |
|---|---|---|
| User Clock Allan variance parameters  10 | $\tau_1$ | .5 sec |
| | $\tau_2$ | 80 sec |
| | $\tau_3$ | $5 \times 10^4$ sec |
| | M | -220 db |
| Ionospheric error correlation time | $\tau_i$ | 4212 sec |
| Ionospheric error[*] 1-$\sigma$ value | | $1.7 \times 10^{-8}$ sec |
| Satellite clock random walk driving noise 1-$\sigma$ value | | $1. \times 10^{-11}$ sec/(sec)$^{\frac{1}{2}}$ |
| EM log Markov error correlation time | $\tau_{EM}$ | 1380 sec |
| EM log Markov error 1-$\sigma$ value | | .079 meters/sec |
| Gyrocompass Markov error correlation time | $\tau_{GC}$ | 1380 sec |
| Gyrocompass Markov error 1-$\sigma$ value | | $6.1 \times 10^{-3}$ radians |
| Omega error correlation time | $\tau_{OM}$ | 3600 sec |
| Omega Markov error 1-$\sigma$ value | | .0223 cycles |
| Omega sinusoid error frequency | | $1.45 \times 10^{-4}$ cycles/sec |

[*]This value is for the single frequency receiver.

107

## Table 4.1. Reference System Parameter Values (Continued)

| Parameter | Value |
|---|---|
| Doppler count integration time | .2 sec |
| Satellite signal frequency | $1.57542 \times 10^9$ cycles/sec |
| Time-of-arrival measurement error 1-$\sigma$ value | $25 \times 10^{-9}$ sec |
| Doppler measurement error 1-$\sigma$ value | .289 counts |
| Gyrocompass measurement error 1-$\sigma$ value | $2.62 \times 10^{-3}$ radians |
| EM log measurement error 1-$\sigma$ value | .14 meters/sec |

## Table 4.2. Reference System Initial Covariance Values
### (Non-zero elements of upper triangle)

| Row | Column | Value |
|-----|--------|-------|
| 1 | 1 | $1 \times 10^8$ meters$^2$ |
| 2 | 2 | $1 \times 10^8$ meters$^2$ |
| 3 | 3 | $1 \times 10^8$ meters$^2$ |
| 4 | 4 | 100 (meters/sec)$^2$ |
| 5 | 5 | 100 (meters/sec)$^2$ |
| 6 | 6 | 100 (meters/sec)$^2$ |
| 7 | 7 | 1 (meter/sec$^2$)$^2$ |
| 8 | 8 | 1 (meter/sec$^2$)$^2$ |
| 9 | 9 | 1 (meter/sec$^2$)$^2$ |
| 10 | 10 | $3.1666 \times 10^{-2}$ |
| 10 | 11 | $3.821 \times 10^{-2}$ |
| 10 | 12 | $3.96 \times 10^{-2}$ |
| 10 | 13 | $1.61 \times 10^{-2}$ |
| 11 | 11 | $5.48 \times 10^{-2}$ |
| 11 | 12 | $6.15 \times 10^{-2}$ |
| 11 | 13 | $1.37 \times 10^{-2}$ |
| 12 | 12 | $7.85 \times 10^{-2}$ |
| 12 | 13 | $1.31 \times 10^{-2}$ |
| 13 | 13 | $6.92 \times 10^{-2}$ |
| 14 | 14 | $1. \times 10^{-18}$ (sec/sec)$^2$ |
| 15 | 15 | $1. \times 10^{-24}$ (sec)$^{-2}$ |
| 16 | 16 | $1. \times 10^{-12}$ (sec)$^2$ |
| 17 | 17 | $.44 \times 10^{-16}$ (sec)$^2$ |
| 18 | 18 | 9. (meters)$^2$ |
| 19 | 19 | 9. (meters)$^2$ |
| 20 | 20 | 9. (meters)$^2$ |

## Table 4.2. Reference System Initial Covariance Values
### (Non-zero elements of upper triangle) (Continued)

| Row | Column | Value |
|-----|--------|-------|
| 21 | 21 | $1. \times 10^{-18}$ (sec)$^2$ |
| 22 | 22 | $1. \times 10^{-24}$ (sec/sec)$^2$ |
| 23 | 23 | * |
| 23 | 29 | * |
| 23 | 35 | * |
| 23 | 41 | * |
| 24 | 24 | 9. (meters)$^2$ |
| 25 | 25 | 9. (meters)$^2$ |
| 26 | 26 | 9. (meters)$^2$ |
| 27 | 27 | $1. \times 10^{-18}$ (sec)$^2$ |
| 28 | 28 | $1. \times 10^{-24}$ (sec/sec)$^2$ |
| 29 | 29 | * |
| 29 | 35 | * |
| 29 | 41 | * |
| 30 | 30 | 9. (meters)$^2$ |
| 31 | 31 | 9. (meters)$^2$ |
| 32 | 32 | 9. (meters)$^2$ |
| 33 | 33 | $1. \times 10^{-18}$ (sec)$^2$ |
| 34 | 34 | $1. \times 10^{-24}$ (sec/sec)$^2$ |
| 35 | 35 | * |
| 35 | 41 | * |
| 36 | 36 | 9. (meters)$^2$ |
| 37 | 37 | 9. (meters)$^2$ |
| 38 | 38 | 9. (meters)$^2$ |
| 39 | 39 | $1. \times 10^{-18}$ (sec)$^2$ |
| 40 | 40 | $1. \times 10^{-24}$ (sec/sec)$^2$ |

*Value computed using satellite/user geometry in formulas given in
section 1.2.2.3 with $\epsilon$ = 17 ft.

## Table 4.2. Reference System Initial Covariance Values
### (Non-zero elements of upper triangle) (Continued)

| Row | Column | Value |
|-----|--------|-------|
| 41 | 41 | * |
| 43 | 43 | $1.61 \times 10^{-2}$ (meters/sec)$^2$ |
| 45 | 45 | $3.721 \times 10^{-5}$ (radians)$^2$ |
| 46 | 46 | $.534$ (radians)$^2$ |
| 47 | 47 | $.31$ (radians)$^2$ |
| 48 | 48 | $.314$ (radians)$^2$ |
| 49 | 49 | $6.6 \times 10^{-9}$ |
| 50 | 50 | $.534$ (radians)$^2$ |
| 51 | 51 | $.31$ (radians)$^2$ |
| 52 | 52 | $.314$ (radians)$^2$ |
| 53 | 53 | $6.6 \times 10^{-9}$ |
| 54 | 54 | $.534$ (radians)$^2$ |
| 55 | 55 | $.31$ (radians)$^2$ |
| 56 | 56 | $.314$ (radians)$^2$ |
| 57 | 57 | $6.6 \times 10^{-9}$ |
| 58 | 58 | $.534$ (radians)$^2$ |
| 59 | 59 | $.31$ (radians)$^2$ |
| 60 | 60 | $.314$ (radians)$^2$ |
| 61 | 61 | $6.6 \times 10^{-9}$ |

*Value computed using satellite/user geometry in formulas given in
section 1.2.2.3 with $\epsilon = 17$ ft.

## Table 4.3. Filter Configuration Matrix

| States | Filter Type | | | | |
|---|---|---|---|---|---|
| | 11-State | 10-State | 8-State | 7-State | $\alpha - \beta$ |
| x-position | yes | yes | yes | yes | yes |
| y-position | yes | yes | yes | yes | yes |
| z-position | yes | yes | yes | yes | yes |
| x-velocity | yes | yes | yes | yes | yes |
| y-velocity | yes | yes | yes | yes | yes |
| z-velocity | yes | yes | yes | yes | yes |
| x-acceleration | yes | yes | no | no | no |
| y-acceleration | yes | yes | no | no | no |
| z-acceleration | yes | yes | no | no | no |
| user clock bias | yes | yes | yes | yes | yes |
| user clock frequency error | yes | no | yes | no | yes |

## Table 4.4. Filter Plant Noise 1-σ Values

| Noise Parameter | Nominal Value | States added to |
|---|---|---|
| $\sigma_{pos}$ | 1 meter/(sec)$^{1/2}$ | x, y, z position |
| $\sigma_{vel}$ | .1 meter/(sec)$^{3/2}$ | x, y, z velocity |
| $\sigma_{acc}$ | .01 meter/(sec)$^{5/2}$ | x, y, z acceleration |
| $\sigma_{uclk}$ | $10^{-12}$ sec/(sec)$^{1/2}$ | bias error |
| $\sigma_{urate}$ | $10^{-11}$ sec/(sec)$^{1/2}$/day | frequency error |

113

In the following subsections, the covariance analysis of the filter development will be presented for several candidate filters. Following this, sensitivity of filter performance to key system parameters will be presented.

### 4.1.5.1 Eleven-State Suboptimal Filter

The eleven-state filter includes all of the candidate states. The first attempt at the eleven-state filter was a Kalman formulation with no modifications made to accommodate unmodelled disturbances in acceleration. The results of this are shown in Figures 4.1 and 4.2.[*] In Figure 4.1, no measurements of doppler shift are made. Figure 4.2 shows the results when doppler measurements are made. The scenario in both cases includes time between measurements of one second, a 5 meter/sec$^2$ step change of acceleration at 20 seconds, and four satellites used at each measurement time. Figures 4.3 and 4.4 show essentially the same cases except that at each measurement only one satellite signal was used in a round-robin fashion using the same four satellites. Figure 4.5 shows the results with a fading memory filter with a boxcar of acceleration uncertainty of 5 meters/sec$^2$ for $20 \leq t \leq 35$. The fading memory filter uses an exponential fade factor. The exponent is .2 times $\Delta t$ (where $\Delta t$ is the integration step size) for $0 \leq t \leq 25$ and $40 < t \leq 50$ and it is .6 for $25 < t \leq 40$.

Examination of Figure 4.1 and 4.2 shows that in the absence of doppler measurements, the filter does not provide good velocity information. The position information is not substantially worse except

---

[*]NOTE: Each figure contains time plots. Plot (a) shows the RSS position error standard deviation versus time and plot (b) shows the RSS velocity error standard deviation versus time. Care should be taken when comparing plots since not all of the scales are the same.
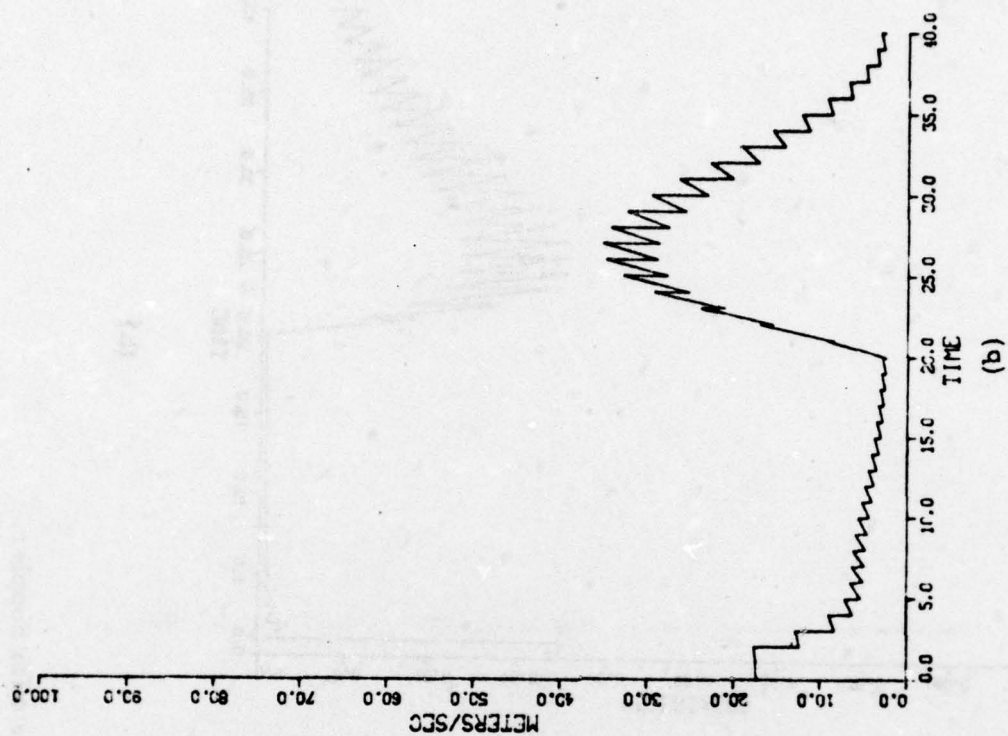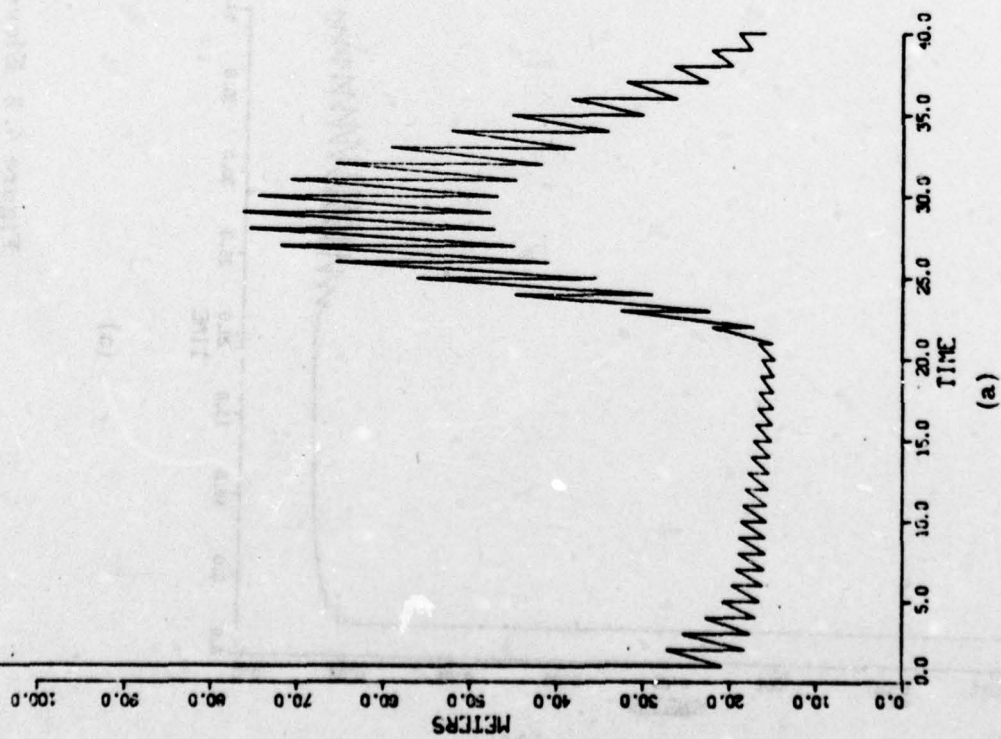
Figure 4.1 Eleven-state filter without doppler.

115
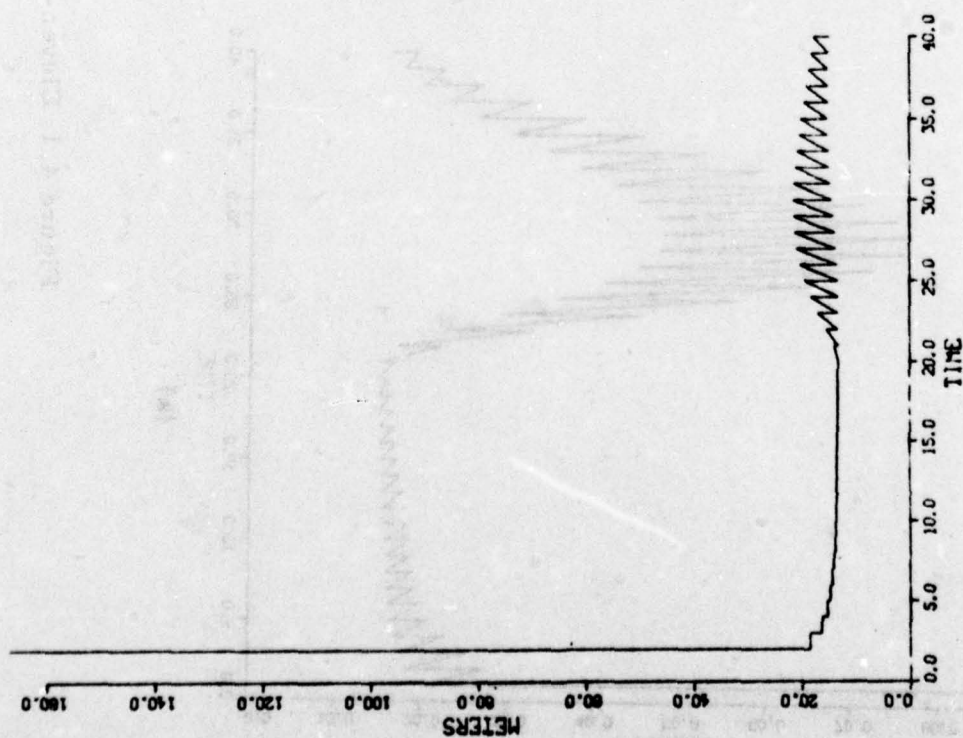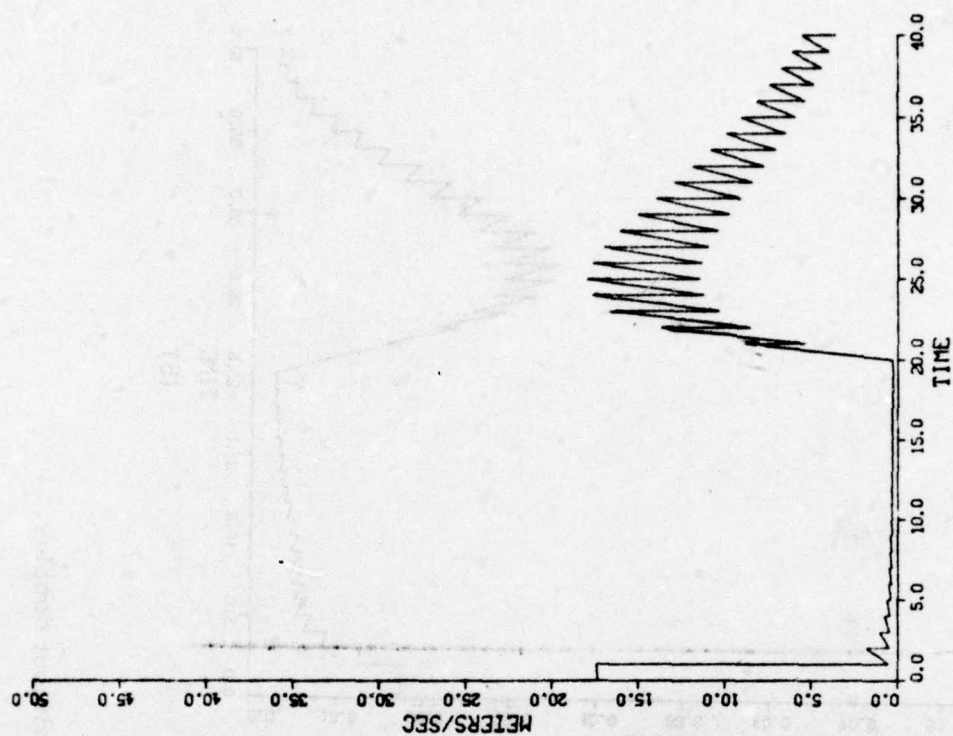
Figure 4.2 Eleven-state filter with doppler.

116
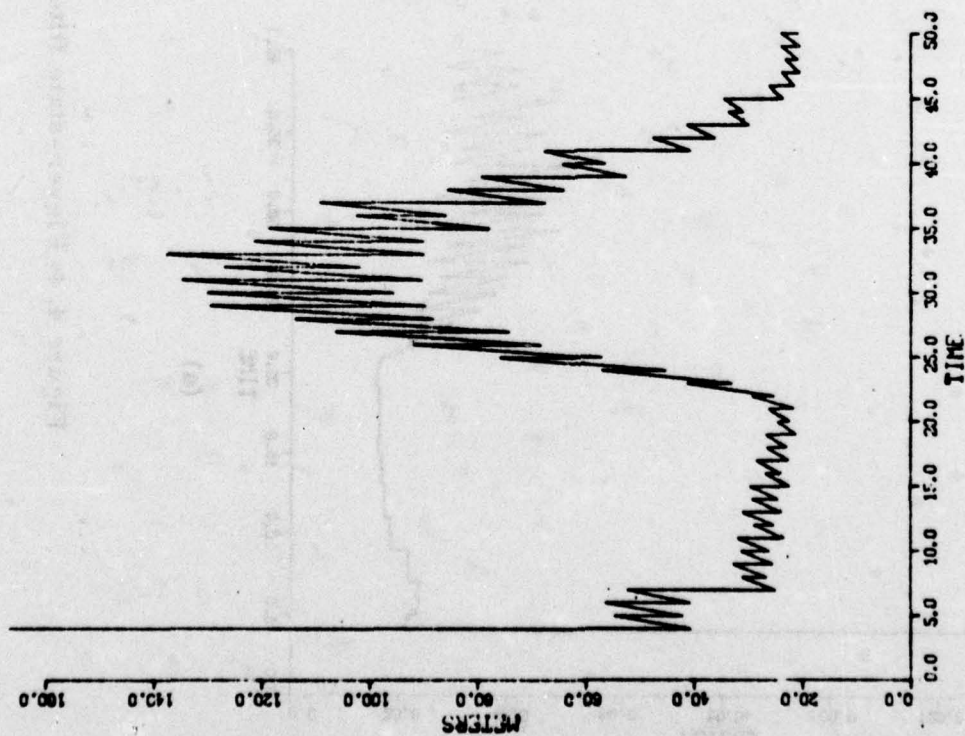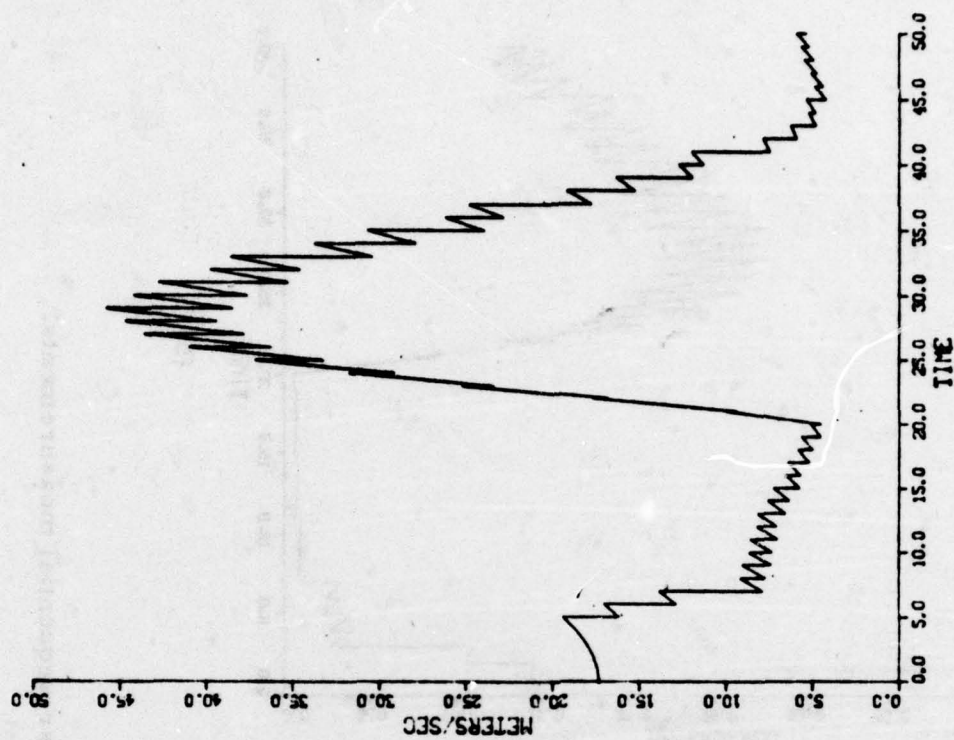
Figure 4.3  Eleven-state filter without doppler-sequential measurements.

117
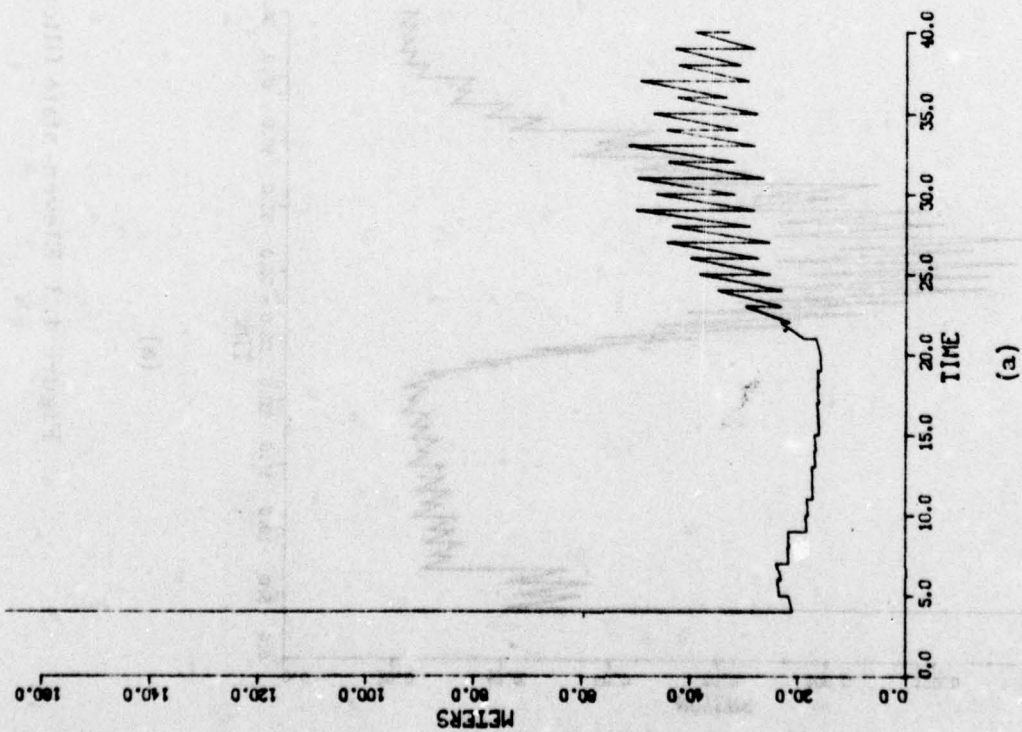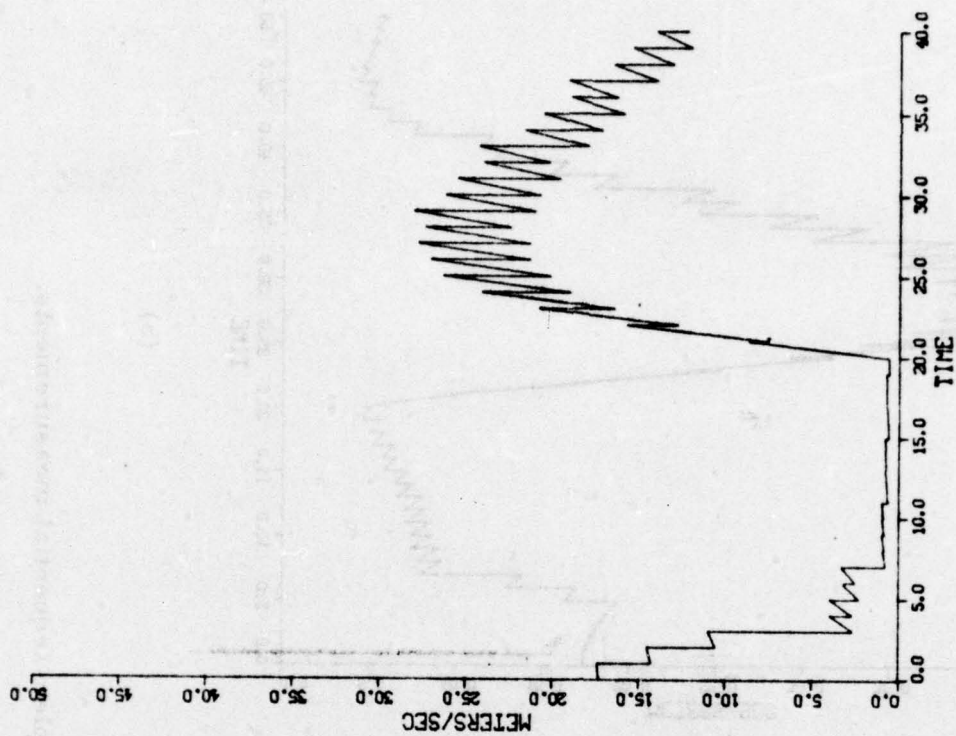
Figure 4.4 Eleven-state filter with doppler-sequential measurements.

118
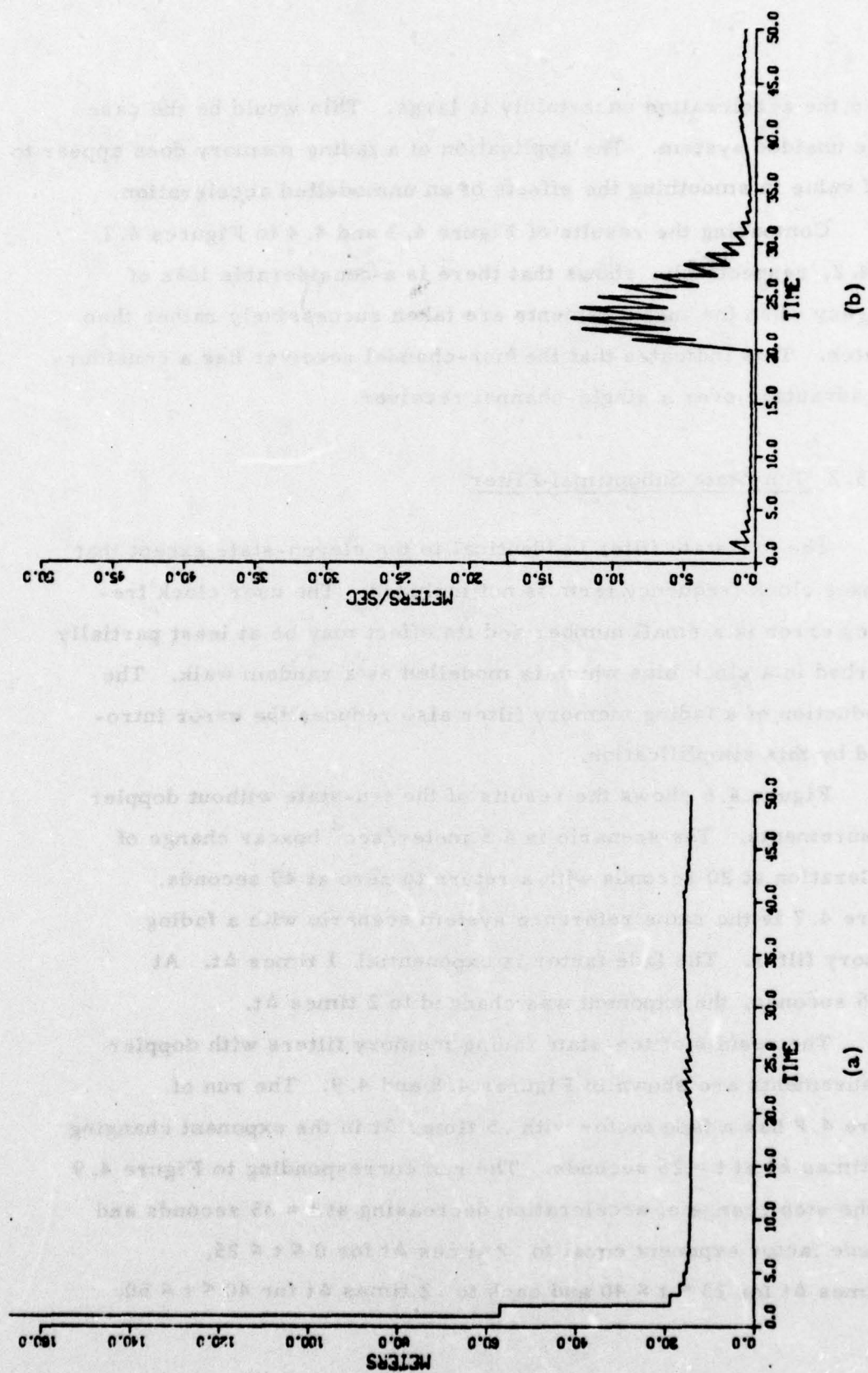
Figure 4.5 Eleven-state filter with doppler and fading memory.

where the acceleration uncertainty is large. This would be the case of the unaided system. The application of a fading memory does appear to be of value in smoothing the effects of an unmodelled acceleration.

Comparing the results of Figure 4.3 and 4.4 to Figures 4.1 and 4.2, respectively, shows that there is a considerable loss of accuracy when the measurements are taken successively rather than in batch. This indicates that the four-channel receiver has a considerable advantage over a single-channel receiver.

### 4.1.5.2 Ten-State Suboptimal Filter

The ten-state filter is identical to the eleven-state except that the user clock frequency term is not included. The user clock frequency error is a small number and its effect may be at least partially absorbed in a clock bias which is modelled as a random walk. The introduction of a fading memory filter also reduces the error introduced by this simplification.

Figure 4.6 shows the results of the ten-state without doppler measurements. The scenario is a 5 meter/sec$^2$ boxcar change of acceleration at 20 seconds with a return to zero at 40 seconds. Figure 4.7 is the same reference system scenario with a fading memory filter. The fade factor is exponential 1 times $\Delta t$. At t = 25 seconds, the exponent was changed to 2 times $\Delta t$.

The results of ten-state fading memory filters with doppler measurements are shown in Figures 4.8 and 4.9. The run of Figure 4.8 has a fade factor with .5 times $\Delta t$ in the exponent changing to 1 times $\Delta t$ at t = 25 seconds. The run corresponding to Figure 4.9 has the step change of acceleration decreasing at t = 35 seconds and the fade factor exponent equal to .2 times $\Delta t$ for $0 \leq t \leq 25$, .6 times $\Delta t$ for $25 < t \leq 40$ and back to .2 times $\Delta t$ for $40 < t \leq 50$.
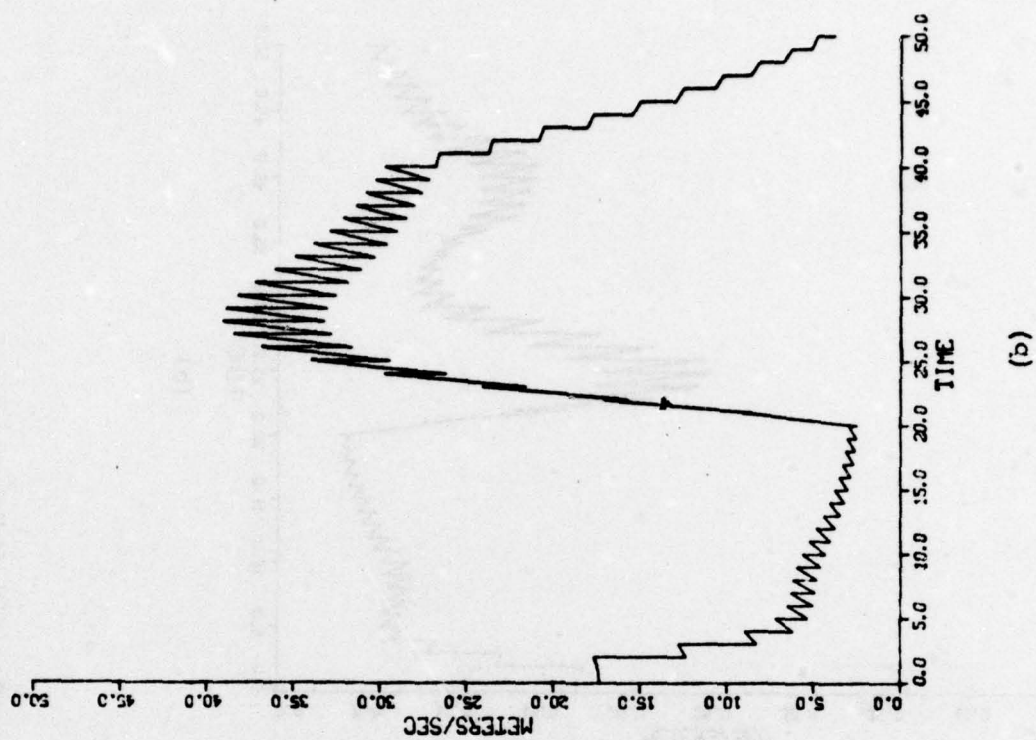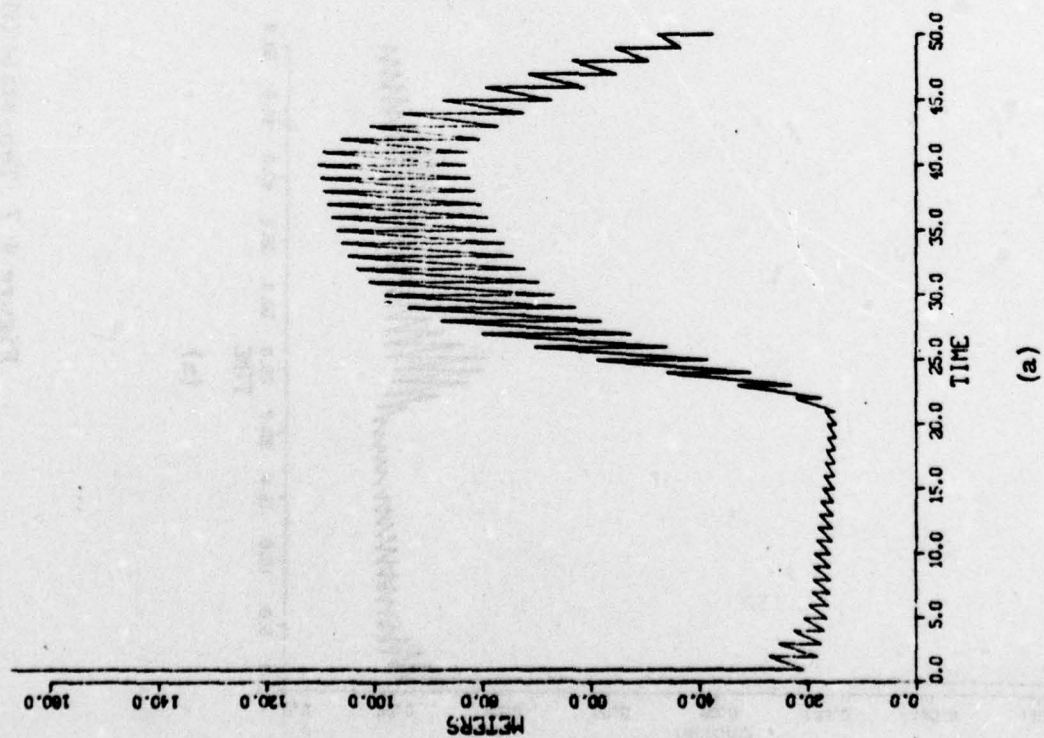
Figure 4.6 Ten-state filter without doppler.

121
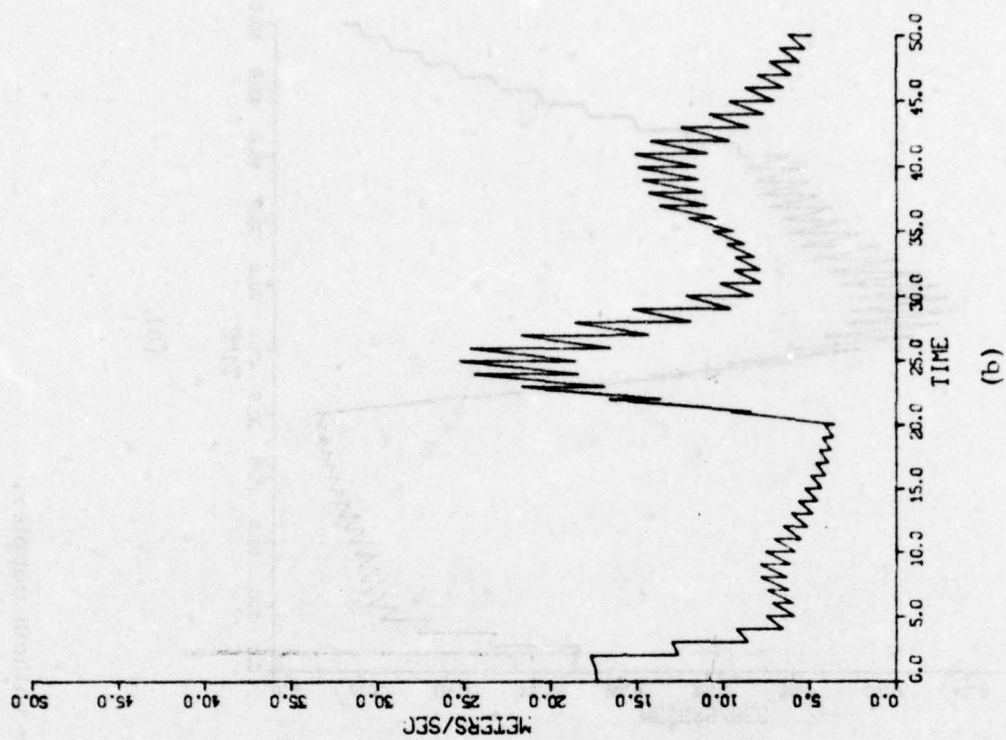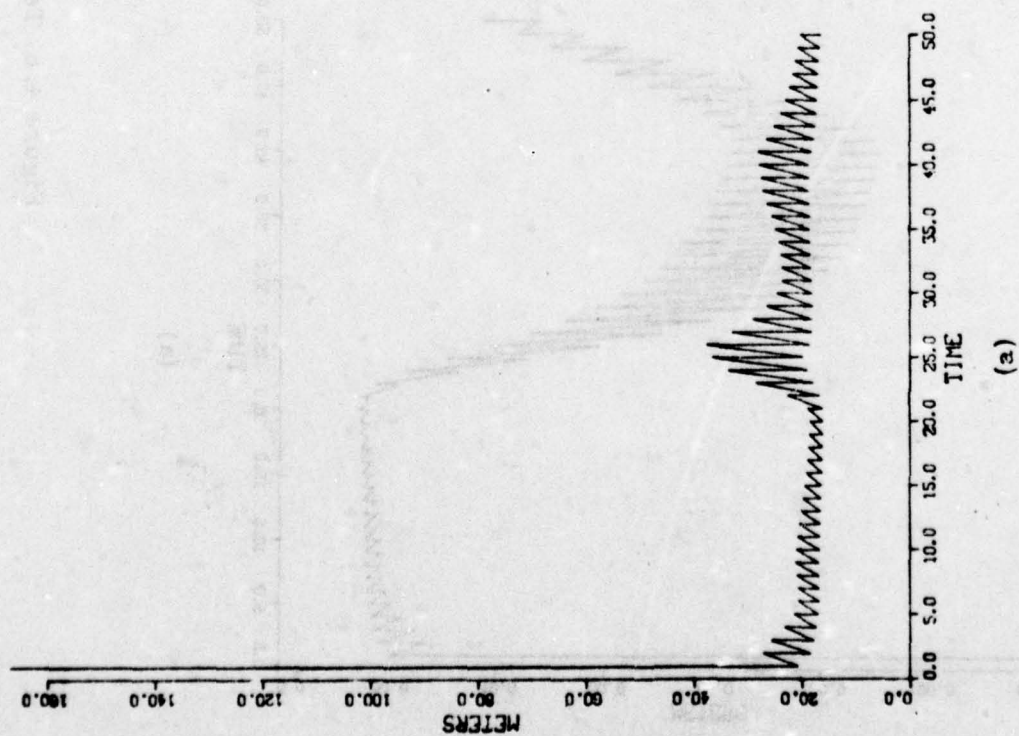
Figure 4.7  Ten-state filter without doppler with fading memory.

122
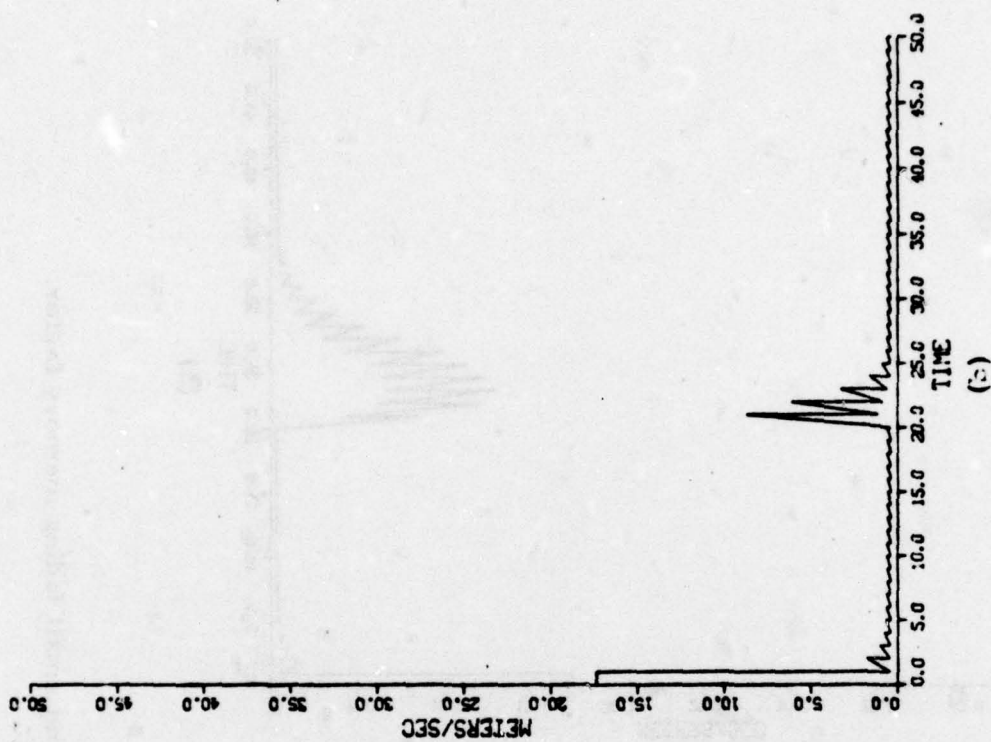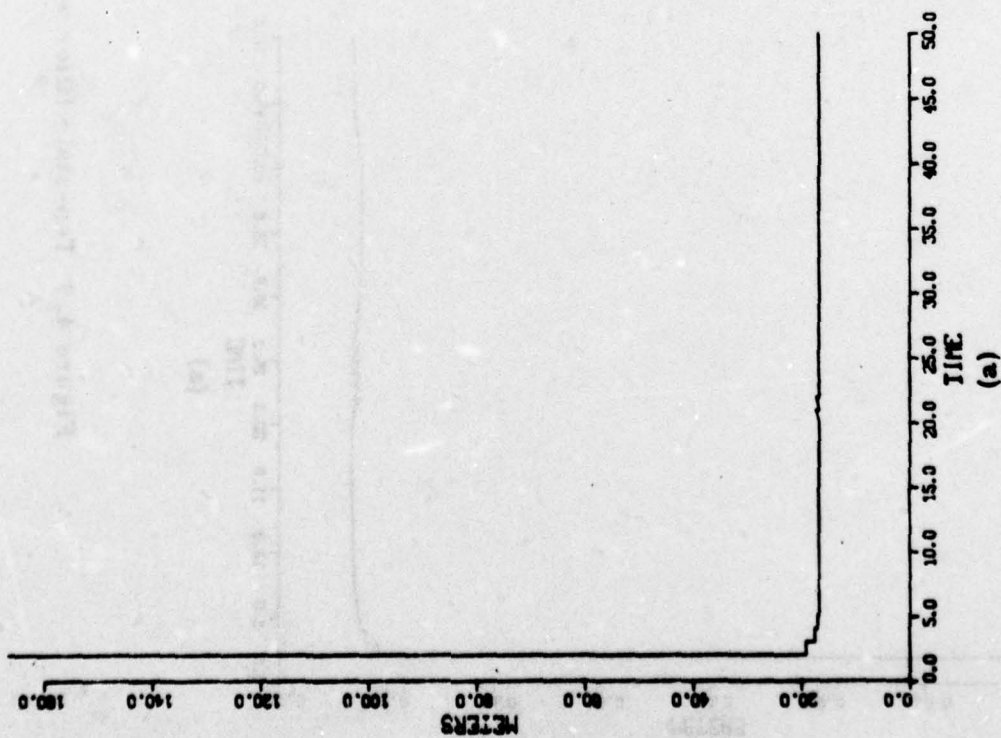
Figure 4.8  Ten-state filter with doppler and large fading memory factor.
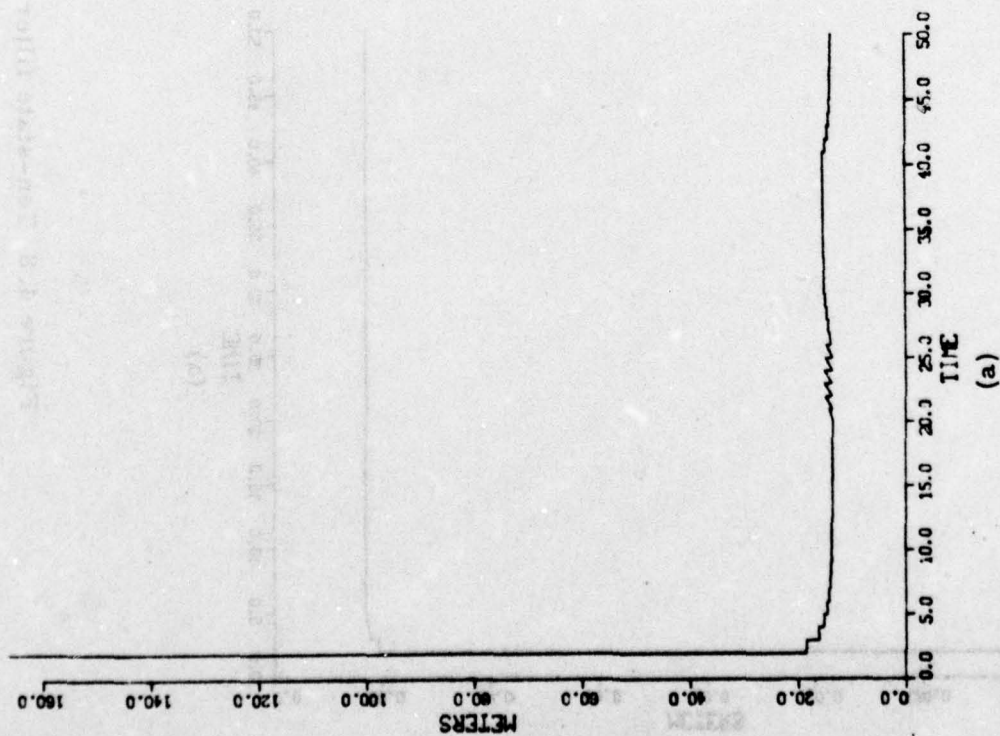
123
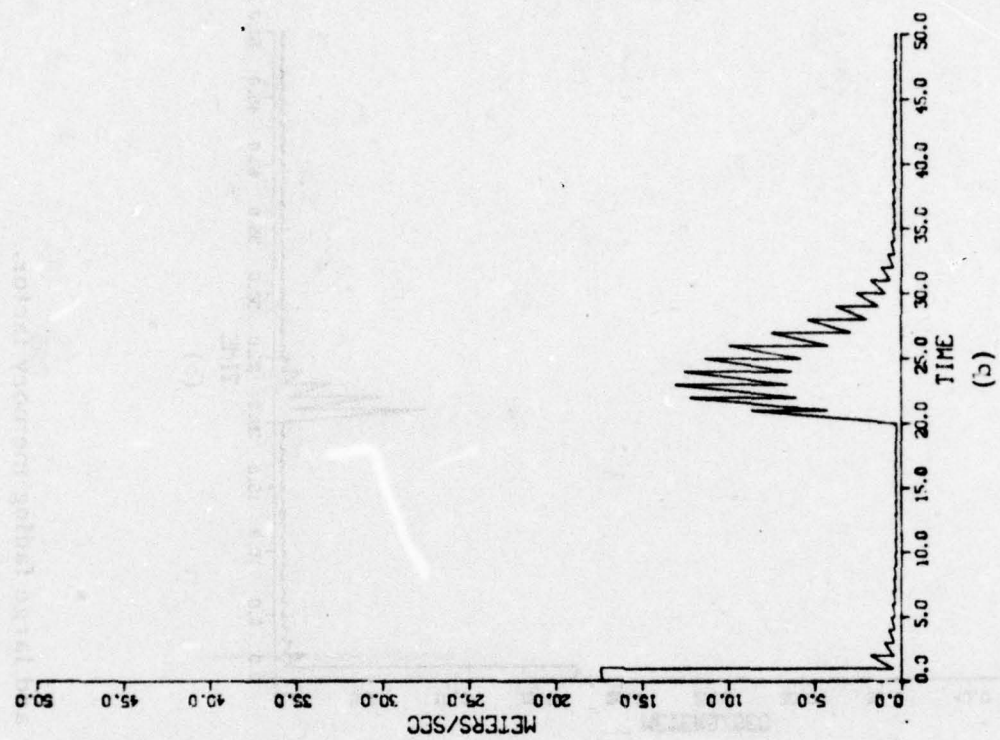
Figure 4.9 Ten-state filter with doppler and small fading memory factor.

The sensitivity of the results to the measurement errors is shown in Figures 4.10 and 4.11. The runs are the same as the one for Figure 4.9, except for the measurement errors. For Figure 4.10, the doppler error was reduced to a one-half cycle truncation error ($\sigma_{DOP}$ = .145 cycles). The results in Figure 4.11 are for a TOA measurement error $\sigma$ of 5 ns and a doppler truncation error of about 22 degrees ($\sigma_{DOP}$ = .01732 cycles).

Comparison of Figure 4.6 and 4.7 shows the advantage to be gained when using a fading memory formulation on the ten-state filter. The fade factor may, however, not be the best. The effects of different fade factors for the case where doppler measurements are made can be seen in Figures 4.8 and 4.9. The filter with the larger fade factor in Figure 4.8 has a better response to transients while the filter with the smaller fade factor has better steady state properties.

The effects of the receiver measurement errors can be determined by comparing Figures 4.9, 4.10 and 4.11. The improvement in velocity accuracy is shown by the change from Figure 4.9 to 4.10 and to 4.11. There does not, however, appear to be any improvement in position error when the TOA measurement error is reduced. This indicates that the position error is more dependent on nonreceiver related errors.

### 4.1.5.3 Eight-State Filter

The eight-state filter models position, velocity, and two-clock states only. The acceleration terms are ignored. It would be expected that the filter would not perform too well if there are accelerations. To partially compensate for this, the fading memory has been used with different fade factors.

125
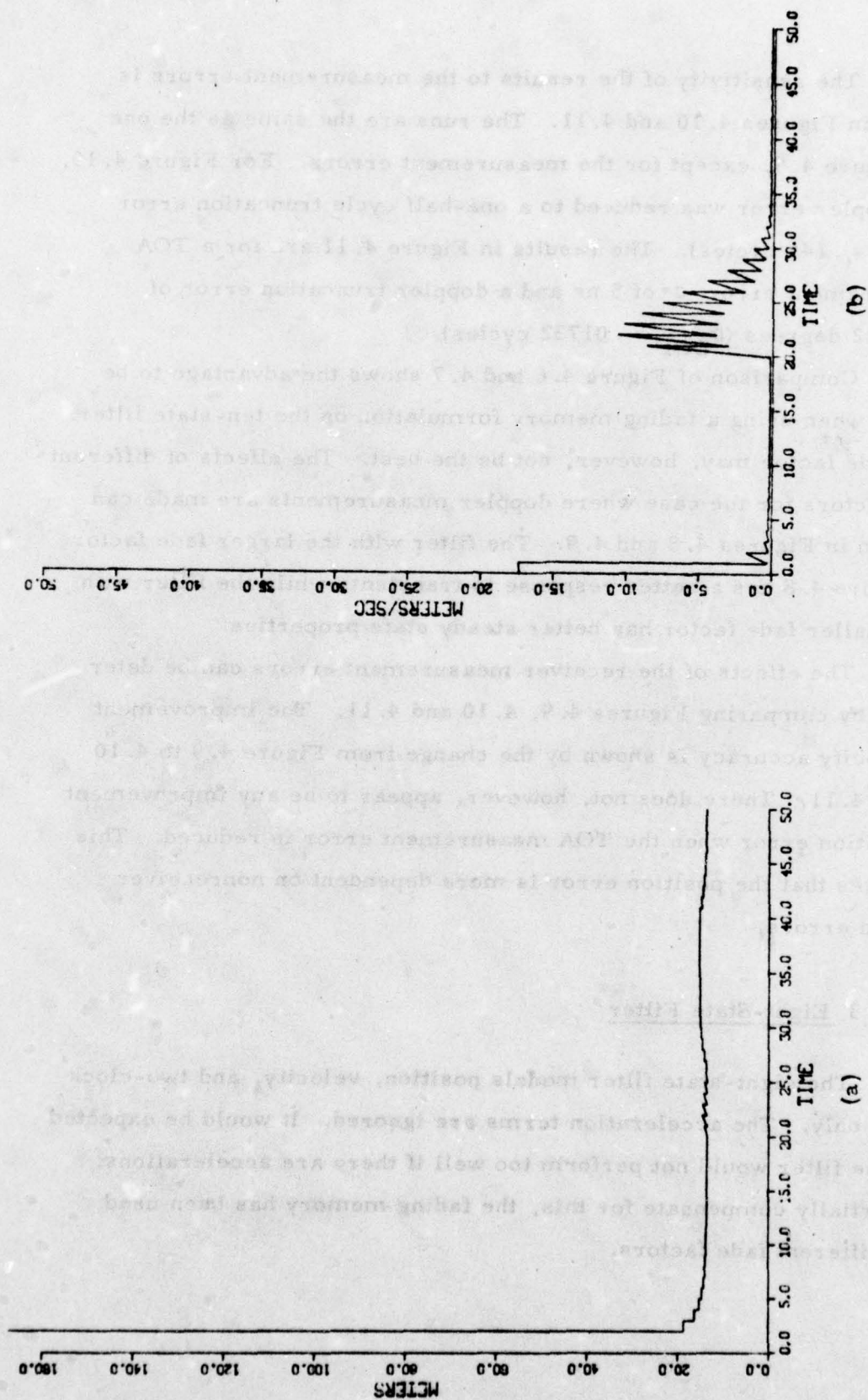
Figure 4.10 Ten-state filter with doppler and reduced doppler measurement error.
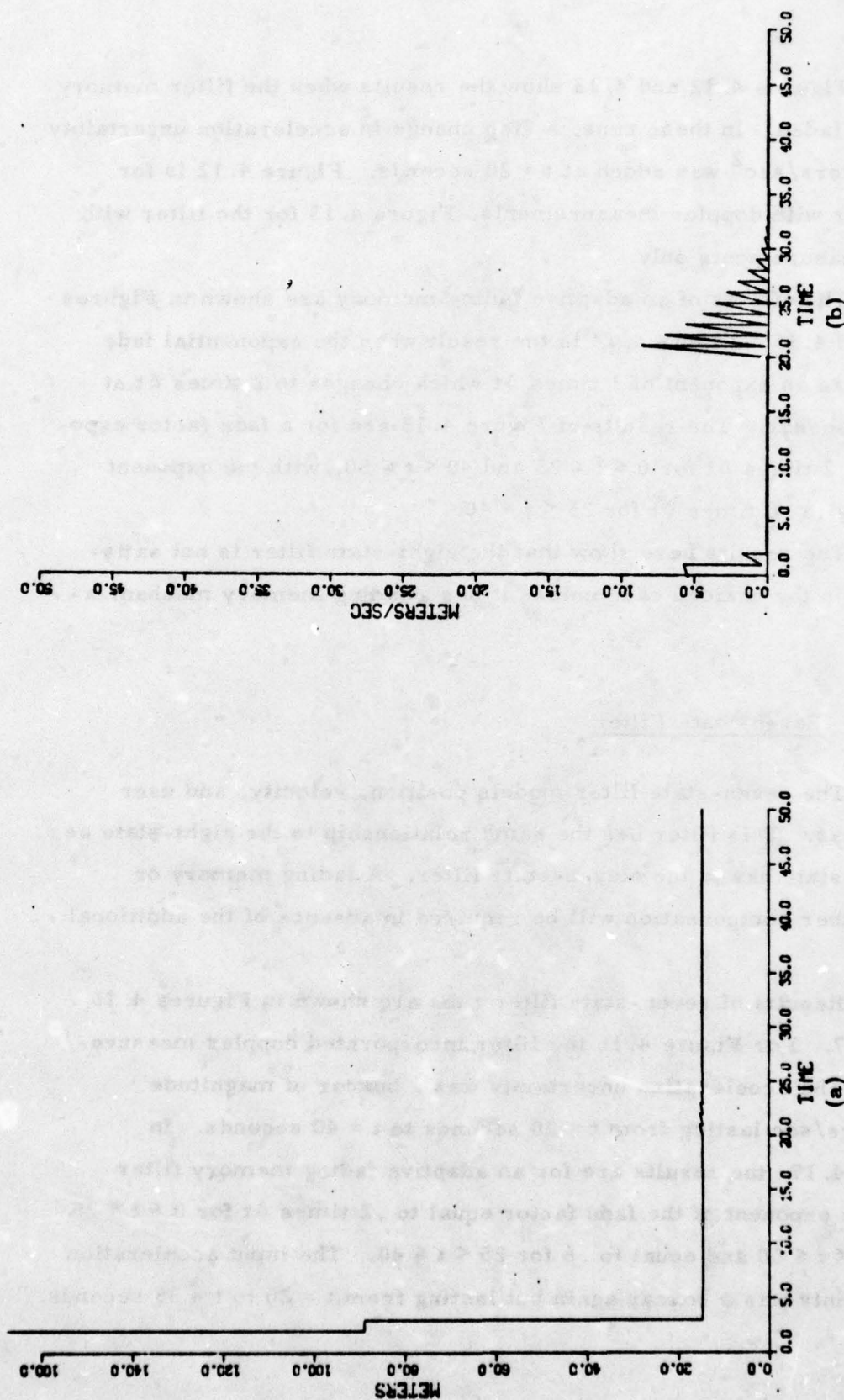
(a)

(b)

TIME

METERS/SEC

METERS

Figure 4.11, Ten-state filter with doppler and minimum measurement errors.

Figures 4.12 and 4.13 show the results when the filter memory was not faded. In these runs, a step change in acceleration uncertainty of 5 meters/sec$^2$ was added at t = 20 seconds. Figure 4.12 is for the filter with doppler measurements, Figure 4.13 for the filter with TOA measurements only.

The effects of an adaptive fading memory are shown in Figures 4.14 and 4.15. Figure 4.14 is the result when the exponential fade factor has an exponent of 1 times $\Delta t$ which changes to 2 times $\Delta t$ at t = 25 seconds. The results of Figure 4.15 are for a fade factor exponent of .2 times $\Delta t$ for $0 \le t \le 25$ and $40 < t \le 50$, with the exponent changing to .6 times $\Delta t$ for $25 < t \le 40$.

The results here show that the eight-state filter is not satisfactory in the unaided case unless it has a fading memory mechanization.

### 4.1.5.4 Seven-State Filter

The seven-state filter models position, velocity, and user clock bias. This filter has the same relationship to the eight-state as the ten-state has to the eleven-state filter. A fading memory or some other compensation will be required in absence of the additional state.

Results of seven-state filter runs are shown in Figures 4.16 and 4.17. For Figure 4.16 the filter incorporated doppler measurement. The acceleration uncertainty was a boxcar of magnitude 5 meters/sec lasting from t = 20 seconds to t = 40 seconds. In Figure 4.17, the results are for an adaptive fading memory filter with the exponent of the fade factor equal to .2 times $\Delta t$ for $0 \le t \le 25$ and $40 < t \le 50$ and equal to .6 for $25 < t \le 40$. The input acceleration uncertainty was a boxcar again but lasting from t = 20 to t = 35 seconds.
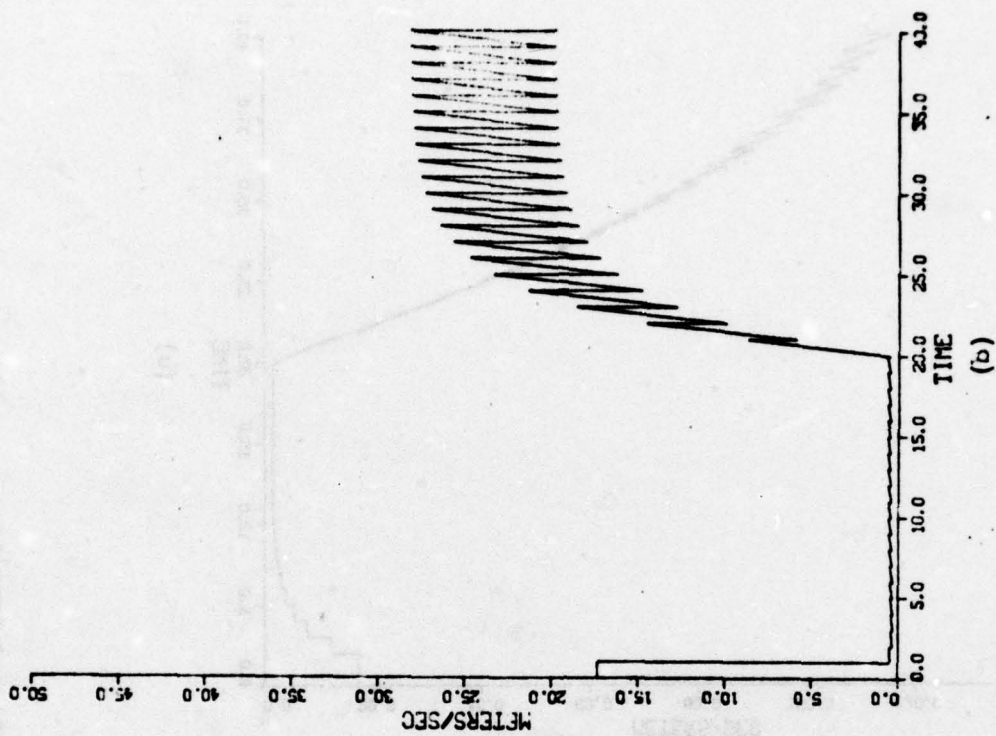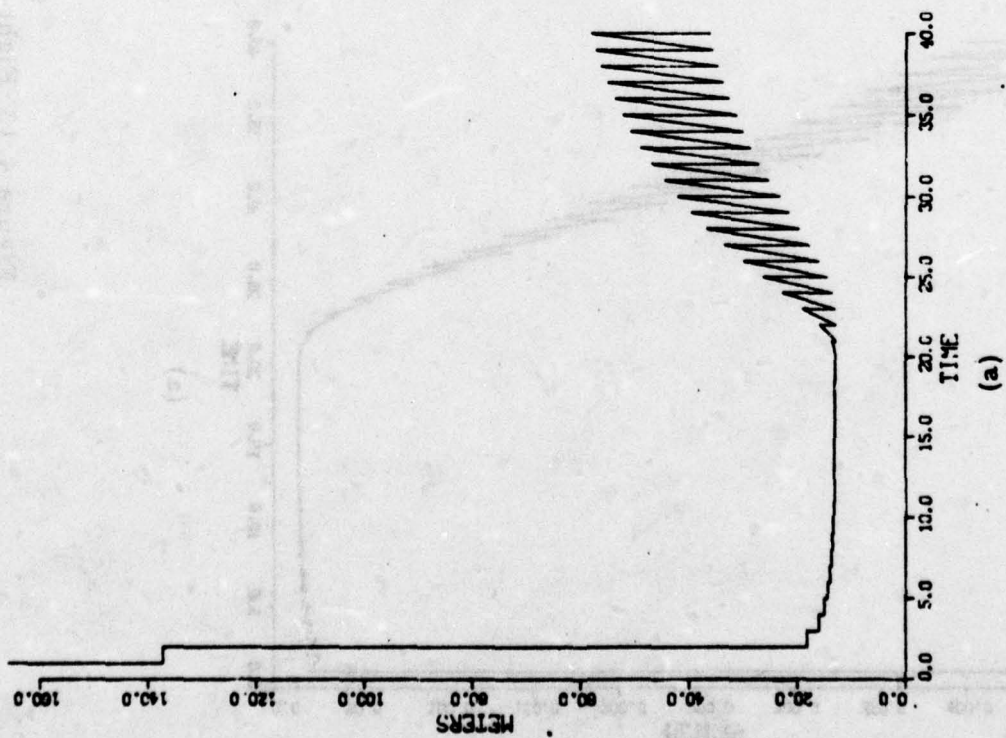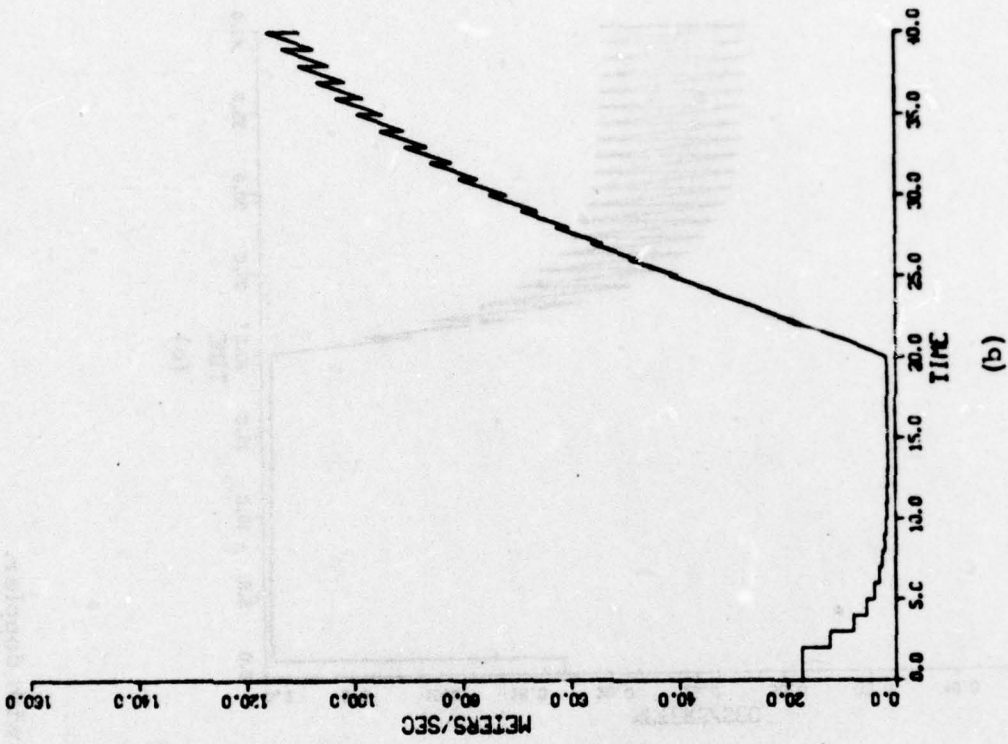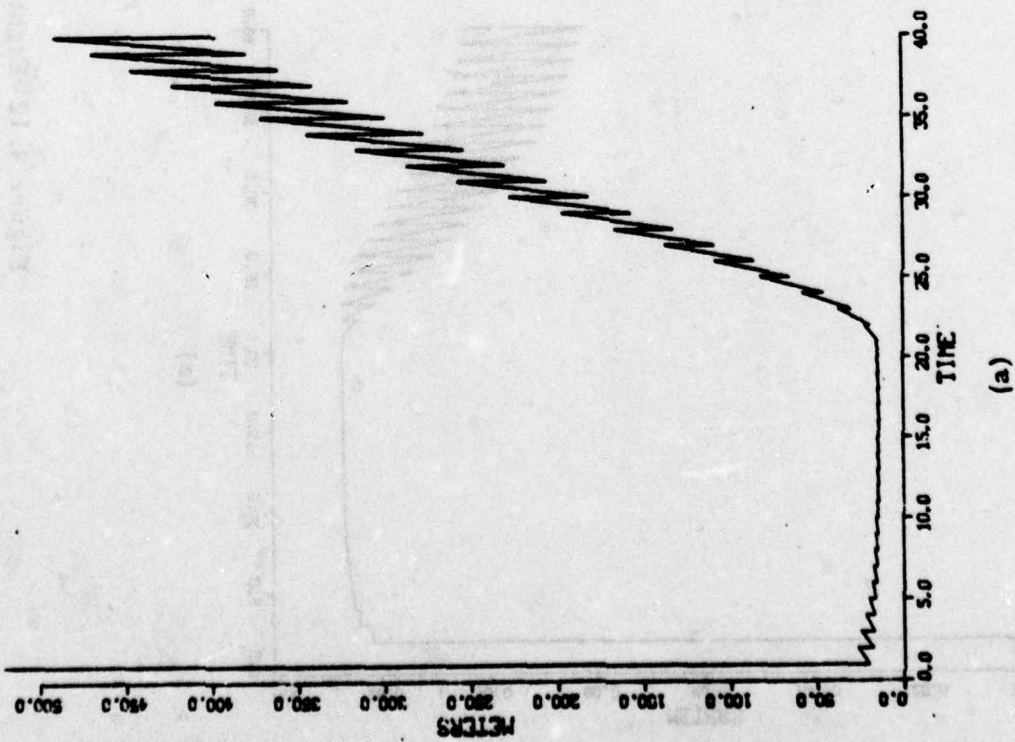
128

Figure 4.12 Eight-state filter with doppler.
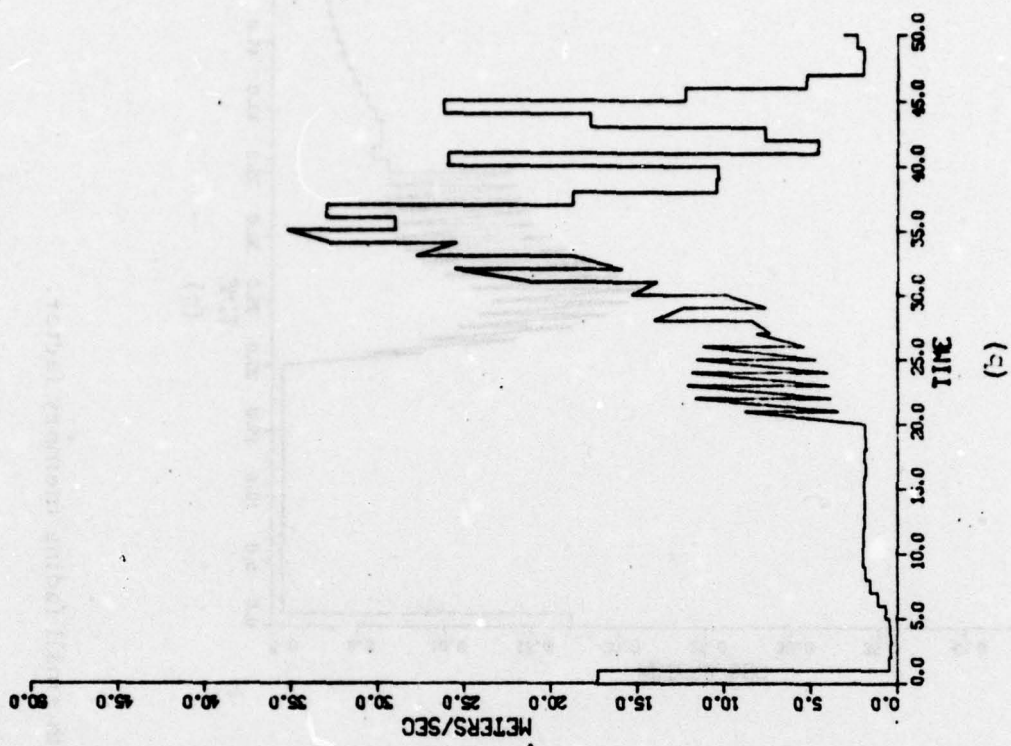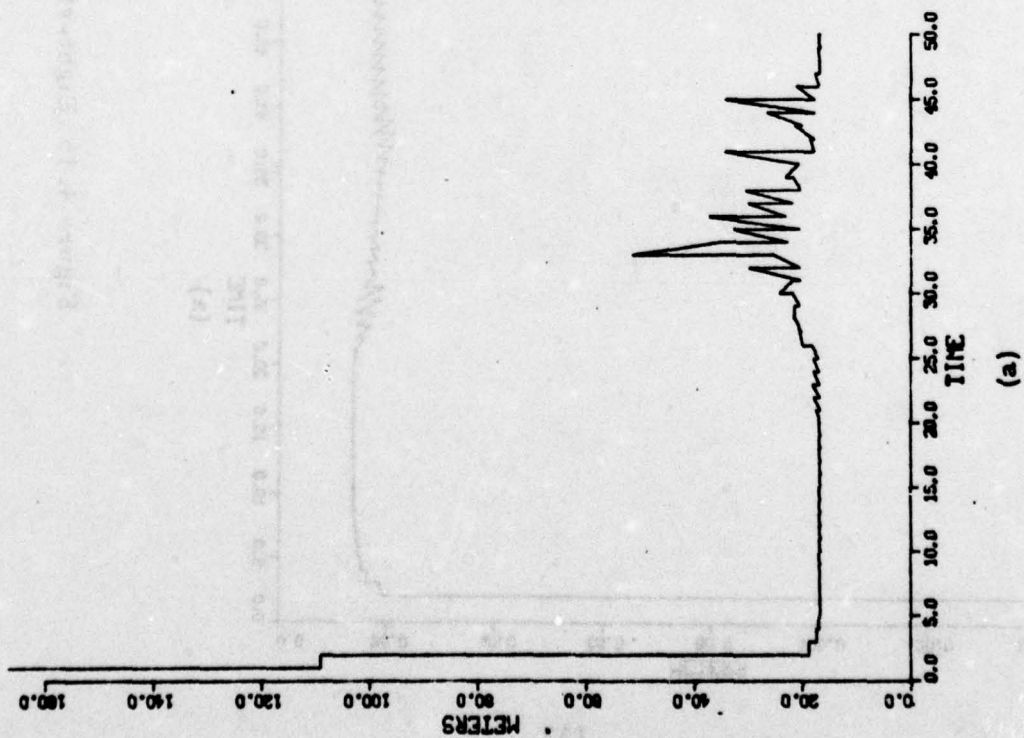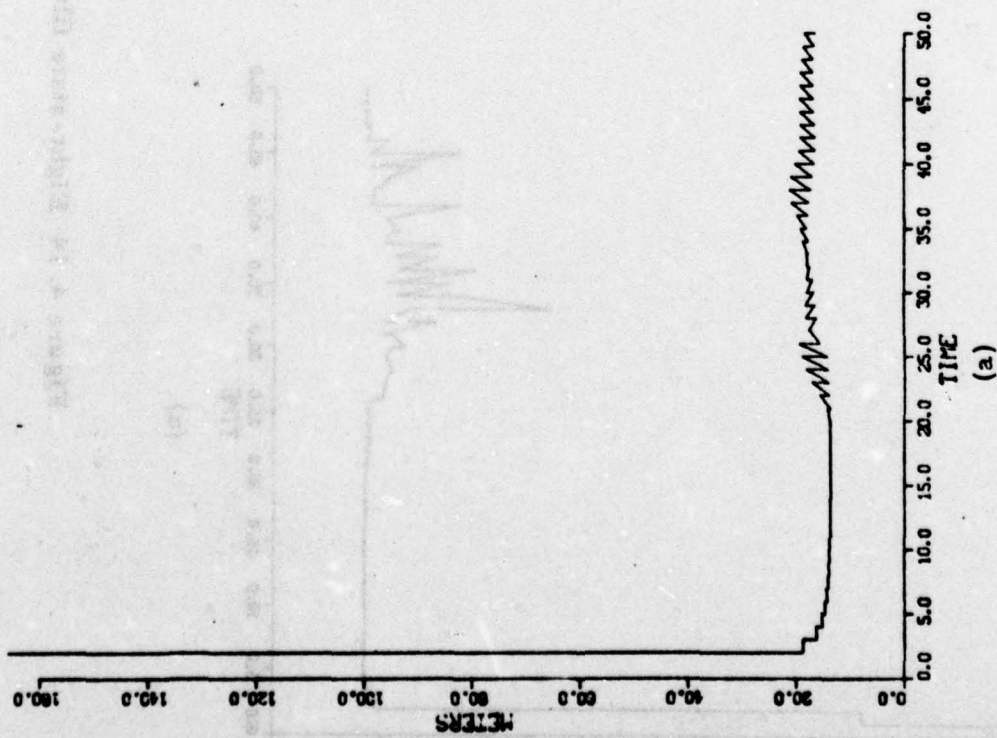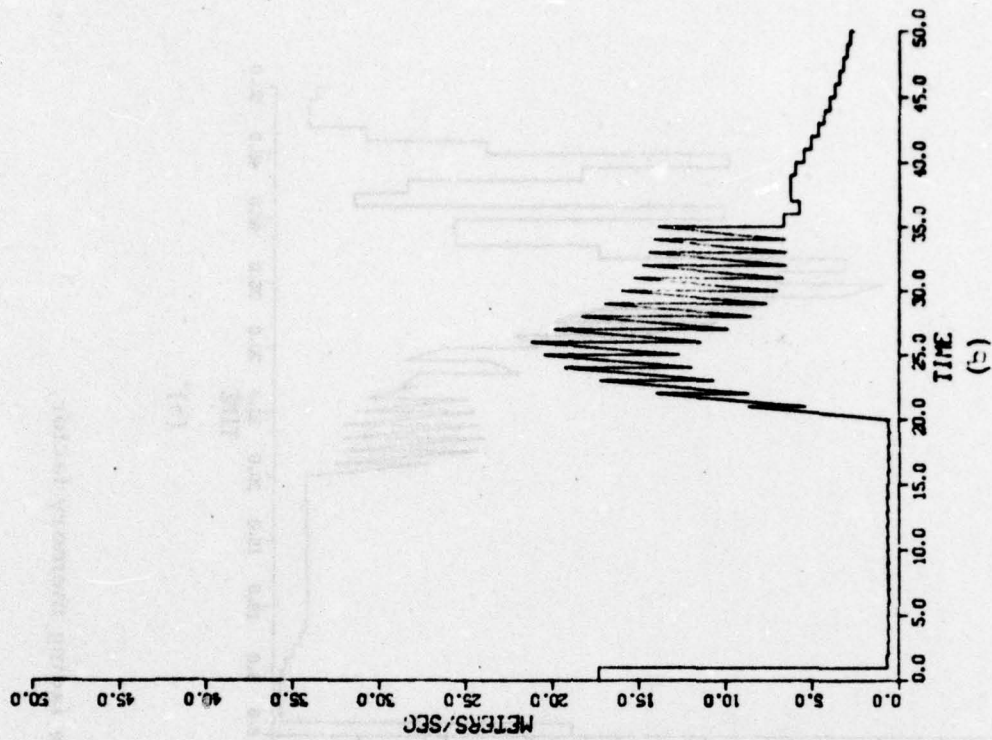
129

Figure 4.13 Eight-state filter without doppler.

130

Figure 4.14 Eight-state filter with large fading memory factor.

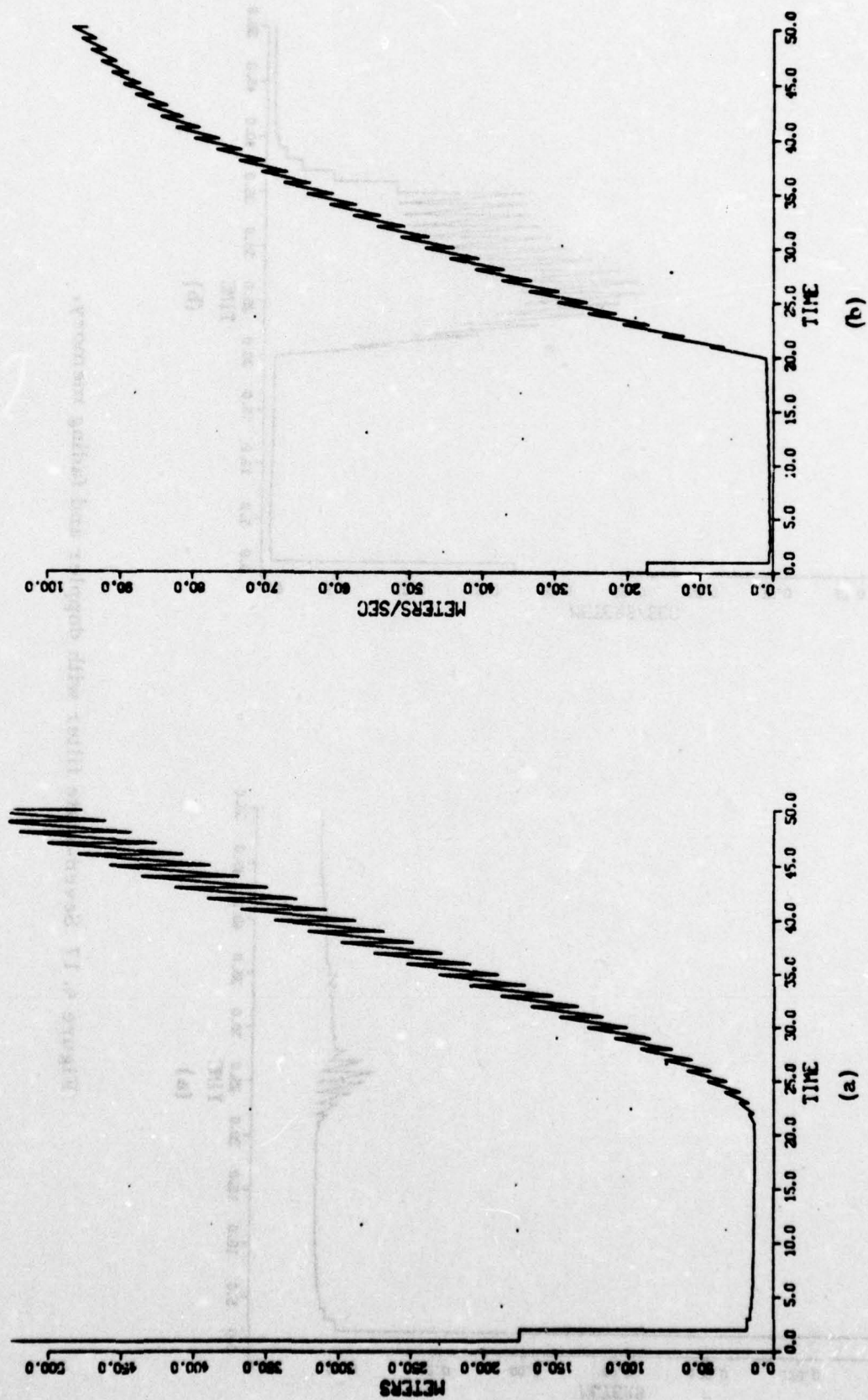Figure 4.15 Eight-state filter with small fading memory factor.

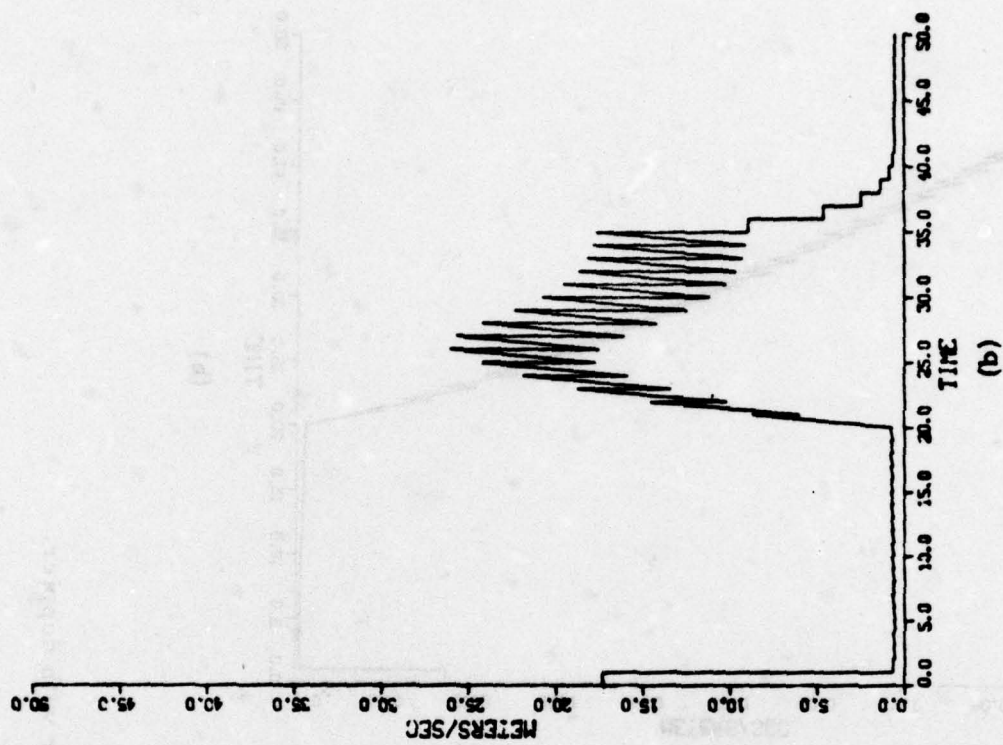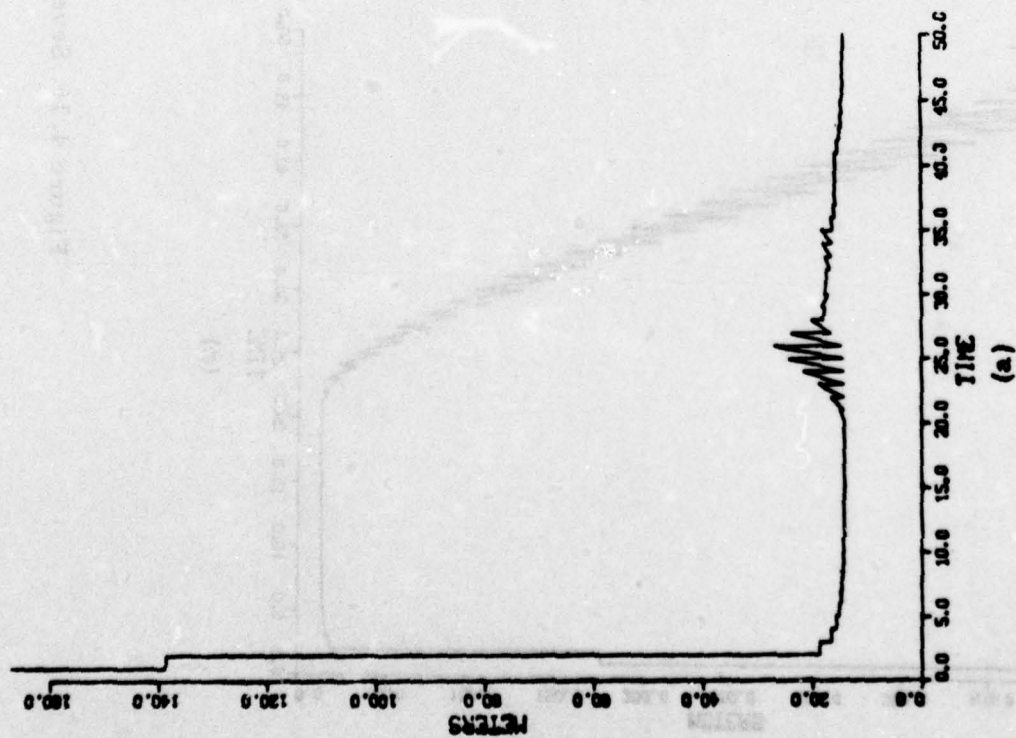Figure 4.16 Seven-state filter with doppler.

133

Figure 4.17 Seven-state filter with doppler and fading memory.

The results show that a fading memory mechanization is needed for the seven-state filter to perform in a satisfactory fashion. In fact, comparison of Figures 4.15 and 4.17 shows that the seven-state fading memory performs better than the eight-state after the transient. This is due to the fact that the time bias rate error (the eighth state) looks like an acceleration error. The additional clock state then adds damping to the filter when unmodelled accelerations are applied.

### 4.1.5.5 $\alpha$-$\beta$ Filter

This is an eight-state filter which has position, velocity, user clock bias, and user clock frequency error. The $\alpha$-$\beta$ filter must have a preprocessor such as a single fix algorithm to supply it with pseudo-measurements. The pseudo-measurements, position and user clock bias, are filtered by four two-state filters, three identical filters in position coordinates and one other for the clock. This filter has no provisions for incorporating doppler measurements.

Figure 4.18 shows the results of a covariance run with a boxcar of 5 meters/sec$^2$ acceleration uncertainty starting at t = 20 seconds and ending at t = 40 seconds. Figure 4.19 shows the results of the same run except that a fading memory filter was employed where the exponent of the fade factor was .5 times $\Delta$t. Figure 4.20 shows the results using an adaptive fading memory. The boxcar of acceleration was shortened to extend from t = 20 to t = 35. The exponent of the fade factor was .3 times $\Delta$t for $0 \leq t \leq 25$ and $40 < t \leq 50$ and it was .9 times $\Delta$t for $25 < t \leq 40$.

The $\alpha$-$\beta$ filter does not work well without a fading memory mechanization. The adaptive fading memory seems to give better steady state response and better transient recovery. The $\alpha$-$\beta$ filter, due to its inability to incorporate doppler measurements, does not give good velocity estimates.
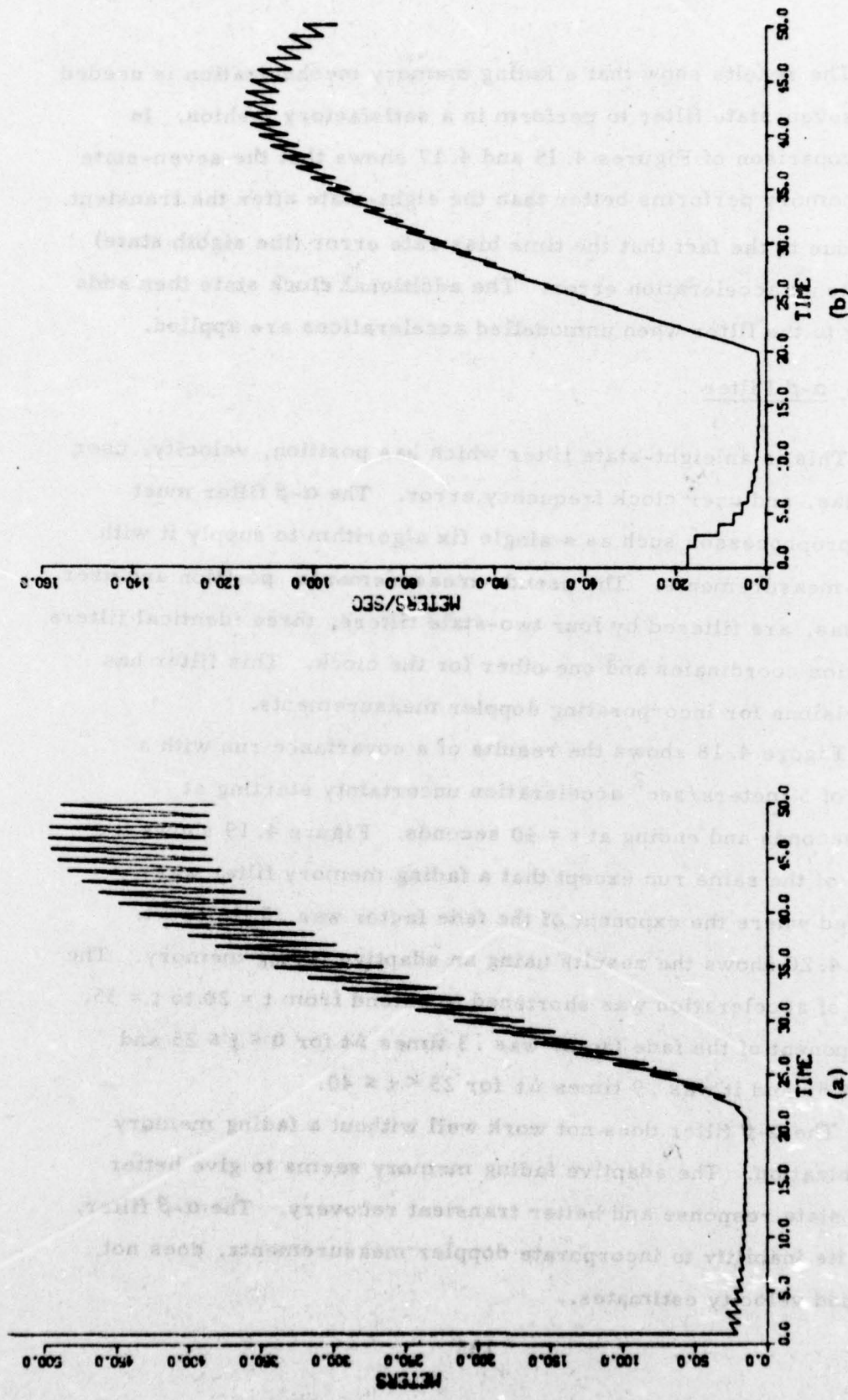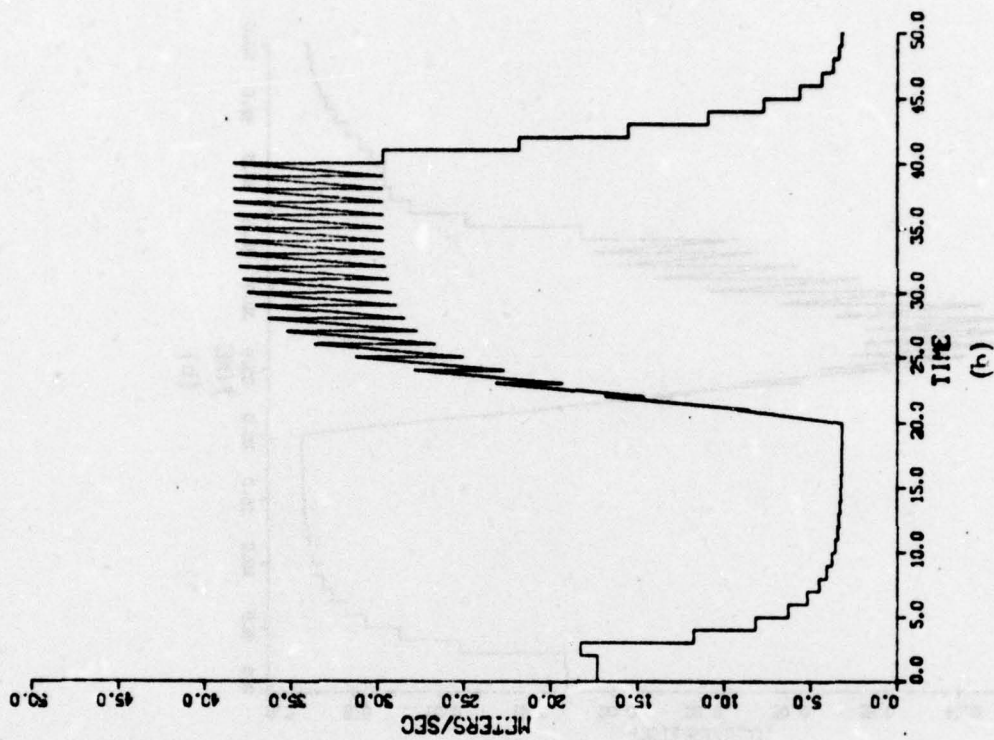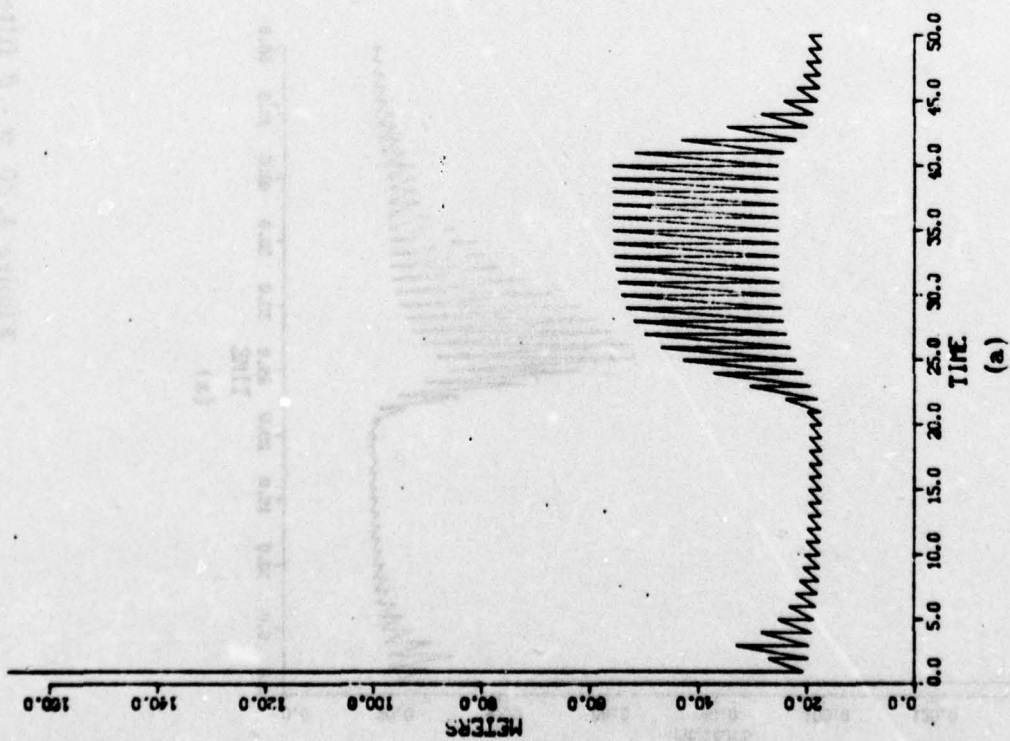
135

Figure 4.18 $\alpha - \beta$ filter.
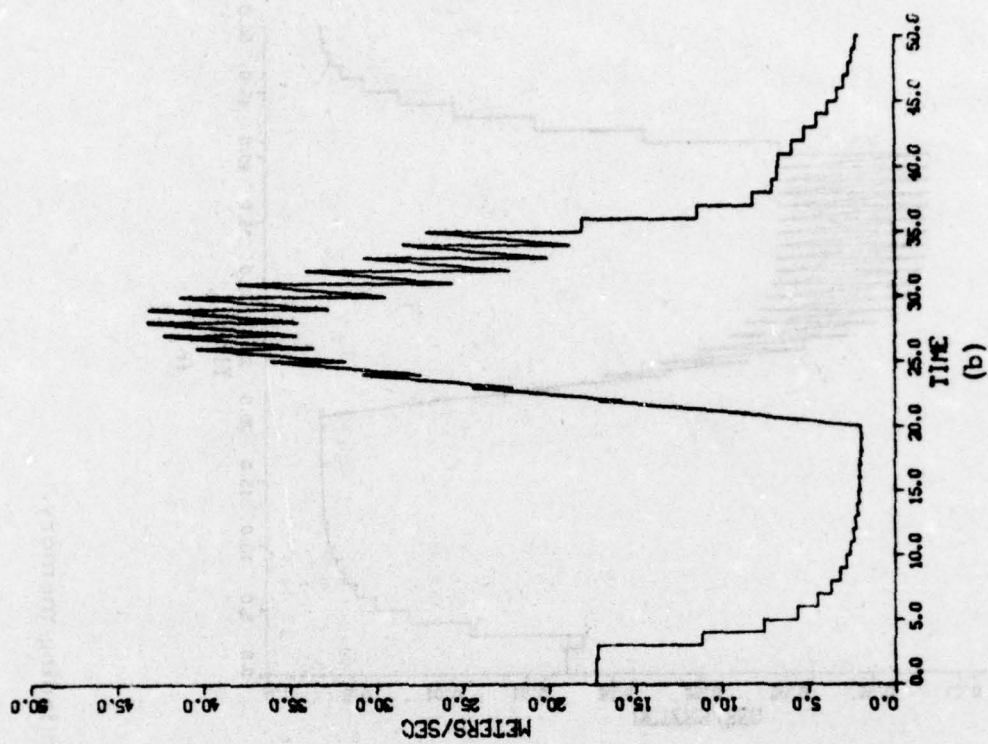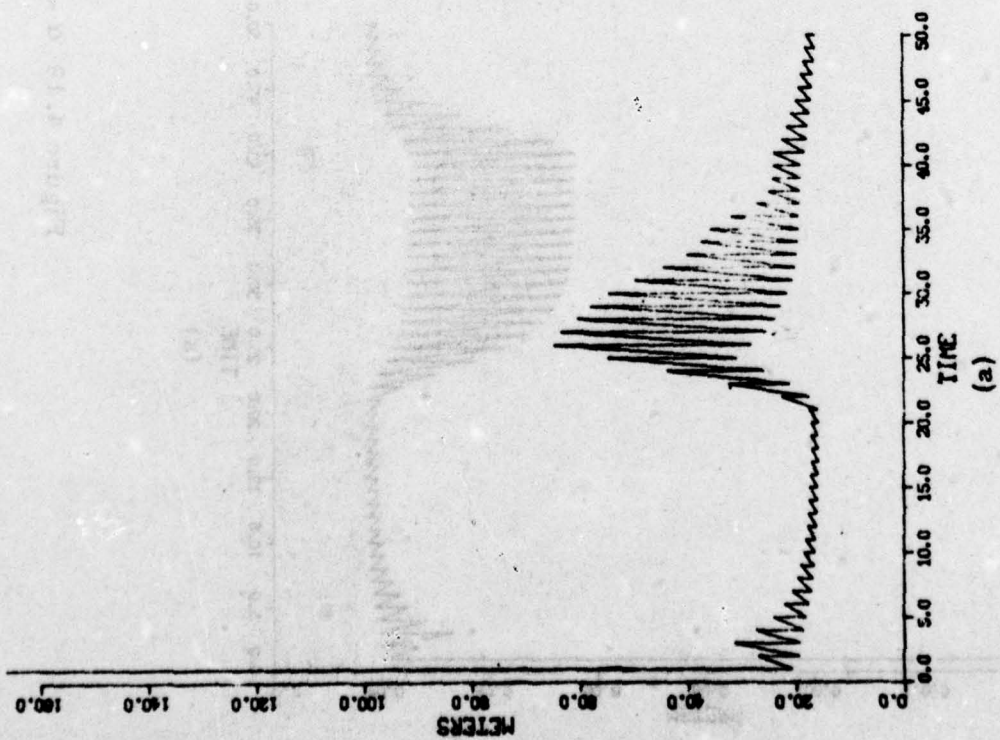
Figure 4.19 $\alpha - \beta$ filter with fading memory.

137

Figure 4.20 $\alpha - \beta$ filter with adaptive fading memory.

138

### 4.1.5.6 Other Factors

There are certain other factors which influence the filter performance which are of interest. These factors are involved in any filter mechanization. Two of these factors, geometry and update time, will be discussed in this section. Rather than carrying out the analysis for all of the filters, one particular filter was chosen as an example. The filter used was the ten-state filter with doppler measurements.

### 4.1.5.6.1 Effects of Geometry

Much analytic work has been done to study the geometric effects of the GPS determined position. The common measure for the geometric error scale factor is GDOP (see discussion in Section 2). GDOP is, however, a static measure based on a single-fix least squares position estimate. GDOP does provide a convenient performance measure to use when selecting a satellite constellation for navigation. Since GDOP was not designed as a performance measure for recursive filtering, it is of interest to use the results of covariance analysis to relate GDOP to the expected navigation error. It is also of interest to relate GDOP to the doppler derived velocity error. Figure 4.21 shows the three-axis RSS $1-\sigma$ navigation error for the ten-state fading memory filter (exponent of .2 times $\Delta t$) with doppler and the parameter values in Tables 4.1 and 4.2. The user was varied in space and time to get a range of GDOP values between 2 and 9. The values represent an approximate steady state error with no acceleration uncertainty in the reference system.
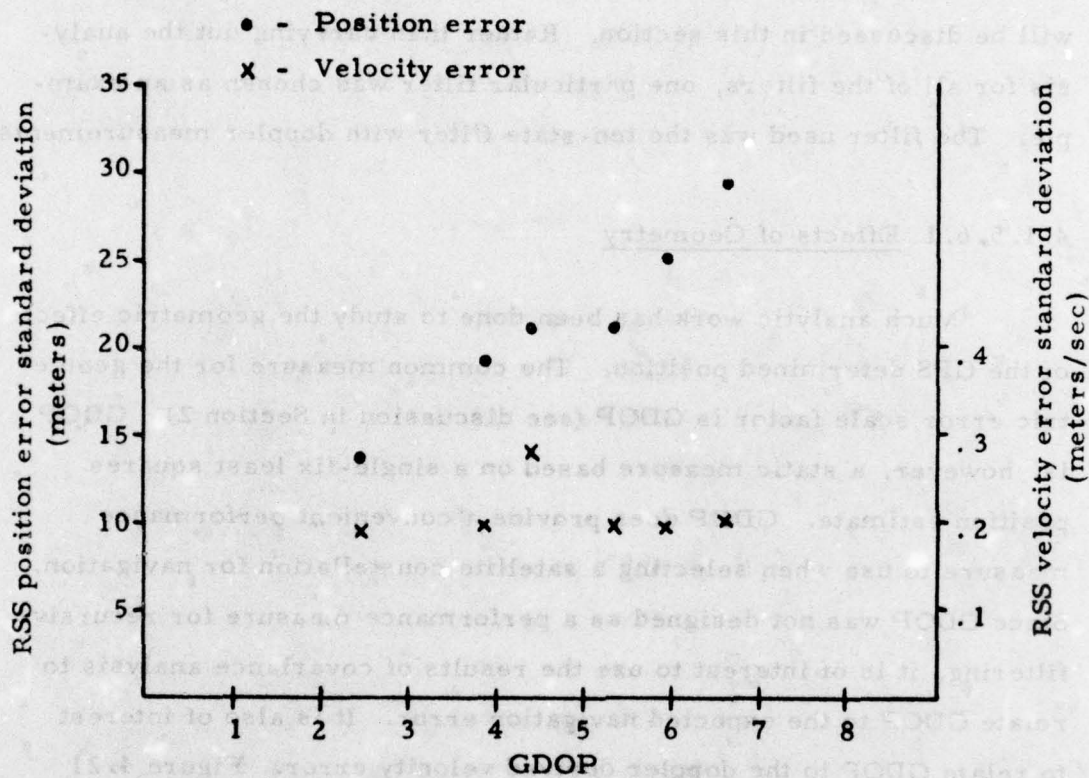
Figure 4.21 Geometric effects on navigation errors.

The results indicate that the RSS position error 1-$\sigma$ value is roughly proportional to GDOP. The RSS doppler determined velocity error 1-$\sigma$ value however appears to be independent of geometric factors. This is probably due to the fact that the dominant errors in the determined velocity are time and frequency factors and not dependent on geometry.

### 4.1.5.6.2 Measurement Rate

In the filter mechanization, the question arises as to how often measurements should be taken. Naturally the more frequent the measurements, the better the accuracy will be up to certain bounds. However, more frequent measurements require more processing of data. This then is an area of tradeoff since requiring high data processing rates implies either a faster processor is required or the processing of other functions will suffer. The sensitivity of filter performance to update time is thus of interest.

Figures 4.22 and 4.23 show the results for a state filter with update rates of 2 seconds and .5 seconds. This is the same filter as the one used to generate the results shown in Figure 4.9.

In Figure 4.24 the sequential channel filter is shown with the update rate increased to four measurements per second. This is roughly equivalent to a four satellite measurement taken every second. This result can then be compared to the results shown in Figure 4.2 which is the same filter with measurements of four satellites taken in batch each second. The result also is to be compared with the results shown in Figure 4.4 which is the sequential channel filter updated once a second or a total of four seconds for an entire round robin.
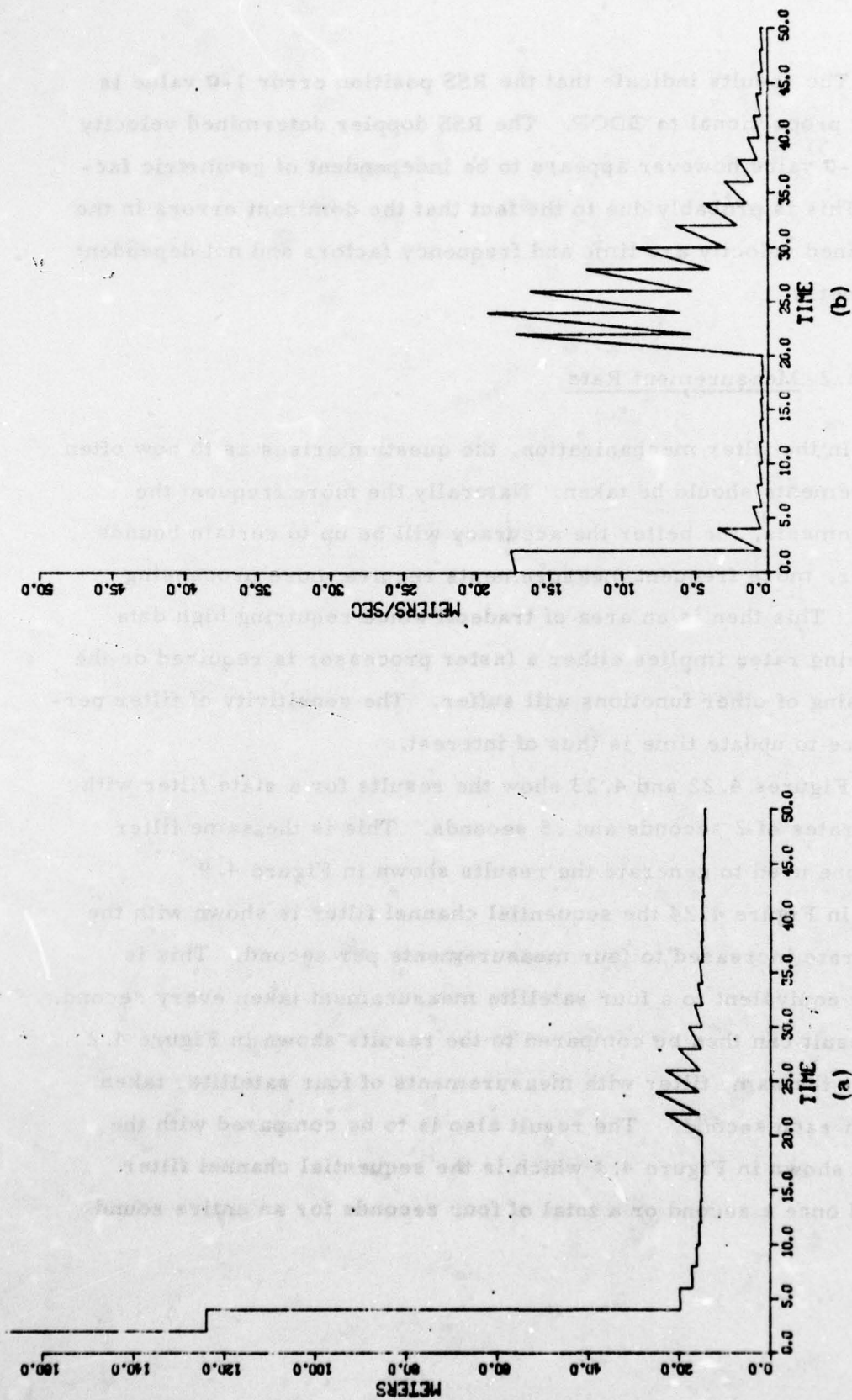
141

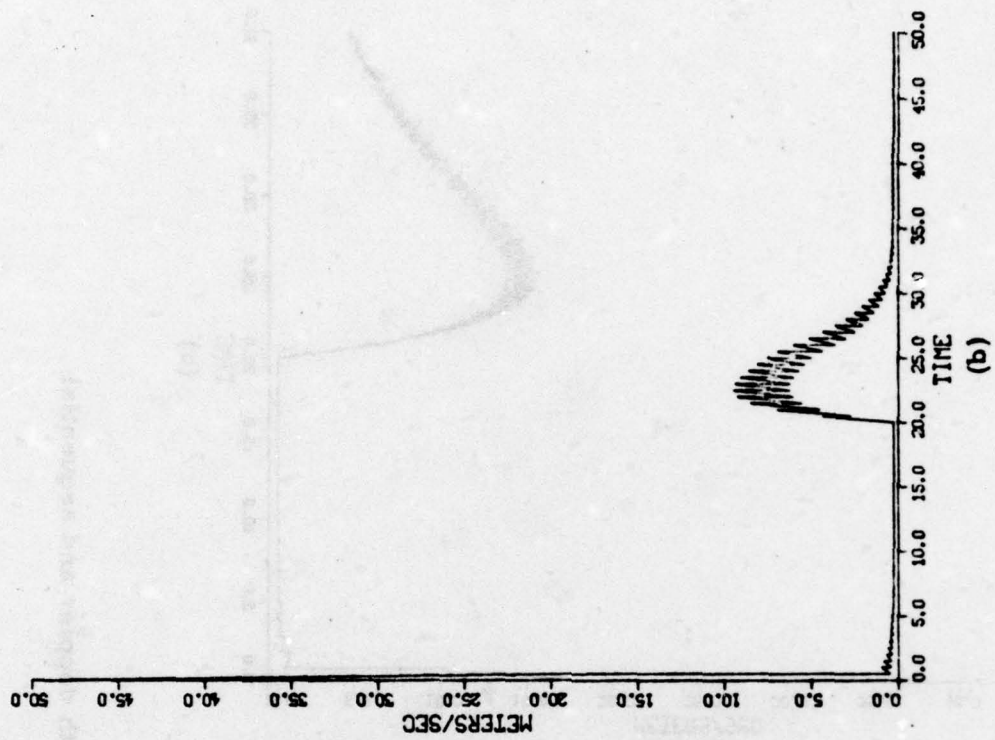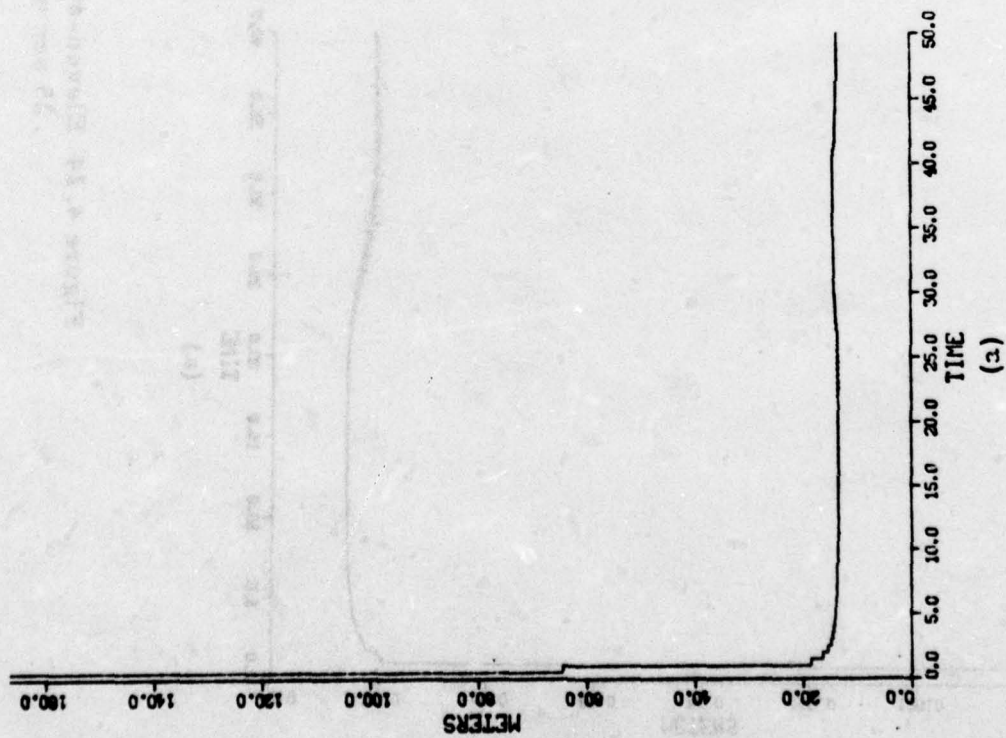Figure 4.22  Ten-state filter with 2 sec update rate.
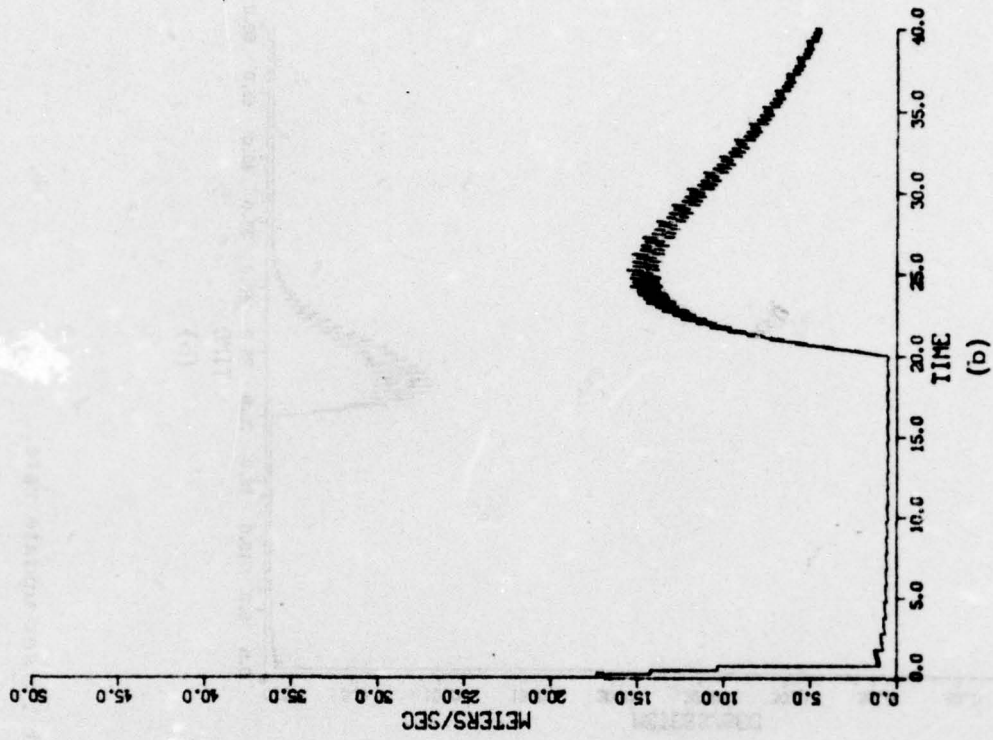
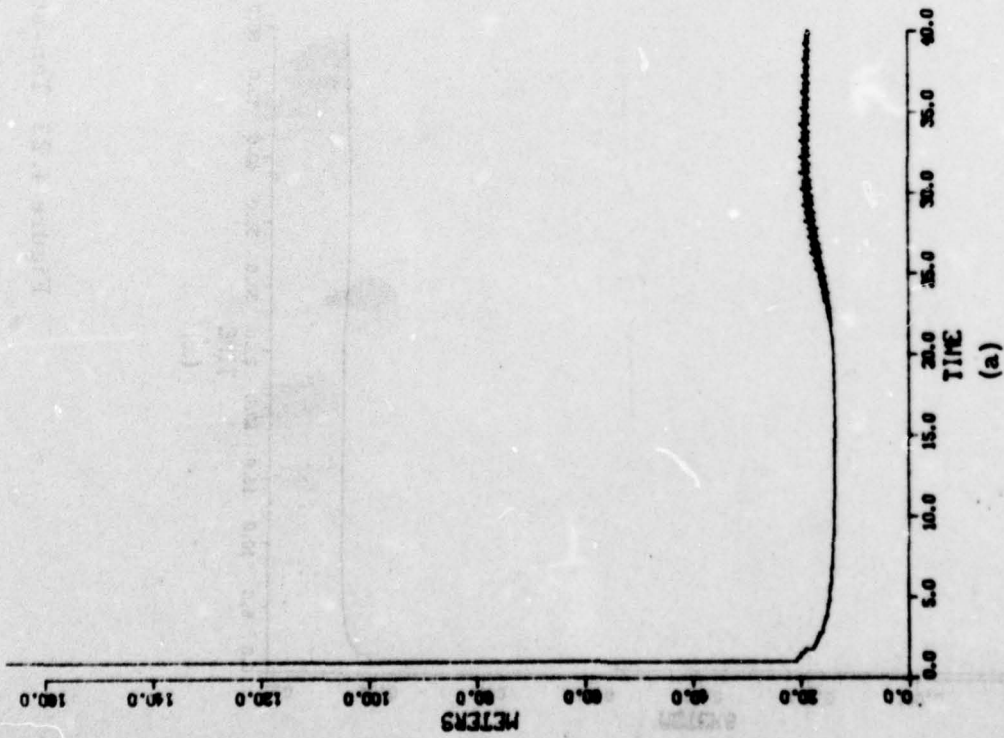Figure 4.23 Ten-state filter with .5 sec update rate.

Figure 4.24 Eleven-state filter with doppler and sequential
.25 sec update rate.

144

#### 4.1.5.7  Error Source Sensitivities

The actual values in an error sensitivity are dependent upon many parameters of the filter mechanization. The idea in this sub-section is to find the approximate sensitivity to the major reference system error sources. The sensitivity to measurement error and geometry have been discussed previously. The error sources to be considered are the ionospheric delay error, the satellite position errors, the satellite clock errors, measurement errors, and the user clock error model. The percent of total error is given in Table 4.5 for the steady state RSS position and velocity error variances for two particular filters. The two filters are the ten-state and the seven-state fading memory filters with a fade constant exponent equal to .2 times $\Delta t$.

#### 4.1.6  Summary

A summary of the covariance analysis runs showing the exact standard deviation values for steady state (just prior to the unmodelled acceleration) and the exact standard deviation values of the peak transient is presented in Table 4.6.

#### 4.2    Monte Carlo Verification

The covariance analysis method employed is only approximate since it attempts to simulate an entire ensemble of maneuvers while using the linearized model which assumes no maneuver. The error made in this approach was assumed a priori to be small. It is neces-sary then to verify this assumption. This will be done by Monte Carlo simulation runs over selected scenarios. It will not be, however, an extensive Monte Carlo analysis.

#### 4.2.1  Monte Carlo Simulation

The Monte Carlo simulation will be done with the same com-puter analysis program, CANOMIS, that was used in the covariance analysis. This ensures that the same models are being used. The difference is that instead of propagating a covariance matrix, a

## Table 4.5 Filter Error Budget

| Error Source | 10-State Filter | | 7-State Filter | |
|---|---|---|---|---|
| | % of 3-axis position error variance sum | % of 3-axis velocity error variance sum | % of 3-axis position error variance sum | % of 3-axis velocity error variance sum |
| Ionospheric delay error | 54.7 | ~ 0 | 53.5 | ~ 0 |
| Satellite position error (all satellite) | 25.7 | ~ 0 | 25.2 | ~ 0 |
| TOA measurement error | 19.2 | ~ 0 | 18.8 | ~ 0 |
| Acceleration disturbance | ~ 0 | ~ 0 | ~ 0 | 47. |
| User clock | ~ 0 | 1. | 2. | 44.7 |
| Doppler measurement error | ~ 0 | 98. | ~ 0 | 8. |

146

## Table 4.6  Covariance Analysis Summary

| Figure No. | Steady State Standard Deviation (Extrapolation Value) | | Peak Standard Deviation during Transient | |
|---|---|---|---|---|
| | Position (Meter) | Velocity (Meter/sec) | Position (Meters) | Velocity (Meters/sec) |
| 4.1 | 16.27 | 2.96 | 76.29 | 35.23 |
| 4.2 | 13.2 | .28 | 21.40 | 17.94 |
| 4.3 | 24.68 | 5.12 | 134.67 | 45.78 |
| 4.4 | 15.92 | .62 | 50.02 | 28.08 |
| 4.5 | 14.03 | .33 | 15.77 | 12.94 |
| 4.6 | 16.27 | 2.98 | 110.46 | 38.94 |
| 4.7 | 18.47 | 4.18 | 37.58 | 25.26 |
| 4.8 | 16.78 | .62 | 17.33 | 8.63 |
| 4.9 | 13.51 | .33 | 15.31 | 13.08 |
| 4.10 | 13.48 | .20 | 15.29 | 10.69 |
| 4.11 | 14.58 | .05 | 15.21 | 8.66 |
| 4.12 | 12.99 | .64 | 58.2 | 28.28 |
| 4.13 | 15.03 | 1.79 | 489.90 | 116.00 |
| 4.14 | 17.01 | 1.92 | 37.45 | 26.12 |
| 4.15 | 13.70 | .67 | 20.92 | 20.51 |
| 4.16 | 13.32 | 1.12 | 557.79 | 96.76 |
| 4.17 | 14.25 | .82 | 27.03 | 26.06 |
| 4.18 | 15.54 | 1.82 | 496.68 | 115.35 |
| 4.19 | 19.36 | 3.21 | 55.86 | 38.38 |

Table 4. 6 (continued)

| | | | | |
|---|---|---|---|---|
| 4.20 | 17.14 | 2.02 | 64.82 | 43.24 |
| 4.22 | 15.14 | .46 | 25.18 | 19.24 |
| 4.23 | 13.44 | .25 | 14.39 | 9.42 |
| 4.24 | 13.94 | .52 | 20.18 | 15.41 |

reference system state vector is propagated and the measurement matrix is linearized about a simulated trajectory.

The Monte Carlo simulations use gains generated by the candidate filter and with these gains process the simulated data according to equation (4.6). The simulated data is generated from equation (4.2) by replacing the noise vectors with white Gaussian pseudo-random number vectors with the appropriate variances.

The scenarios used are the ones outlined in Section 1. The satellite selection was done using the approximate volume minimization algorithm described in Section 2. The verification runs were made with the ten-state filter, the eight-state filter, and the $\alpha$-$\beta$ filter, all using doppler measurements but otherwise unaided. These were chosen as representative of all the filters analyzed.

As in Section 4.1, the results will be shown via plots of the 3-axis RSS position and velocity error. The (a) part of each figure is the position error and the (b) part is the velocity error.

### 4.2.2 Monte Carlo Results

The results of several Monte Carlo simulations are shown in Figures 4.25 through 4.31. Figures 4.25 and 4.26 show the results of the eight-state fading memory filter with the fade constant exponent equal to .33 times $\Delta t$. Figure 4.25 shows the results for the ship scenario and Figure 4.26 for the aircraft scenario. The results for a ten-state fading memory filter with the fade constant exponent equal to .33 times $\Delta t$ applied to the ship scenario are shown in Figure 4.27. Figures 4.28 to 4.30 are a series of ten-state fading memory filters with different fade constants (exponents equal to .2 $\Delta t$, .33 $\Delta t$, and .5 $\Delta t$, respectively) applied to the aircraft

(a)
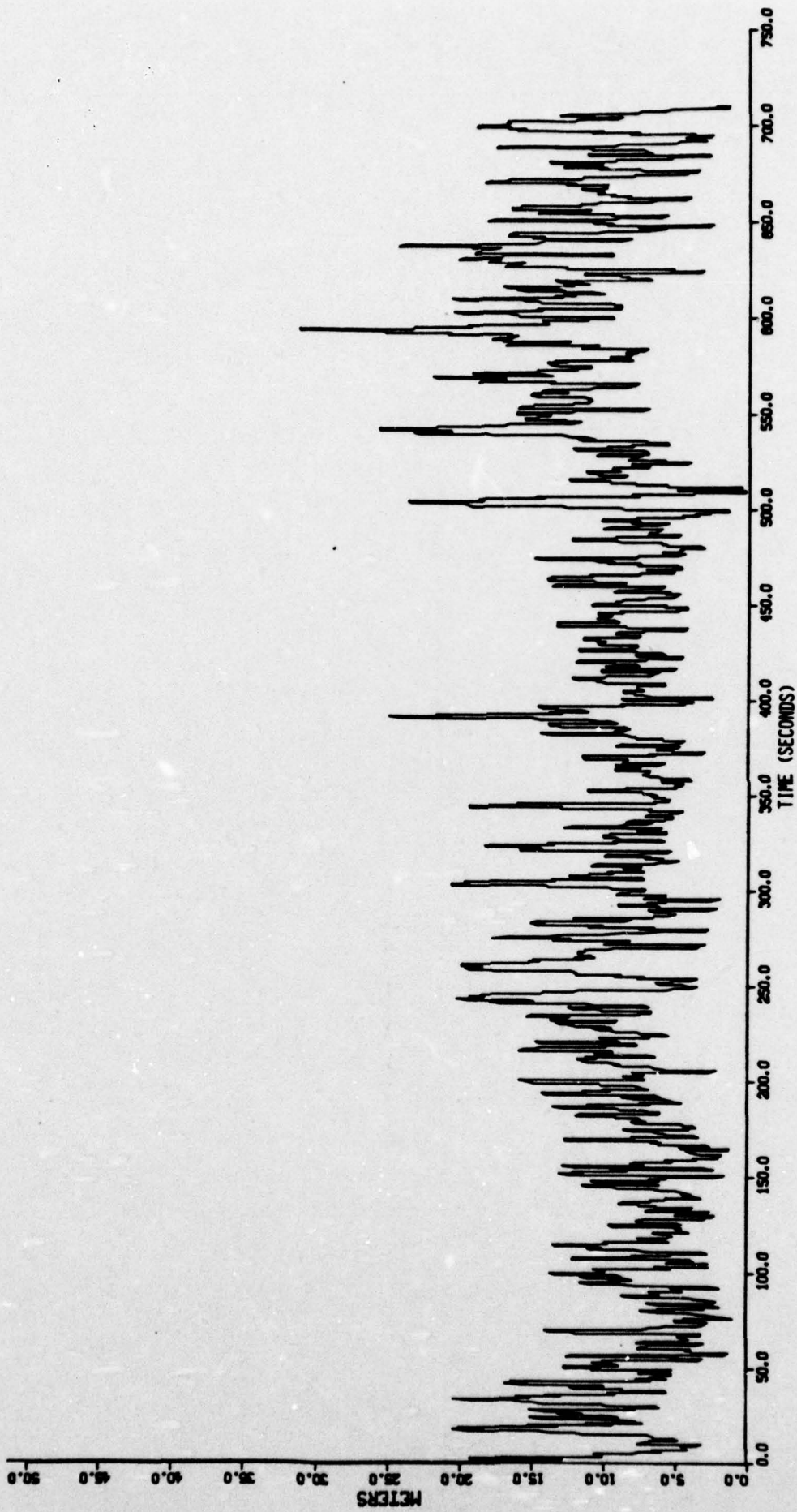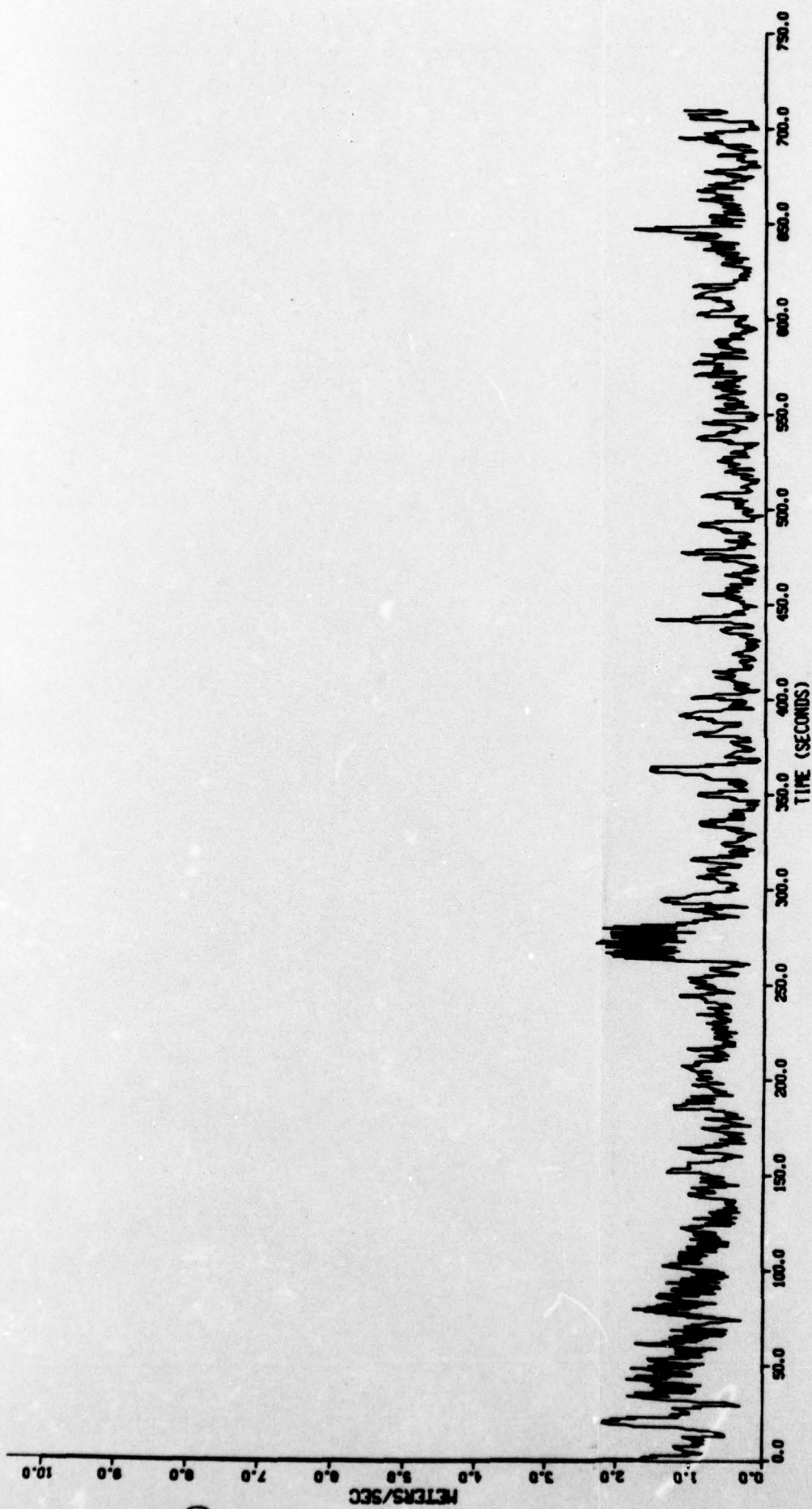
Figure 4.25 Eight-state fading memory filter with ship scenario.

(b)

150

(a)
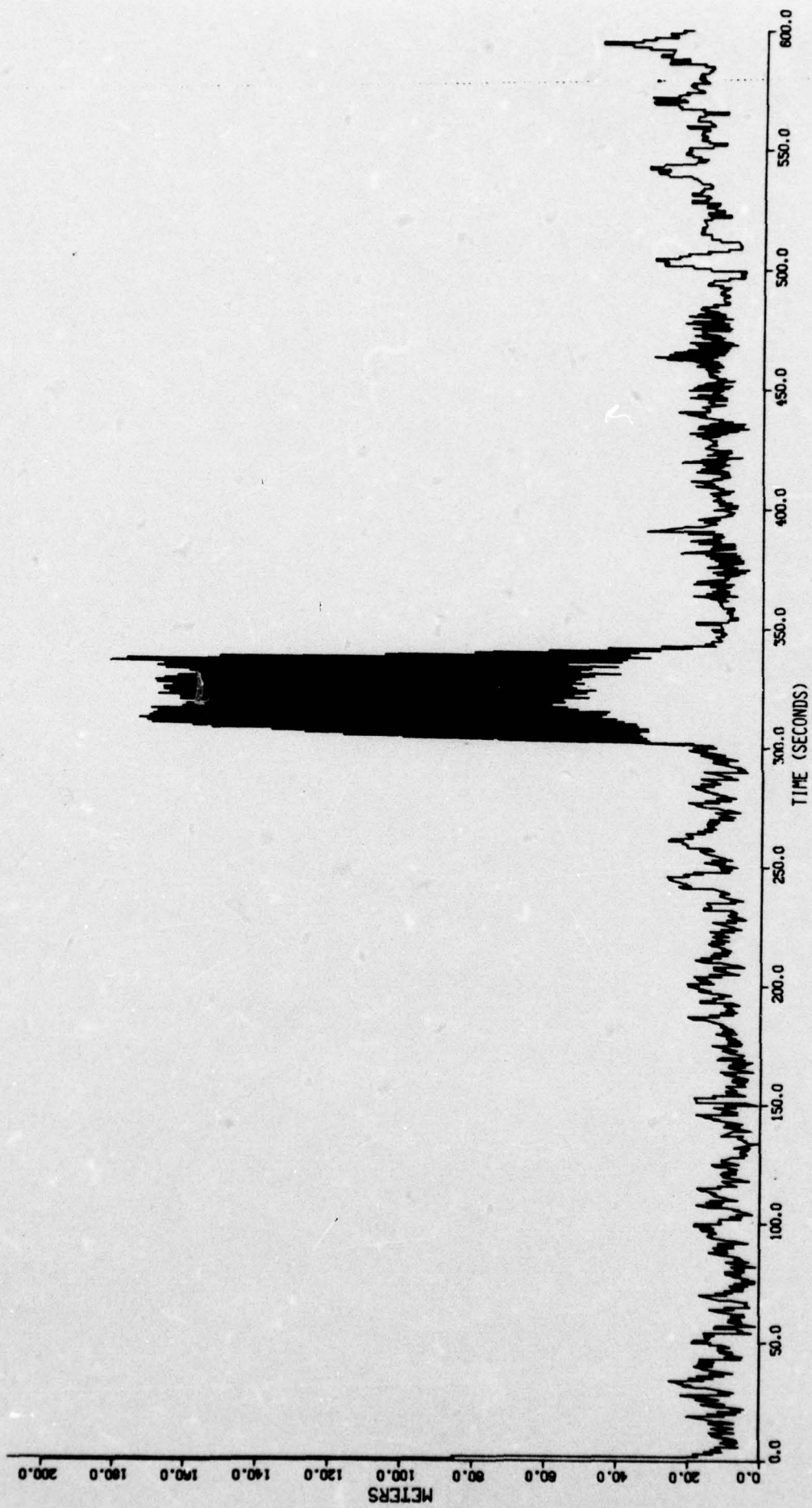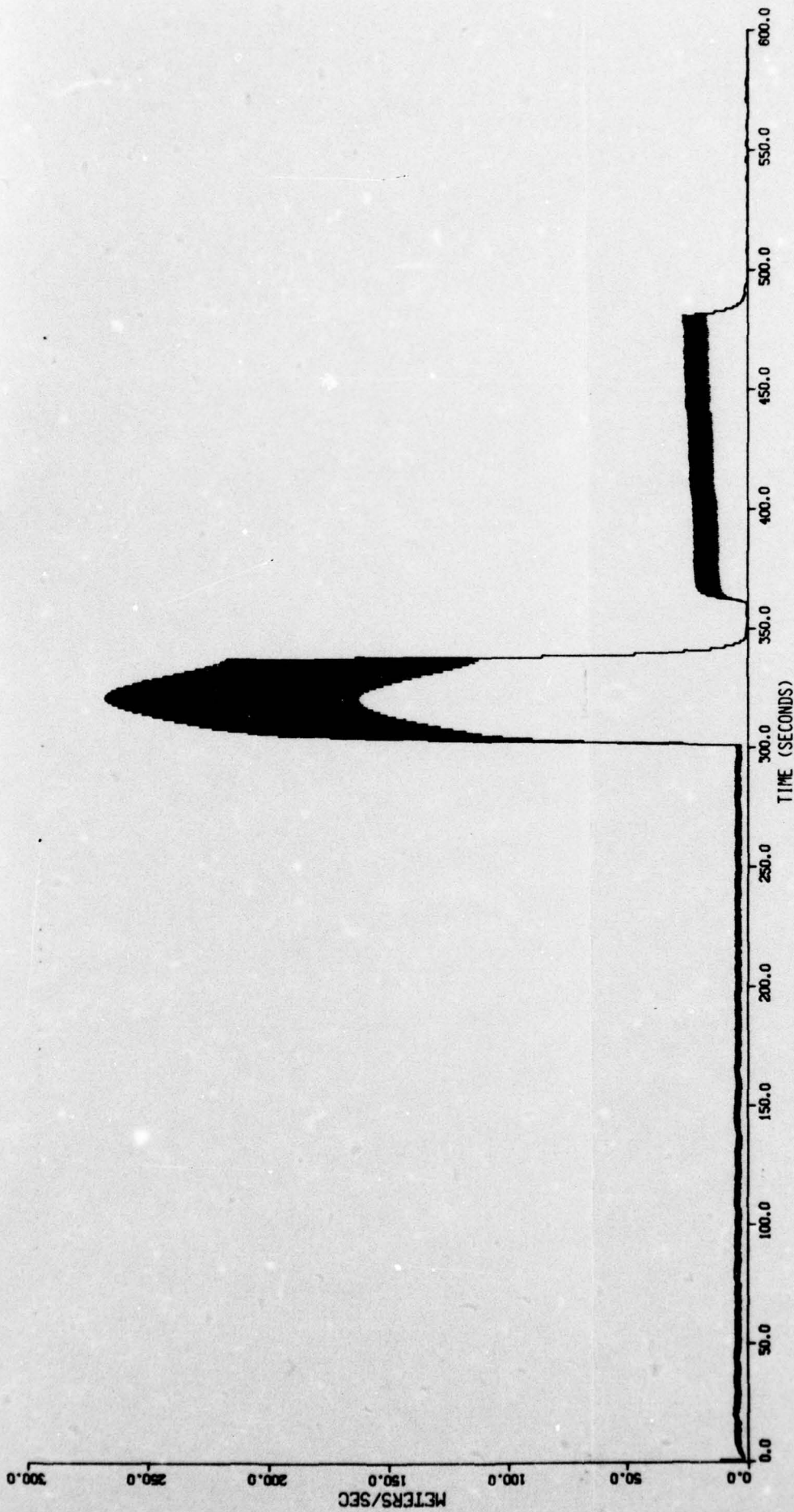
Figure 4.26 Eight-state fading memory filter with aircraft scenario.

(b)

151

(a)
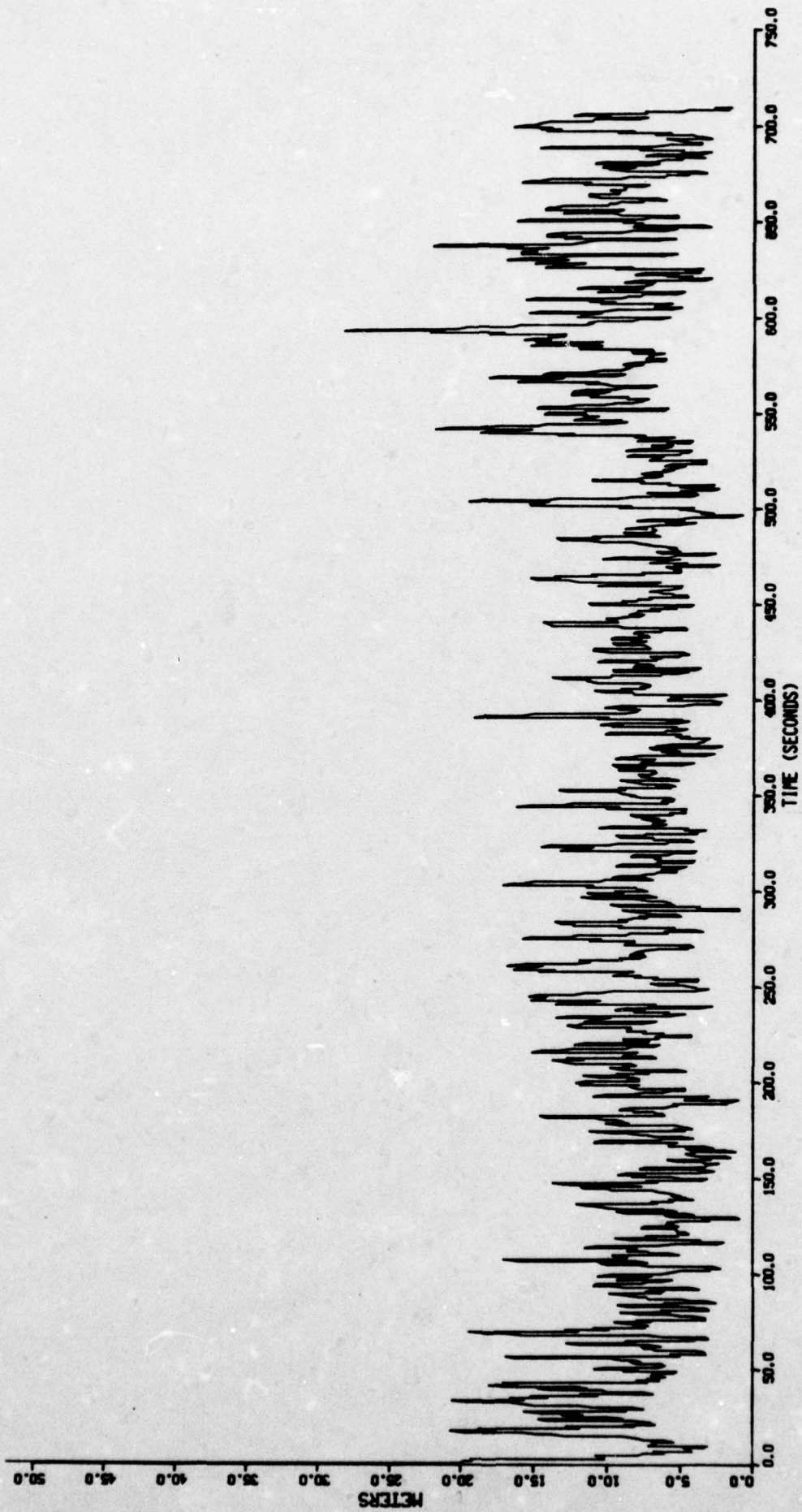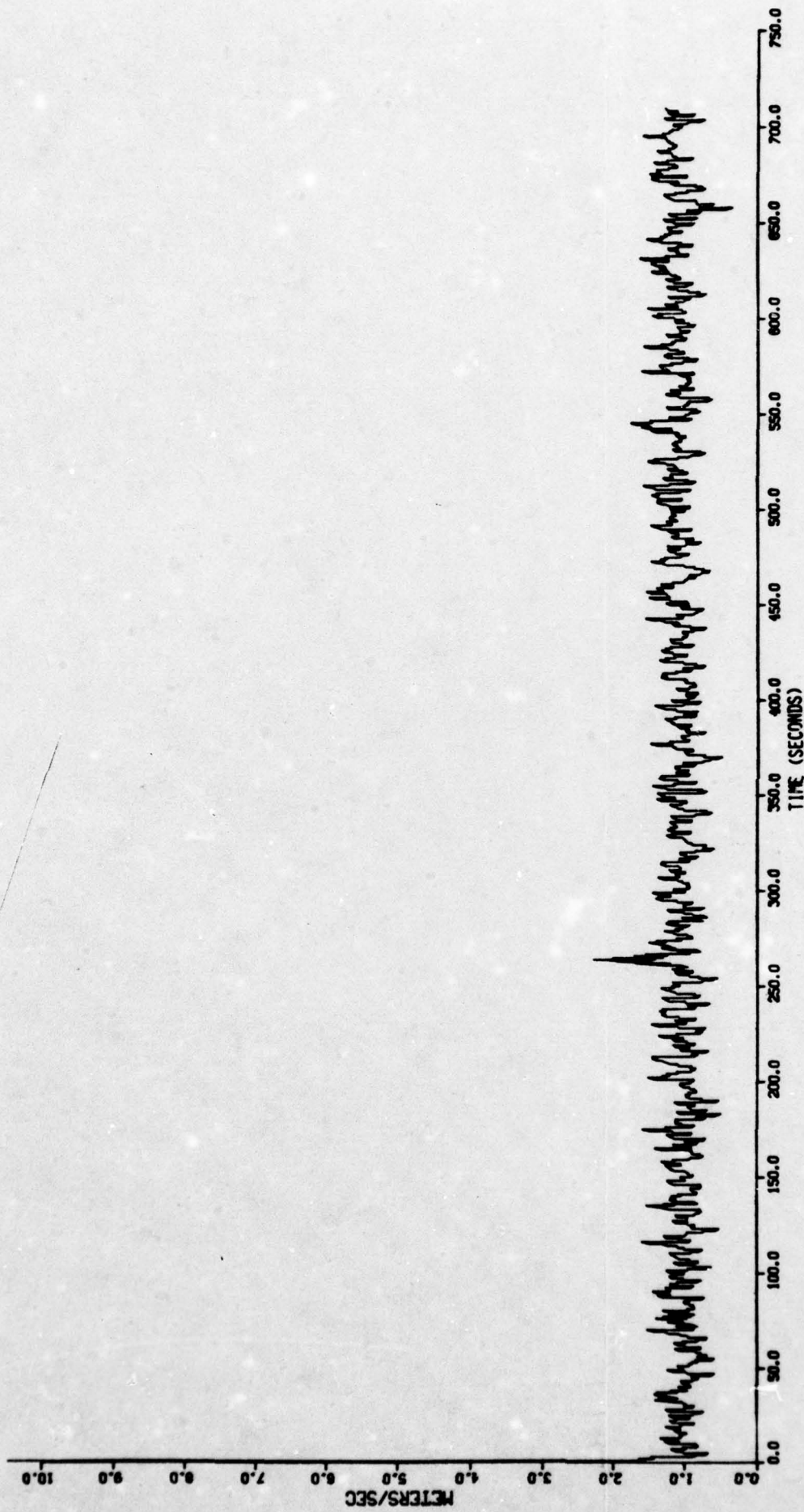
Figure 4.27 Ten-state fading memory filter with ship scenario.

(b)

(a)
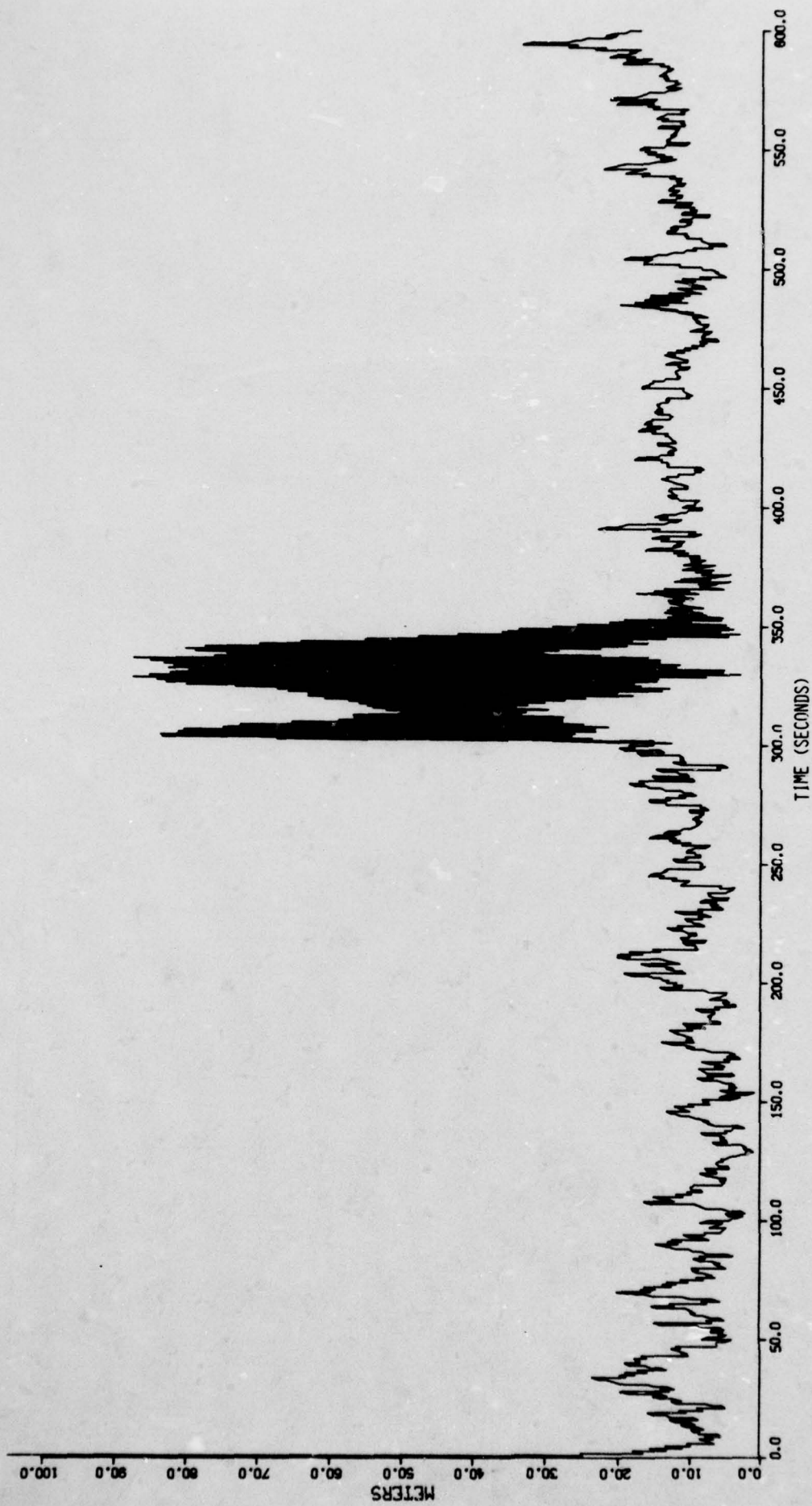
Figure 4.28  Ten-state fading memory filter with aircraft scenario (small fade factor).

(b)

153

(a)

Figure 4.29  Ten-state fading memory filter with aircraft scenario (medium fade factor).

(b)

154

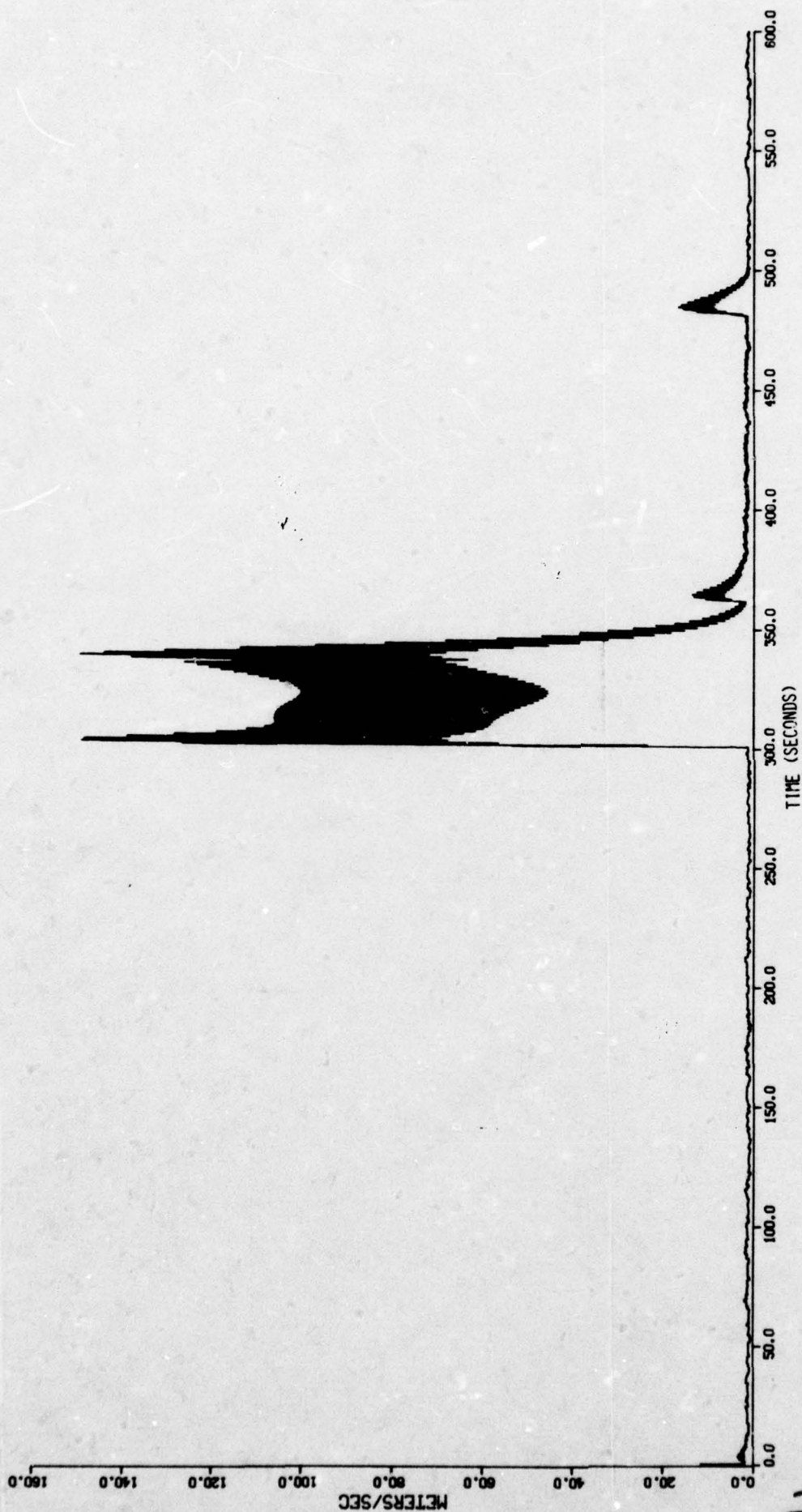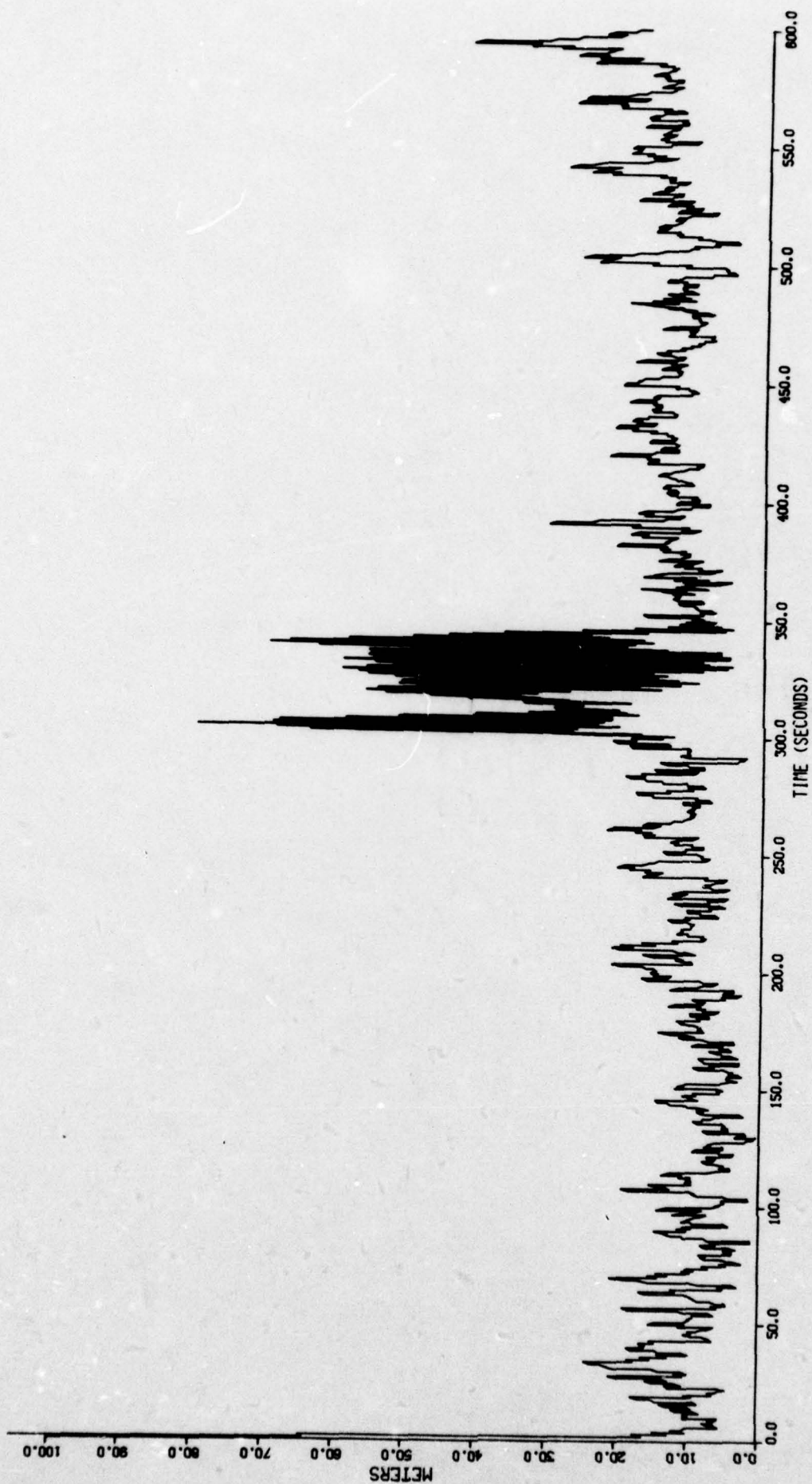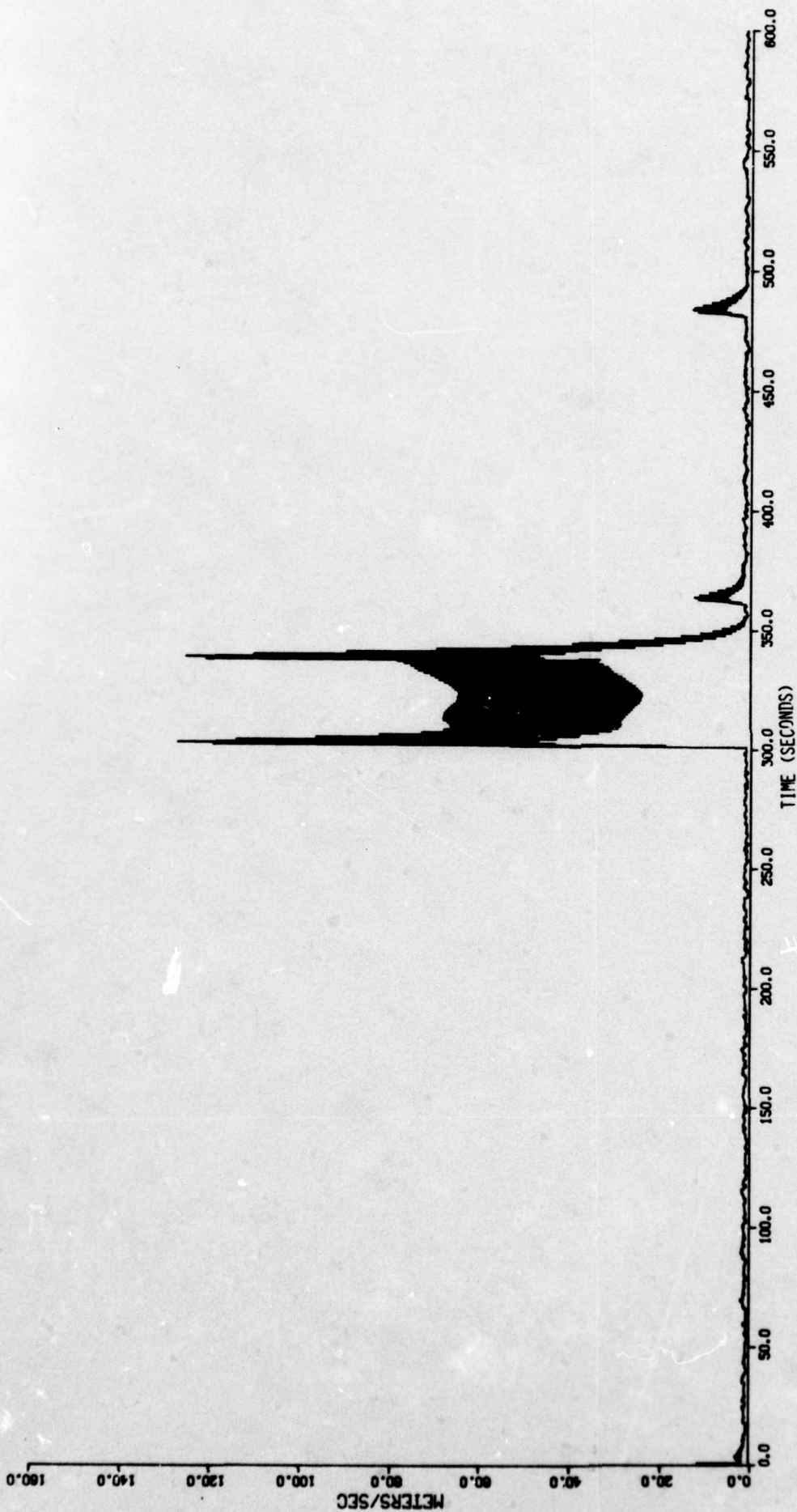(a)
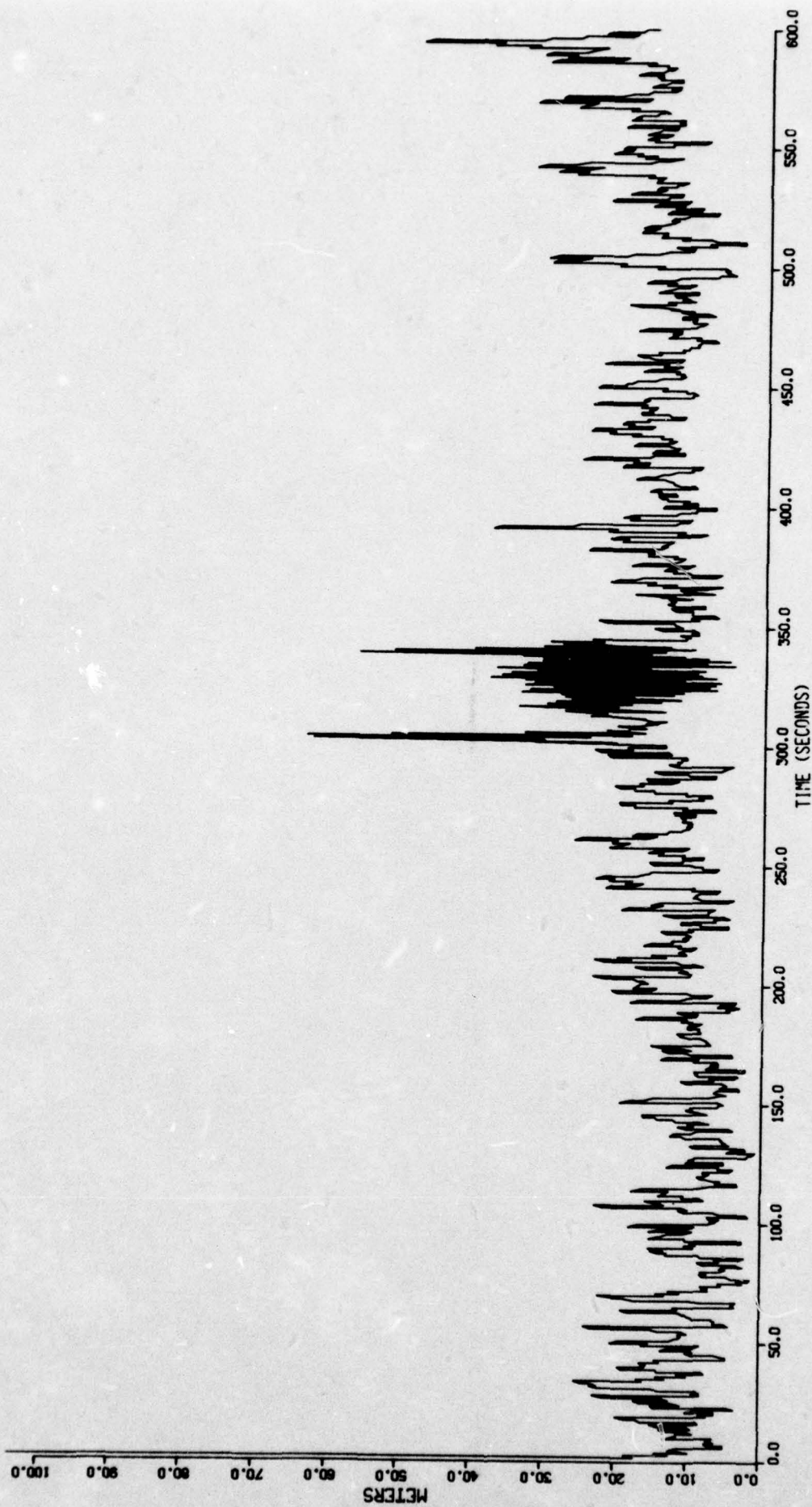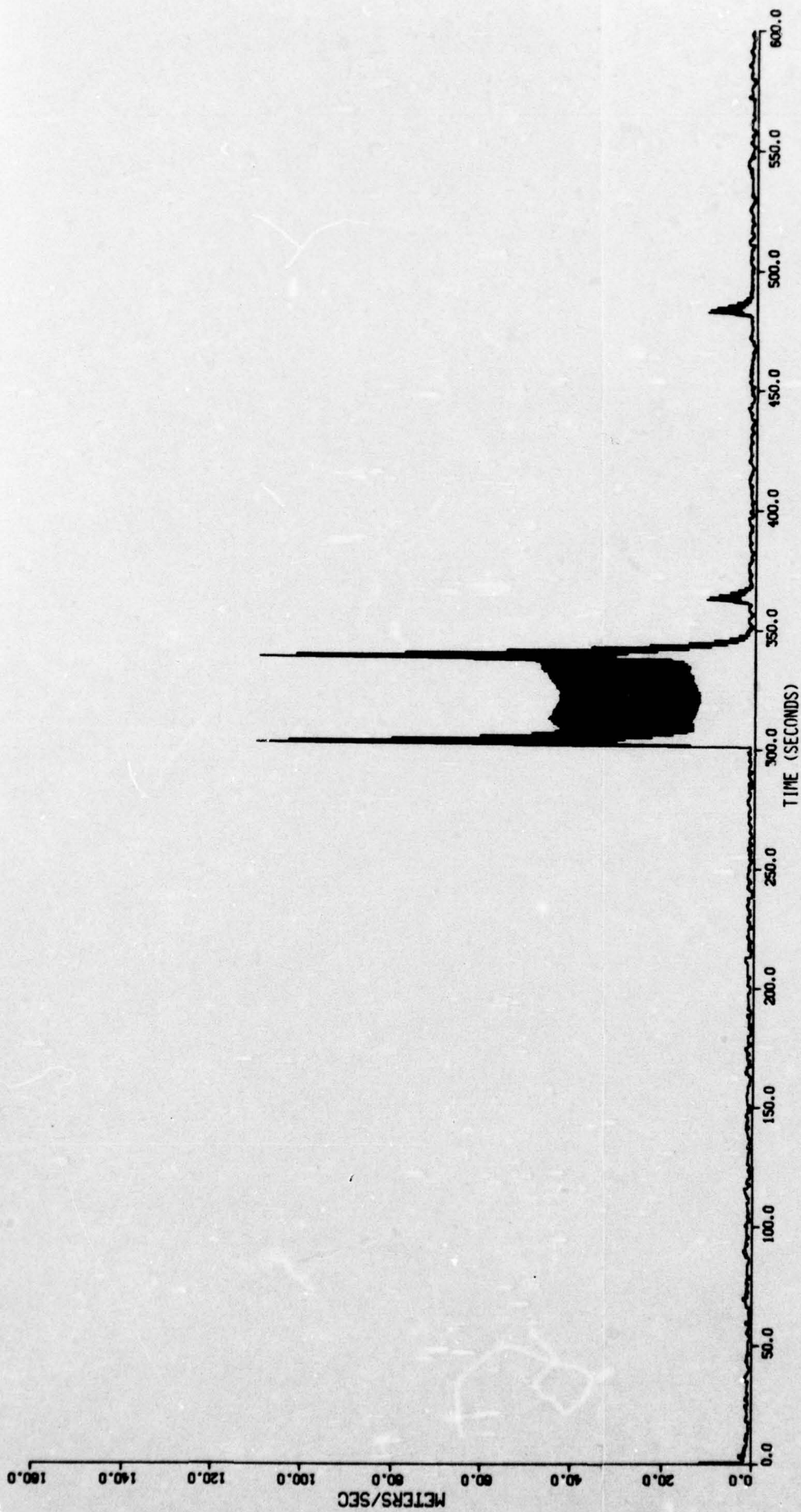
Figure 4.30 Ten-state fading memory filter with aircraft scenario (large fade factor).

(b)

155

(a)
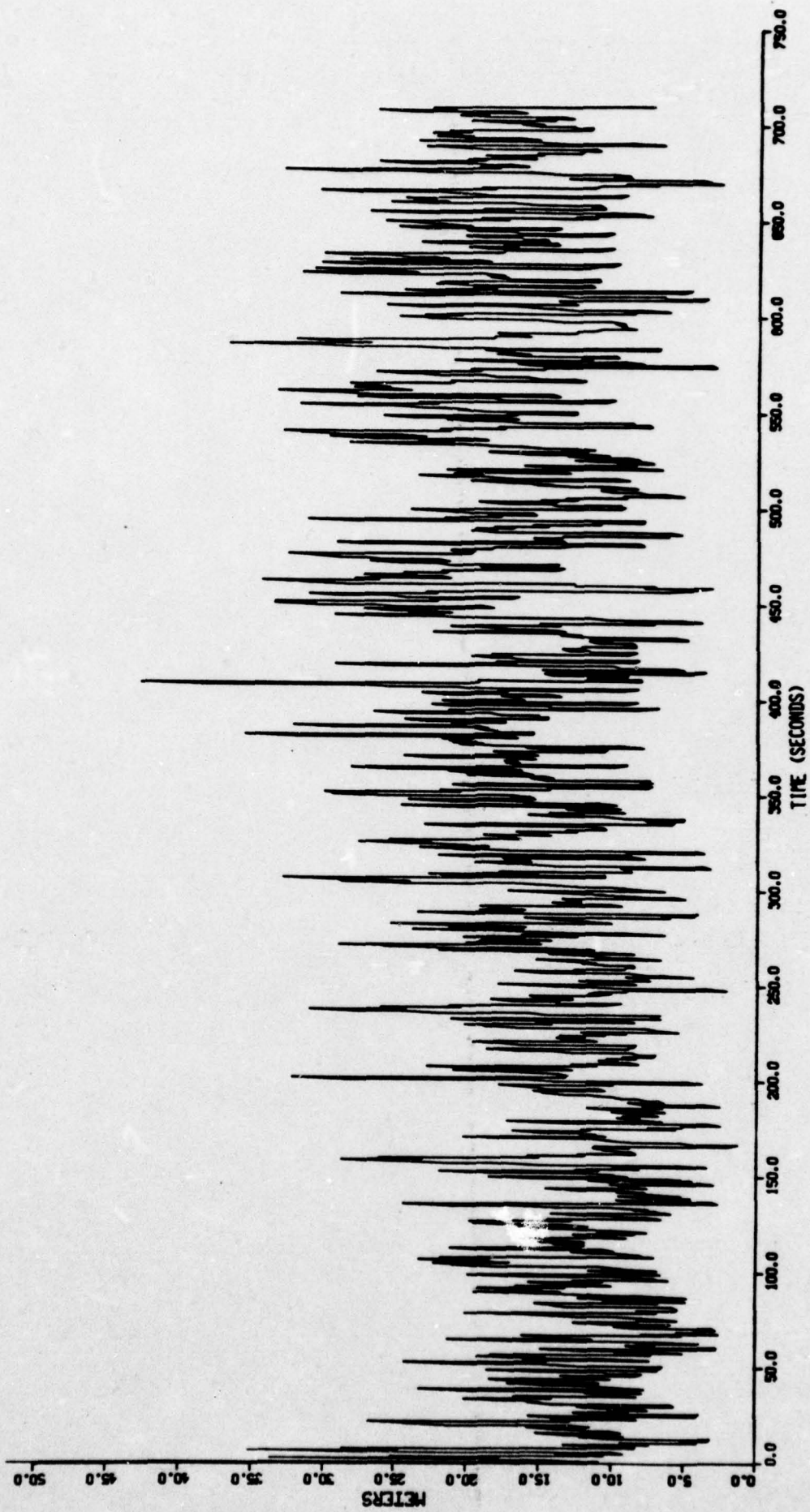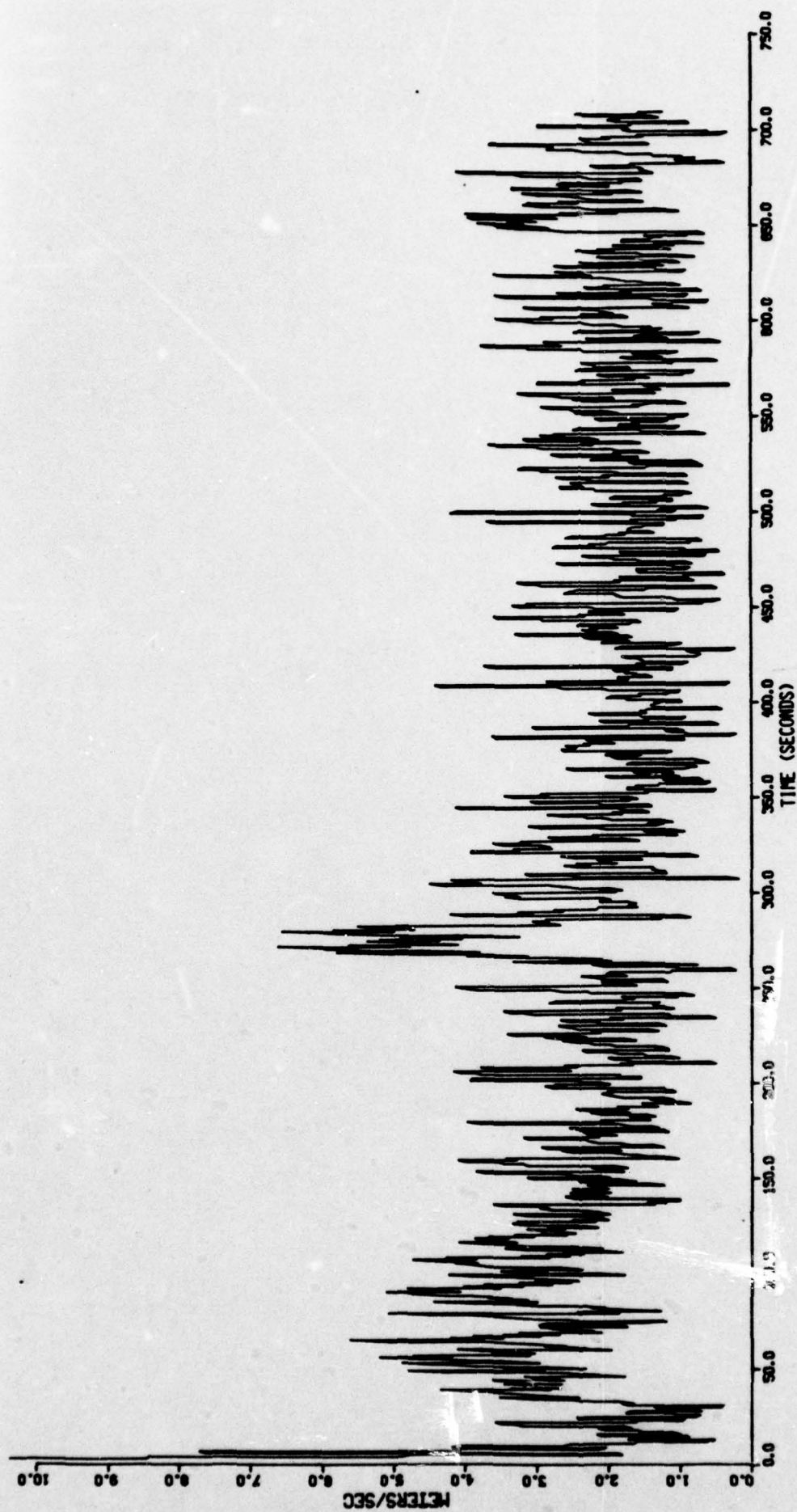
Figure 4.31 $\alpha - \beta$ fading memory filter with ship scenario.

(b)

156

scenario.  The results may be validly compared since the pseudo-random number generator was started from the same value in each case.  Finally, Figure 4.31 shows the results using a fading memory $\alpha$-$\beta$ filter with the fade constant exponent equal to .33 times $\Delta t$.

The results from the two eight-state filter runs (Figures 4.25 and 4.26) confirm the covariance analysis results.  The mean RSS position error in Figure 4.25 (a) appears to be below the value predicted by the covariance analysis.  The velocity error shown in Figure 4.25 (b) is within the limits predicted by the covariance analysis.  The one notable deviation in the velocity error is at t = 260, where the ship undergoes a 3 degree/sec turn at 15 knots.  This turn is an acceleration of approximately .04 g so that the velocity error is to be expected.  The velocity errors shown in Figure 4.26 (b) are for the aircraft scenario.  The aircraft turns at t = 300 and t = 360 are approximately 5 g and .5 g turns, respectively.  The velocity errors in these turns are again what the covariance analysis would predict when the acceleration uncertainties are scaled to the values in the scenario.  The RSS position error from Figure 4.26 (a) is approximately at the 1-$\sigma$ value from the covariance analysis, except during the 5 g maneuver.  The unusual curve shape starting just prior to t = 500 is due to the fact that the acceleration goes to zero there.

The results for the ten-state fading memory filter applied to the ship scenario (Figure 4.27) show good position results.  The velocity estimation error is somewhat larger than the steady state 1-$\sigma$ values predicted by the covariance analysis.  The results of the aircraft case (Figures 4.28 through 4.30) give results which are again in good agreement with the covariance analysis.  Variation of the fade factor shows the larger fade factor reduces the magnitude of the transient errors during periods of large acceleration while the steady state

errors increase. This again is the result which would be expected after examining the covariance analysis results. The shape of the velocity error curves indicate the ten-state filter is able to track accelerations after an initial transient. This can be seen from the small "bumps" on the curve at t = 360 and t = 480.

The last Monte Carlo results shown (Figure 4. 31) confirm good agreement between the covariance analysis and the simulation for the fading memory $\alpha$-$\beta$ filter.

In the simulation runs, the fading memory filters were mechanized with the same fade factor throughout. An analysis into making the fade factor a function of the measurement residuals in probably worth while as a future task.

## Section 5. - COMPUTER PROGRAM SIZING

### 5.0    Introduction

This section addresses the final task of the algorithm development study. This task was to determine the computational requirements (i.e., arithmetic operations and storage locations) for the candidate algorithms. These results will provide an input to the effort establishing the computer program size. The results to be presented here do not account for computer word length. The true computer size requirement will probably depend on the word length used in the computer. This problem has been considered to be beyond the scope of this study, though ORINCON is aware that it must be addressed somewhere.

The actual computer mechanization of the navigation equations can be divided in two parts. The first part is the preprocessing of the raw measurement data to obtain the measurables for the filter. The second part is the filtering of these measurables to obtain the actual navigation information. It is the latter problem which will receive the most attention in this section. The first part is more dependent on factors outside this study.

### 5.1    Common Requirements

All of the candidate filters fall into the category of extended filters. By this it is meant that the filter is linearized about the current estimate. The measurables for this type of filter are the difference between the predicted value of the measurement and the actual measured value. The computation of the expected measurement is a common requirement of all of the filter mechanizations.

The following steps are required to perform the measurable computation:

(a)    Determination of the time of transmission of the received signal. This can be accomplished from knowledge of the system requirements which specify the times of transmission.

(b)    Determination of the satellite positions at the time of signal transmission. This can be done using the equations for this purpose presented in Section 1.

(c)    Correction of the measured time for satellite clock errors and ionospheric delay errors. This is done by using the received data and the algorithms for these purposes presented in Section 1.

(d)    Computation of expected measurement values. This computation involves using the estimate of the user position and velocity at the time of reception and the computed satellite locations. From these, expected range and range-rate values can be computed.

(e)    Formation of the filter measurables. This final step is done by differencing the expected measurements and the actual corrected measurements.

Other common requirements include the alert computation (such as the candidates outlined in Section 2), general matrix operation subroutines, and special mathematical functions (e.g., square root, vector norm, etc.).

## 5.2    Filter Requirements

In this subsection, the computer requirements for a general Kalman filter and the specific candidate filters will be presented. This includes the storage requirements and the operation counts.

### 5.2.1    General Kalman Filter [25]

The computational requirements for the Kalman filter are given in Table 5.1. Here n is the number of states and m is the number of measurables. This does not include the computation for guaranteeing symmetry (Item 15). The computation time is represented by the number of multiplications since it is largely governed by the number of multiplications. Additions and subtractions normally require far less time in most computers. In any case, these operations are of the same order as the number of multiplications so, for purposes of comparing algorithms, this operation count is considered to be valid.

It will be noted below that for the simple dynamics assumed in each of the candidate filters that items 4 and 6 may be done more efficiently. Implementation of a fading memory filter adds up to an addition $n^2$ multiplications to item 6.

### 5.2.2    Eleven-State Suboptimum Filter

For the eleven-state filter the simple dynamics mean that steps 4 and 6 in Table 5.1 each require $10n$ multiplications instead of $n^3$. Also there is no requirement for storage for the state transition matrix. The measurement noise covariance matrix is also diagonal so that only m storage locations are needed. Another consequence of the uncorrelated measurement errors will be discussed below in Section 5.3.

161

## Table 5.1. Computational Requirements for the Kalman Filter

| Quantity | Multiplications | Storage |
|----------|-----------------|---------|
| 1. $\hat{\underline{x}}_k$ | | $n$ |
| 2. $P_{k-1}$ | | $n^2$ |
| 3. $\Phi_{k,k-1}$ | | $n^2$ |
| 4. $\Phi_{k,k-1}P_{k-1}$ | $n^3$ | Store in $P_{k-1}$ |
| 5. $Q_k$ | | $n^2$ |
| 6. $P'_k = \Phi_{k,k-1}P_{k-1}\Phi^T_{k,k-1}+Q_k$ | $n^3$ | Store in $\Phi P$ |
| 7. $H_k$ | | $mn$ |
| 8. $P'_k H^T_k$ | $mn^2$ | Store in $P_k$ |
| 9. $R_k$ | | $m^2$ |
| 10. $H_k P'_k H^T_k + R_k$ | $m^2 n$ | $m^2$ |
| 11. $(H_k P'_k H^T_k + R_k)^{-1}$ | $m^3$ | Store in $HPH^T + R$ |
| 12. $K_k = P'_k H^T_k(H_k P'_k H^T_k + R_k)^{-1}$ | $m^2 n$ | $mn$ |
| 13. $\underline{z}_k$ | | $m$ |
| 14. $\hat{\underline{x}}_k = K_k \underline{z}_k$ | $mn$ | Store in $\hat{\underline{x}}_k$ |
| 15. $P_{k/k} = P_{k/k-1}-K_k(P_{k/k-1}H^T_k)^T$ | $mn^2$ | Store in $P_k$ |
| 16. Scratch storage | | $n^2$ |
| **TOTALS** | $2n^3+2mn^2$ $+m^3+2m^2n+mn$ | $4n^2+n+2mn+2mn^2+m$ |

162

### 5.2.3  Ten-State Suboptimum Filter

In the ten-state filter, steps 4 and 6 of Table 5.1 reduce to 9n multiplications each with again no requirement for a state transition matrix. The computational requirements for this filter are in Table 5.2.

### 5.2.4  Eight-State Suboptimal Filter

The simple dynamics used in the eight-state filter mean that steps 4 and 6 of Table 5.1 reduce to 4n multiplications. The results are presented in Table 5.2.

### 5.2.5  Seven-State Suboptimal Filter

The transition steps for the seven-state filter given in steps 4 and 6 of Table 5.1 require only 3n multiplications and no state transition matrix storage. The results are given in Table 5.2.

### 5.2.6  $\alpha$-$\beta$ Filter

The $\alpha$-$\beta$ is an eight-state filter which is composed of four two-state filters. The transition steps reduce to 8 multiplications and there is only one observable per filter. The results given in Table 5.2 do not include the prefiltering of the data.

### 5.3  Additional Considerations

In this subsection, additional considerations which impact the computational requirements are discussed.

Table 5.2. Computational Requirements for Candidate Filters*

| Filter | Computational Requirements | | TOA Measurements Only (m = 4) | | TOA and Doppler Measurements (m = 8) | |
|---|---|---|---|---|---|---|
| | Multiplications | Storage | Multiplications | Storage | Multiplications | Storage |
| 11-State | $2m^2n+2mn^2+m^3+mn+20n$ | $3n^2+n+2m+2mn+m^2$ | 1648 (1336) | 486 | 4164 (2484) | 630 |
| 10-State | $2m^2n+2mn^2+m^3+mn+18n$ | $3n^2+n+2m+2mn+m^2$ | 1404 (1116) | 414 | 3652 (2084) | 550 |
| 8-State | $2m^2n+2mn^2+m^3+mn+8n$ | $3n^2+n+2m+2mn+m^2$ | 800 (560) | 352 | 2688 (1344) | 408 |
| 7-State | $2m^2n+2mn^2+m^3+mn+6n$ | $3n^2+n+2m+2mn+m^2$ | 750 (534) | 290 | 2290 (1058) | 346 |
| $\alpha$-$\beta$ | $4(2n+2n^2+1+n+n)$ | $4(3n^2+n+2+2n+1)$ | 52 | 84 | -- | -- |

* Note: Numbers in parentheses are for sequential processing of data.

164

### 5.3.1 Sequential Processing

Since the measurement errors in the GPS receiver are uncorrelated (i.e., the R matrix is diagonal) the data may be processed sequentially even though it is received in batch [26] with exactly the same results. Processing the data sequentially always requires fewer multiplications than batch processing [25]. For scalar sequential measurements, the totals in Table 5.2 (except the $\alpha$-$\beta$ filter which already uses this advantage) can be reduced by [25]

$$\Delta M = m^3 - m + 2nm^2 - 2nm$$

$$= m(m-1)(m+2n)$$

The numbers in parentheses in Table 5.2 are the number of multiplications reduced by $\Delta M$. Since the measurement errors are all uncorrelated in the GPS environment, the sequential processing should be implemented.

### 5.3.2 Computational Form of the Filter

Much work has been done in other studies on the computational form of the filter. Selection of the form may have considerable impact on numerical errors. The most common numerical error seems to be that the filter covariance matrix loses its positive definiteness.

One method of solving the numerical problems of the covariance matrix is to use the "stabilized" form of the filter. This is done by replacing step 15 of Table 5.1 by the equivalent form given in equation (3.6d) of Section 3. This form of the filter requires considerably more multiplications. Another stabilization procedure is to force

165

the result of the covariance reset in step 15 of Table 5.2 to be sym-
metric by averaging the off-diagonal elements, i.e.,

$$\tilde{P}_{ij} = \tilde{P}_{ji} = \frac{P_{ij} + P_{ji}}{2}$$

where

$\tilde{P}_{ij}$, $\tilde{P}_{ji}$ are the new values

$P_{ij}$, $P_{ji}$ are the results of step 15.

Both of these techniques do not necessarily solve the precision
problem.

A different approach is through the square root formulation
of the filter. Carlson [26] and others have developed square root
formulations which solve the positive definiteness problem and also
alleviate precision problems. These methods are well documented
in the literature [26, 27]. Another covariance factorization technique,
the U-D filter, which is not quite so well known is presented in refe-
rence 28. This formulation is equivalent in numerical performance
to the other square root formulations, but it does not require a square
root to be taken at each point of propagation. For a small processor,
this can lead to a significant time savings.

A summary of the U-D filter equations for the case of scalar
measurements is presented here. The reader is referred to reference
28 for a thorough explanation of the U-D mechanization.

Suppose, the n-dimensional error covariance matrix, $P$, is
factored such that

$$P = UDU^T \tag{5.1}$$

166

where $U$ is upper triangular with unity diagonal elements and $D = \text{diag}(d_1, \ldots, d_n)$. The matrices $U$ and $D$ are referred to as the U-D factors of $P$. They are unique, provided that $P$ is positive definite, and can be constructed using a Cholesky factorization [20].

## U-D Measurement Update Algorithm

Given a priori covariance factors $\tilde{U}$ and $\tilde{D}$ and scalar measurement $z = Hx + v$, where $E(v^2) = r$, the updated U-D covariance factors and the Kalman gain (U, D and K respectively) can be obtained as follows:

$$f^T = H\tilde{U} \quad ; \quad f^T = (f_1, \ldots, f_n) \tag{5.2}$$

$$v = \tilde{D}f \quad ; \quad v_j = \tilde{d}_j f_j \tag{5.3}$$

$$\bar{K}_1^T = (v_1, 0, \overbrace{\ldots}^{n-1}, 0) \tag{5.4}$$

$$\alpha_1 = r + v_1 f_1 \tag{5.5}$$

$$d_1 = (r/\alpha_1)\tilde{d}_1 \tag{5.6}$$

For $j = 2, \ldots, n$ cycle through

$$\alpha_j = \alpha_{j-1} + v_j f_j \tag{5.7}$$

$$d_j = (\alpha_{j-1}/\alpha_j)\tilde{d}_j \tag{5.8}$$

$$\lambda_j = -f_j/\alpha_{j-1} \tag{5.9}$$

167

$$U_j = \tilde{U}_j + \lambda_j \bar{K}_{j-1} \qquad (5.10)$$

$$\bar{K}_j = \bar{K}_{j-1} + v_j \tilde{U}_j \qquad (5.11)$$

where $U = [U_1, U_2 \ldots, U_n]$. The component $U$ vectors have the form

$$U_j^T = (U_j(1), \ldots U_j(j-1), 1, 0, \ldots, 0)$$

and $D = \text{diag}(d_1, \ldots, d_n)$. The Kalman gain is given by

$$K = K_n / \alpha_n \qquad (5.12)$$

The salient feature of this algorithm is the way in which the updated diagonal $D$ elements are computed. Since the quantities $\alpha_j$ are calculated as positive sums, it follows that the updated d's are fractions of their a priori values and therefore cancellation errors present in the conventional measurement updating equation are avoided. The positivity of $D$, and hence of $P$, is therefore assured. Furthermore, the elements of $D$ can diminish to near-zero without affecting the stability of the algorithm.

Modified Givens techniques can be employed to accomplish time updating of the $U-D$ factors, and the resulting algorithm is the following: Let

$$W = \left[ G \vdots \Phi U \right] = \left[ w_1, w_2, \ldots, w_{n+k} \right]$$

$$\bar{D} = \text{Diag}(D, I) = \text{Diag}(\bar{d}_1, \ldots, \bar{d}_{n+k}); \quad k = \text{no. of columns of } G$$

The $U-D$ factors of $\tilde{P} = W\bar{D}W^T$ can be computed as follows: For $j = n, \ldots, 1$ cycle through the following as indicated.

$$m: = j + k \qquad (5.13)$$

---

The symbol " : = " denotes replacement (i. e. , replace m by j+k).

For $i = m-1, \ldots, 1$ evaluate Eqs. (5-14) - (5.27) as indicated.

$$\alpha_: = \bar{d}_m w_m(j) \tag{5.14}**$$

$$\beta_: = \bar{d}_i w_i(j) \tag{5.15}$$

$$d'_m_: = \alpha w_m(j) + \beta w_i(j) \tag{5.16}**$$

$$\bar{s}_: = \beta / d'_m \tag{5.17}$$

$$\bar{d}_i_: = \bar{d}_i \bar{d}_m / d'_m \tag{5.18}$$

$$v_: = w_i \tag{5.19}$$

If $i = m-1$ evaluate Eqs. (5.20) - (5.23)

$$\bar{c}_: = \alpha / d'_m \tag{5.20}$$

$$\left. \begin{array}{l} w_i(\ell)_: = w_m(j)v(\ell) - v(j)w_m(\ell) \\[2em] w_m(\ell)_: = \bar{c}w_m(\ell) + \bar{s}v(\ell) \end{array} \right\} \ell = 1, \ldots, j-1 \tag{5.21} \tag{5.22}$$

$$w_i(j)_: = 0, \quad w_m(j)_: = 1 \tag{5.23}$$

If $i < m-1$ evaluate

$$\left. \begin{array}{l} w_i(\ell)_: = v(\ell) - v(j)w_m(\ell) \\[2em] w_m(\ell)_: = w_m(\ell) + \bar{s}w_i(\ell) \end{array} \right\} \ell = 1, \ldots, j-1 \tag{5.24} \tag{5.25}$$

---

**When $i < m-1$, $w_m(j) \equiv 1$

169

$$w_i(j): = 0 \tag{5.26}$$

$$\bar{d}_m : = d'_m \tag{5.27}$$

Upon completion of this recursion the $W$ and $D$ arrays contain $U$ and $D$, stored as follows

$$W = [\, \underbrace{0}_{k} \mid \underbrace{U}_{n}\,]\}n \tag{5.28}$$

$$\tilde{d}_j = \bar{d}_{j+k} \qquad j=1,\ldots,n \tag{5.29}$$

170

# SECTION 6. - CONCLUSIONS

## 6.0 Conclusions of the Study

The purposes of this study were to develop and analyze navigation algorithms for use in Navy NAVSTAR/GPS navigation receivers. By performing algorithm design and analysis for various receiver configurations, it was possible to provide data useful in certain trade-offs. This report has presented much data and many results from which the reader may derive his own conclusions. Changing requirements and hardware specifications may at some point in time invalidate certain of the results summarized below. Nonetheless the following conclusions have been drawn by ORINCON.

A.  The Alert algorithm based on the approximate volume maximization or exhaustive search should be used.

B.  The successive linearizations of the measurement matrix method should be used to provide single fixes or pseudo-measurements.

C.  The multi-channel receiver gives better transient response than the single channel receiver if the frequency of measurements is the same. The single channel performance is nearly equivalent to the multi-channel when the data rate is equal. This means that if the single channel receiver can make n-measurements in the same time that the n-channel receiver makes one measurement, then the single channel performance is on a par with the n-channel reciever. (This conclusion does not take into account the possibility of reducing ionospheric errors by using different frequency channels. This is a different issue).

D.  In order to provide good velocity estimates from the GPS data, doppler measurements must be made. Without the doppler measurements, position estimates are only slightly degraded, however the

171

velocity errors are of the order of several knots.

E. The addition of acceleration states in the filter provides a better velocity estimate in both the steady state and in the transient response to unmodelled acceleration.

F. The addition of a fading memory to the filter improves the performance of the filter when unmodelled acceleration are present. This is at the expense of the steady state performance when there are no acceleration disturbances. Some sort of adaptive fading memory would provide a good compromise solution.

G. The measurement update rate (within certain bounds) does not appear to be a significant consideration in systems where there are no unmodelled accelerations. The update rate becomes significant when there are unmodelled accelerations.

H. The ionospheric errors appear to be a significant error source. The value of the error source is an uncertain quantity at this time. More data should be gathered on the proposed ionospheric correction schemes for the single and dual frequency receivers.

I. The receiver TOA measurement error is not as significant an error source in relation to the overall position error as is the doppler measurement error in relation to the overall velocity error. This is of course only in the ranges considered in this study. Emphasis should be placed on improving the doppler measurement accuracy.

J. For low accuracy systems where an accurate velocity estimate is not needed, the $\alpha$-$\beta$ filter provides a computationally simple filter when combined with the pseudo-measurements generated by the successive linearizations algorithms.

K. Sequential processing of the data should be done to save computer storage and computation time. Also a factorization technique should

probably be used.

In all of the above conclusions, the unmodelled accelerations refer
to unaided systems. The amount which the response to unmodelled accel-
erations should be weighed in making any design trade-offs is of course
dependent on the expected amount of acceleration disturbances (both
frequency and magnitude of disturbances).

173

# Section 7. - REFERENCES

1. Navstar Global Positioning System - An Evolutionary Research and Development Program," Space And Missile Systems Organization/YEC Briefing (1974).

2. Bate, R.R., Mueller, D.D., and White, J.E., Fundamentals of Astrodynamics, Dover Publications, Ind., New York (1971).

3. "A Proposal to SAMSO/JPO for the Navstar-GPS," General Dynamics Proposal P3631007, Volumes 1 and 4 (June 1974).

4. "Space Vehicle Navigation System and NTS PRN Navigation Assembly/User System Segment and Monitor Station," Rockwell International, ICD MH08-00002-400, Rev. E (September 21, 1975).

5. White, D.M., and Silberman, S.R., "Simulation of 2D Radar Automatic Detection and Tracking Systems: Baseline Program," Technology Service Corporation Report No. TSC-W8-60 (August 19, 1975).

6. "System Segment Specification for the User System Segment of the NAVSTAR Global Positioning System, Phase I," Space and Missile Systems Organization, Report SS-US-101-B (December 30, 1974).

7. Nash, J.M., "Covariance Analysis of the DD 963 Navigation System," Naval Electronics Laboratory Center, Report TR 1967 (November 1975).

8. Goodyear, W.H., "Completely General Closed-Form Solution for Coordinate and Partial Derivatives of the Two-Body Problem," Astronomical Journal, Vol. 70, No. 3 (April 1965).

9. "System Specification for the Navstar Global Positioning System, Phase I," Space and Missile Systems Organization/YEN, Report SS-GPS-101B, Code Identification 07868 (August 15, 1974).

10. Meditch, J.S., "Clock Error Models for Simulation and Estimation," Aerospace Corporation Report No. TOR-0076(6474-01)-2 (July 7, 1975).

11. "Concept for a Satellite-Based Advanced Air Traffic Management System," Department of Transportation, Transportation Systems Center, Report No. DOT-TSC-OST-73-29 (October 1973).

12. Mallinckrodt, A.J., "Notes for a UCLA Short Course, Satellite Based Navigation, Traffic Control and Communication to Mobile Terminals," (October 1969).

13. Kreigsman, B., "Refraction Error Model for One-Way Doppler," The Charles Stark Draper Laboratory, Memo No. 21-73 (March 8, 1973).

14. Duiven, E. M. and Le Schack, A. R., "Global Positioning System Simulation Development and Analysis," TASC Report TR-428-2, (December 15, 1974).

15. "Navigation Signal Structure," General Dynamics Electronics and Magnavox (June 3, 1975).

16. Wolfe, C. A., "Single-Fix Algorithm Report for the NAVSTAR/GPS Navigation Analysis and Algorithm Development Study," ORINCON Corp. Report OC-75-82-2 (April 1, 1976).

17. Dahlquist, G., Bjork, A., and Anderson, N., "Numerical Methods," Prentice-Hall, Englewood Cliffs, New Jersey, 1974.

18. Noe, P. S. and Myers, K. A., "A Position Fixing Algorithm for the Low-Cost GPS Receiver," IEEE Transactions on Aerospace and Electronics Systems, Vol. AES-12 No. 2 March 1976.

19. Meditch, J. S., Stochastic Optimal Linear Estimation and Control, McGraw-Hill, New York (1969).

20. Forsythe, G. and Molen, C. B., Computer Solution of Linear Algebraic Systems, Prentice-Hall, Englewood Cliffs, N. J. (1967).

21. Sorenson, H. W. and Sacks, J. E., "Recursive Fading Memory Filtering," Information Sciences 3, pp. 101-119 (1971).

22. Schooler, C. C., "Optimal $\alpha$ - $\beta$ Filters for Systems with Modeling Inaccuracies," IEEE Transactions on Aerospace and Electronic Systems, Vol. AES-11, No. 6 (November 1975).

23. "Systems Specification for the Navstar Global Positioning System, Phase I," Space and Missile Systems Organization/YEN, Report SS-GPS-101B, Code Identification 07868 (August 15, 1974).

24. Hewlett-Packard 10544A Quartz Crystal Oscillator Specifications, (July 1975).

25. "ORINCON Corporation Short Course on Estimation Theory for Nonlinear Stochastic Systems," ORINCON Corporation, La Jolla, California, 1976.

26. Carlson, N. A., "Fast Triangular Formulation of the Square Root Filter," AIAAJ., 11(9): 1259-1265, September 1973.

27.     Andrews, A. "A Square Root Formulation of the Kalman Covariance Equations," _AIAAJ._, 6(6): 1165-1166, June 1968.

28.     Thornton, C. L. "Triangular Covariance Factorizations for Kalman Filtering," Jet Propulsion Laboratory Technical Memorandum 33-798, Oct. 15, 1976.

176

## APPENDIX A

### Filter Sensitivity to a Class of
### Unmodelled Errors

In this appendix, a simple method will be developed for attacking a particular problem in the covariance analysis of suboptimal filters. The problem being considered is that of determining sensitivity to unmodeled error sources of a certain class. The class of unmodeled errors is somewhat restrictive, but it is rich enough to be of practical importance.

The setting for covariance analysis is as follows. First a reference system is defined which contains all of the error sources modeled.

$$\underline{X}_k = \varphi_{k, k-1} \underline{X}_{k-1} + \Gamma_{k, k-1} \underline{U}_k$$

$$\underline{Z}_k = H_k \underline{X}_k + \underline{V}_k \tag{A-1}$$

where

$\underline{X}_k$      is the $n_s$ state vector at time k

$\varphi_{k, k-1}$      is the $n_s \times n_s$ state transition matrix from time k-1 to k

$\Gamma_{k, k-1}$      is the $n_s \times r_s$ input disturbance at time k

$\underline{Z}_k$      is the $m_s$ observation vector at time k

$H_k$      is the $m_s \times n_s$ measurement matrix at time k

$\underline{V}_k$      is the $m_s$ observation noise vector at time k

$\underline{U}_k$      is the $r_s$ vector of input noise at time k

It is desirable to estimate certain states of $\underline{X}_k$, but due to computer size restrictions certain of the states will not be modeled in the "suboptimal filter". Let $\underline{\tilde{X}}_k$ be the $n_f$ state vector of the suboptimal filter. The model for $\underline{\tilde{X}}_k$ is

$$\underline{\tilde{X}}_k = \tilde{\varphi}_{k,k-1} \underline{\tilde{X}}_{k-1} + \tilde{\Gamma}_{k,k-1} \underline{\tilde{U}}_k$$

$$\underline{\tilde{Z}}_k = \tilde{H}_k \underline{\tilde{X}}_k + \underline{\tilde{V}}_k \tag{A-2}$$

Based upon the model in (A-2) (and possibly other constraints) a set of filter gains are computed. Consider the case[†] where $\underline{\tilde{X}}_k$ is a subvector of $\underline{X}_k$. It is of interest to look at the difference between the estimate of $\underline{\tilde{X}}_k$ (denoted $\underline{\hat{X}}_k$) and the reference vector $\underline{X}_k$. In particular, consider the covariance matrix P defined by

$$P_k = E[(\underline{X}_k - \underline{\hat{X}}_k^*)(\underline{X}_k - \underline{\hat{X}}_k^*)^T] \tag{A-3}$$

where the * indicates the vector has been augmented with zeroes sufficient to make the subtraction well defined.

Let $\underline{X}_k^s$ denote the vector difference $(\underline{X}_k - \underline{\hat{X}}_k^*)$. With $\tilde{\varphi}_{k,k-1}$ a submatrix of $\varphi_{k,k-1}$ and $\tilde{H}_k$ a submatrix of $H_k$, the time evolution of $\underline{X}_k^s$ can be described by

$$P_k = \varphi_{k,k-1} P'_{k-1} \varphi_{k,k-1}^T + \Gamma_{k,k-1} \Gamma_{k,k-1}^T \tag{A-4a}$$

$$P'_k = \left\{ I_{n_s} - (K_k H_k)^* \right\} P_k \left\{ I_{n_s} - (K_k H_k)^* \right\}^T + K^* R_k K^{*T} \tag{A-4b}$$

where $I_{n_s}$ is the $n_s \times n_s$ identity matrix

and the * indicates that the matrix with $n_f$ rows has been augmented with $(n_s - n_f)$ rows of zeroes so that the matrix operations are well defined.

---

[†]A more general case which includes errors in $\tilde{\varphi}$, $\tilde{\Gamma}$ and $\tilde{H}$ may also be considered.

The matrices $P_k'$ and $P_k$ contain the information about the variances of the error in the estimate $\underline{\hat{X}}_k$. With the filter gain matrix $K_k$ defined, equations (A-4a) and (A-4b) are linear equations for the covariance matrix $P_k$ for all $k$. It thus makes sense to determine the sensitivity of the variance of the filter states to the variances of the unmodeled error sources. It has been suggested [A-1] that to do this, each individual error source be evaluated separately by propagating equations (A-4a) and (A-4b) for each error source. However, for a certain class of unmodeled error sources, the sensitivity may be determined in the presence of other error sources in just one propagation of equations (A-4a) and (A-4b). To define this class of error sources, partition $\underline{X}_k^s$ as follows:

$$\underline{X}_k^s = \begin{pmatrix} \underline{X}_k^1 \\ \underline{X}_k^2 \end{pmatrix}$$

where

$\underline{X}_k^1$ is the subset of $\underline{X}_k^s$ not in the class of interest $\underline{X}_k^1$ is a $n_c$-vector where $n_c \geq n_f$

$\underline{X}_k^2$ is the subset of $\underline{X}_k^s$ which is the class of interest $\underline{X}_k^2$ is a $(n_s - n_c)$-vector

The class of error source for $\underline{X}_k^2$ is characterized by

$$\begin{pmatrix} \underline{X}_k^1 \\ \underline{X}_k^2 \end{pmatrix} = \begin{pmatrix} \varphi_{11} & \varphi_{12} \\ 0 & \varphi_{22} \end{pmatrix}_{k, k-1} \begin{pmatrix} \underline{X}_{k-1}^1 \\ \underline{X}_{k-1}^2 \end{pmatrix} + \begin{pmatrix} \Gamma_{k, k-1} \\ 0 \end{pmatrix} \underline{U}_k \qquad \text{(A-5)}$$

179

where the partitioning is comformable with the state vector partition.

To show how the sensitivity of an error source in this class may be determined in the presence of other error sources, the equations for the propagation of the inverse of $P_k$ will be developed. It will be apparent from these equations that the effects of the class of error sources considered may be easily removed from the inverse covariance matrix. Reinverting the remaining part of the inverse covariance matrix will yield the estimation error covariance matrix in the absence of the error source. The decrease in variance divided by the variance of the error source used in the covariance analysis defines the sensitivity.

Using the state transition matrix and input noise distribution matrix from (A-5) in (A-4a), the following is obtained

$$
P_k = \begin{pmatrix} \varphi_{11} & \varphi_{12} \\ O & \varphi_{22} \end{pmatrix}_{k,k-1} P_k' \begin{pmatrix} \varphi_{11}^T & O \\ \varphi_{12}^T & \varphi_{22}^T \end{pmatrix}_{k,k-1} + \begin{pmatrix} \Gamma_{k,k-1}\, \Gamma_{k,k-1}^T & O \\ O & O \end{pmatrix} \quad (A-6)
$$

where again the partitioning is comformable with $\begin{pmatrix} \underline{x}_k^1 \\ \underline{x}_k^2 \end{pmatrix}$

180

This may be rewritten as

$$P_k = \begin{pmatrix} \varphi_{11} & \varphi_{12} \\ O & \varphi_{22} \end{pmatrix}_{k,k-1} \left( P'_{k-1} + \begin{pmatrix} \varphi_{11} & \varphi_{12} \\ O & \varphi_{22} \end{pmatrix}_{k-1,k} \begin{pmatrix} \Gamma_{k,k-1} \Gamma^T_{k,k-1} & O \\ O & O \end{pmatrix} \begin{pmatrix} \varphi^T_{11} & O \\ \varphi^T_{12} & \varphi^T_{22} \end{pmatrix}_{k-1,k} \right)$$

$$\begin{pmatrix} \varphi^T_{11} & O \\ \varphi^T_{12} & \varphi^T_{22} \end{pmatrix}_{k,k-1}$$

$$= \begin{pmatrix} \varphi_{11} & \varphi_{12} \\ O & \varphi_{22} \end{pmatrix}_{k,k-1} \left( P'_{k-1} + \begin{pmatrix} \varphi_{11} \Gamma_{k,k-1} \Gamma^T_{k,k-1} \varphi^T_{11} & O \\ O & O \end{pmatrix} \right)_{k,k-1}$$

$$\begin{pmatrix} \varphi_{11} & O \\ \varphi^T_{12} & \varphi^T_{22} \end{pmatrix}_{k,k-1} \tag{A-7}$$

where use has been made of the property that $(\varphi_{k,k-1})^{-1} = \varphi_{k-1,k}$ for any state transition matrix.

Likewise the covariance after estimation, equation (A-4b) may be rewritten as

$$P'_k = \left\{ I_{n_s} - (K_k H_k)^* \right\} \left( P_k + \left( I_{n_s} - (K_k H_k)^* \right)^{-1} K^* R_k K^{*T} \left( I_{n_s} - (K_k H_k)^* \right)^{T-1} \right)$$

$$\left\{ I_{n_s} - (K_k H_k)^* \right\}^T \tag{A-8}$$

181

Before proceeding to simplify (A-8) further, the following result which will prove useful is noted.

$$\begin{pmatrix} A & B \\ O & C \end{pmatrix}^{-1} = \begin{pmatrix} A^{-1} & -A^{-1}BC^{-1} \\ O & C^{-1} \end{pmatrix} \tag{A-9}$$

for arbitrary size partitions when A and C are nonsingular and O is a matrix of zero.

Using the fact that $\widetilde{H}_k$ is the submatrix of $H_k$, which is conformable with the filter state vector and (A-9) in (A-8), the following is obtained

$$P'_k = \left\{ I_{n_s} - (K_k H_k)^* \right\} \left( P_k + \begin{pmatrix} \left( I_{n_f} - K_k \widetilde{H}_k \right)^{-1} KRK^T \left( I_{n_f} - K_k \widetilde{H}_k \right)^{T^{-1}} & O \\ O & O \end{pmatrix} \right) \right)$$

$$\left\{ I_{n_s} - (K_k H_k)^* \right\}^T \tag{A-10}$$

Equations (A-7) and (A-10) may now be inverted with relative ease. The only hard part is the matrix sum sandwiched in both equations. Since they both have the same basic form, they can be looked at as inverting the following

$$\left( P_k + \begin{pmatrix} Q & O \\ O & O \end{pmatrix} \right)^{-1} = \left( I + P_k^{-1} \begin{pmatrix} Q & O \\ O & O \end{pmatrix} \right)^{-1} P_k^{-1} \tag{A-11}$$

$P_k^{-1}$ be partitioned as (using the known symmetry)

$$P_k^{-1} = \begin{pmatrix} P_{11} & P_{12} \\ P_{12}^T & P_{22} \end{pmatrix}_k \quad \text{and} \quad P_k'^{-1} = \begin{pmatrix} P_{11}' & P_{12}' \\ P_{12}' & P_{22}' \end{pmatrix}_k$$

The (A-11) becomes

$$\left( P_k + \begin{pmatrix} Q & O \\ O & O \end{pmatrix} \right)^{-1} = \left( I + \begin{pmatrix} P_{11} Q & O \\ P_{12}^T Q & O \end{pmatrix}_k \right)^{-1} \begin{pmatrix} P_{11} & P_{12} \\ P_{12}^T & P_{22} \end{pmatrix}_k$$

and using the transpose of (A-9)

$$\left( P_k + \begin{pmatrix} Q & O \\ O & O \end{pmatrix} \right)^{-1} = \begin{pmatrix} (I + P_{11}Q)^{-1} & O \\ -P_{12}^T Q(I + P_{11}Q)^{-1} & I \end{pmatrix}_k \begin{pmatrix} P_{11} & P_{12} \\ P_{12}^T & P_{22} \end{pmatrix}_k$$

$$= \begin{pmatrix} (I + P_{11}Q)^{-1} P_{11} & (I + P_{11}Q)^{-1} P_{12} \\ -P_{12}^T Q(I + P_{11}Q)^{-1} P_{11} + P_{12}^T & -P_{12}^T Q(I + P_{11}Q)^{-1} P_{12} + P_{22} \end{pmatrix}_k$$

$$= \begin{pmatrix} (I + P_{11}Q)^{-1} P_{11} & (I + P_{11}Q)^{-1} P_{12} \\ P_{12}^T (I + P_{11}Q)^{-1} & -P_{12}^T Q(I + P_{11}Q)^{-1} P_{12} + P_{22} \end{pmatrix}_k \quad (A-12)$$

Now if in equation (A-7) $\varphi_{11} \Gamma_{k, k-1} \Gamma_{k, k-1}^T \varphi_{11}^T = \psi_{k, k-1}$ is identified with Q in equation (A-12), then the extrapolation for the inverse covariance matrix is

$$
P_k^{-1} = \begin{pmatrix} \varphi_{11}^T & O \\ \\ \varphi_{12}^T & \varphi_{22}^T \end{pmatrix}_{k-1, k}
$$

$$
\begin{pmatrix} (I + P'_{11} \psi_{k, k-1})^{-1} P'_{11} & (I + P'_{11} \psi_{k, k-1})^{-1} P'_{11} \\ \\ P'^T_{12} (I + P'_{11} \psi_{k, k-1})^{-1} & -P'^T_{12} \psi_{k, k-1} (I + P'_{11} \psi_{k, k-1})^{-1} P'_{12} + P'_{22} \end{pmatrix}_{k-1}
$$

$$
\begin{pmatrix} \varphi_{11} & \varphi_{12} \\ \\ O & \varphi_{22} \end{pmatrix}_{k-1, k} \tag{A-13}
$$

Now in equation (A-10) identify with Q an $n_c \times n_c$ matrix

$$
\begin{pmatrix} \left(I_{n_f} - K_k \widetilde{H}_k\right)^{-1} KRK \left(I_{n_f} - K_k \widetilde{H}_k\right)^{T^{-1}} & O \\ \\ O & O \end{pmatrix} = \Xi_k \tag{A-14}
$$

where the zeroes are matrices of appropriate size to make up the difference $(n_c - n_f)$.

184

Also let

$$H_k = [H_k^1 : H_k^2] \tag{A-15}$$

Then a partition of $\left\{ I_{n_s} - (K_k H_k)^* \right\}^{-1}$ conformable with

the partition of $\begin{pmatrix} \underline{X}_k^1 \\ \underline{X}_k^2 \end{pmatrix}$ can be obtained using equation (A-9) as

$$\left\{ I_{n_s} - (K_k H_k)^* \right\}^{-1} = \begin{pmatrix} I_{n_c} - \begin{pmatrix} K_k H_k^1 \\ O \end{pmatrix} & \begin{pmatrix} K_k H_k^2 \\ O \end{pmatrix} \\ O & I_{n_s - n_c} \end{pmatrix}^{-1}$$

$$= \begin{pmatrix} \left( I_{n_c} - \begin{pmatrix} K_k H_k^1 \\ O \end{pmatrix} \right)^{-1} & - \left( I_{n_c} - \begin{pmatrix} K_k H_k^1 \\ O \end{pmatrix} \right)^{-1} \begin{pmatrix} K_k H_k^2 \\ O \end{pmatrix} \\ O & I_{n_s - n_c} \end{pmatrix} \tag{A-16}$$

185

Using equations (A-10), (A-12), (A-14), and (A-16), the inverse of $P'_k$ can be expressed

$$P'^{-1}_k = \begin{pmatrix} \left(I_{n_c} - \begin{pmatrix} K_k H_k^1 \\ O \end{pmatrix}\right)^{T^{-1}} & O \\ -\begin{pmatrix} K_k H_k^2 \\ O \end{pmatrix}^T \left(I_{n_c} - \begin{pmatrix} K_k H_k^1 \\ O \end{pmatrix}\right)^{T^{-1}} & I_{n_s - n_c} \end{pmatrix}$$

$$\begin{pmatrix} (I + P_{11} \Xi_k)^{-1} P_{11} & (I + P_{11} \Xi)^{-1} P_{12} \\ P_{12}^T (I + P_{11} \Xi_k)^{-1} & -P_{12}^T \Xi_k (I + P_{11} \Xi_k)^{-1} P_{12} + P_{22} \end{pmatrix}_k$$

$$\begin{pmatrix} \left(I_{n_c} - \begin{pmatrix} K_k H_k^1 \\ O \end{pmatrix}\right)^{-1} & -\left(I_{n_c} \begin{pmatrix} K_k H_k^1 \\ O \end{pmatrix}\right)^{-1} \begin{pmatrix} K_k H_k^2 \\ O \end{pmatrix} \\ O & I_{n_s - n_c} \end{pmatrix}$$

(A-17)

Now from equations (A-13) and (A-17) it is apparent that the upper left block of the inverse covariance matrix (i. e., the part associated with the state in $\underline{X}_k^1$) is unaffected by the model for the error states in $\underline{X}_k^2$. In fact, the propagation of the upper left block is the same as it would be if the states $\underline{X}_k^2$ were not even considered. Thus, the effect of this class of error source may be removed from the covariance matrix at any point in time simply by removing the appropriate rows and columns from the inverse and then reinverting the remaining submatrix.

It may be noted at this point that the inverting of a large covariance matrix, elimination of a few rows and columns and reinversion of the remaining matrix is a rather cumbersome procedure. This is especially true for large matrices and for may sets of error sources to be examined. So at this point, it will be shown that the desired result may be obtained without inverting any large matrices. The only inverse required has the dimension of the error model whose sensitivity is desired.

From the partition of $P_k^{-1}$, the desired matrix for the sensitivity analysis is $P_{11}^{-1}$. First partition $P_k$ conformable to the partition of $P_k^{-1}$

$$
P_k = \begin{pmatrix} \widetilde{P}_{11} & \widetilde{P}_{12} \\ \widetilde{P}_{12}^T & \widetilde{P}_{22} \end{pmatrix} = \begin{pmatrix} P_{11} & P_{12} \\ P_{12}^T & P_{22} \end{pmatrix}^{-1}
\tag{A-18}
$$

Then look at the product $P_k^{-1} P_k = I$ in terms of the partitioned blocks of (A-18) and in particular note

$$
P_{11}\widetilde{P}_{11} + P_{12}\widetilde{P}_{12}^T = I
\tag{A-19a}
$$

$$
P_{11}\widetilde{P}_{12} + P_{12}\widetilde{P}_{22} = O
\tag{A-19b}
$$

From the relations in (A-19), the matrix $P_{11}^{-1}$ may be obtained explicitly in terms of the submatrices of $P_k$ as follows. From (A-19a)

$$P_{11} = (I - P_{12}\widetilde{P}_{12}^T)\,\widetilde{P}_{11}^{-1} \qquad (A-20)$$

From (A-19b)

$$P_{12} = -P_{11}\widetilde{P}_{12}\widetilde{P}_{22}^{-1} \qquad (A-21)$$

With (A-21) in (A-20)

$$P_{11} = (I + P_{11}\widetilde{P}_{12}\widetilde{P}_{22}^{-1}\widetilde{P}_{12}^T)\,\widetilde{P}_{11}^{-1}$$

$$= \widetilde{P}_{11}^{-1} + P_{11}\widetilde{P}_{12}\widetilde{P}_{22}^{-1}\widetilde{P}_{12}^T\widetilde{P}_{11}^{-1}$$

Then

$$P_{11}(I - \widetilde{P}_{12}\widetilde{P}_{22}^{-1}\widetilde{P}_{12}^T\widetilde{P}_{11}^{-1}) = \widetilde{P}_{11}^{-1}$$

Finally

$$P_{11}^{-1} = (I - \widetilde{P}_{12}\widetilde{P}_{22}^{-1}\widetilde{P}_{12}^T\widetilde{P}_{11}^{-1})\,\widetilde{P}_{11}$$

$$= \widetilde{P}_{11} - \widetilde{P}_{12}\widetilde{P}_{22}^{-1}\widetilde{P}_{12}^T \qquad (A-22)$$

188

So if each error source is considered individually, the only inversion required is a matrix of the order of the error model. In the case of an error model which contains only one state, equation (A-22) is particularly simple. In fact, if it is only of interest to determine the variance reduction, then for each state in $\underline{X}_k^1$ the following holds

$$\sigma_i'^2 = \sigma_i^2 (1 - r_i^2) \tag{A-23}$$

where

$\sigma_i'^2$     is the new variance of the $i^{th}$ state of $\underline{X}_k^1$ with the error removed

$\sigma_i^2$     is the variance of the $i^{th}$ state before the error is removed

$r_i$     is the correlation coefficient between the $i^{th}$ state of $\underline{X}_k^1$ and the removed error state.

The sensitivity of the $i^{th}$ state of $\underline{X}_k^1$ to the error removed is thus

$$\alpha_i = \frac{r_i^2 \sigma_i^2}{\sigma^2} \tag{A-24}$$

where

$\alpha_i$     is the sensitivity to the removed error state

$\sigma^2$     is the variance of the error state which was used to determine $\sigma_i^2$.

## Reference

A-1. Gelb, A., ed., Applied Optimal Estimation, the MIT Press, Cambridge, Massachusetts, 1974.

## Appendix B
## Model for Correlated Ionospheric Delay Errors

The model given in [1] for the ionospheric delay error indicates that in addition to the time correlation, there is a spatial correlation. In the case of a single satellite signal, this spatial correlation was converted to an equivalent time correlation by using the constant speed of the ionospheric pierce point of the signal. However, this spatial correlation term introduces cross-correlations among the various satellite signals. Ignoring these correlations in the reference system model would yield error analysis results which are pessimistically large.

A model which produces the appropriate autocorrelation for the ionospheric delay error is given by

$$\dot{x} = -\frac{1}{\tau} x + \sqrt{\frac{2}{\tau}} \sigma u(t) \qquad (B-1)$$

where

$\sigma^2$ is the variance of the state x

$\tau$ is the associated time constant

$u(t)$ is a white noise with unity PSD

This standard model for a Gauss-Markov process can be used to generate the ionospheric residual error for each satellite signal. In addition to requirements on the autocorrelation, it is desired to have the model generate the proper cross correlation. In particular, let $x_1$ and $x_2$ denote the ionospheric delay error states for two satellite signals.

$$\dot{x}_1 = -\frac{1}{\tau} x_1 + \sqrt{\frac{2}{\tau}} \sigma_1 u_1(t)$$

190

$$\dot{x}_2 = -\frac{1}{\tau} x_2 + \sqrt{\frac{2}{\tau}} \sigma_2 u_2(t) \qquad (B-2)$$

From [1], the desired cross covariance is

$$R_{x_1 x_2}(0) = \sigma_1 \sigma_2 \exp(-\Delta\rho / 2500 \text{ km}) \qquad (B-3)$$

where

$$\sigma_i = \epsilon \csc[\sqrt{E_i^2 + (18^\circ)^2}]$$

$\epsilon$ is the correction residual

$E_i$ is the elevation angle of the LOS vector

$\Delta\rho$ is the distance between the ionospheric pierce points
$= |R_1 - R_2|$ where $R_i$ is the position of the pierce point

Using the steady state values for $x_1$ and $x_2$

$$R_{x_1 x_2}(0) = E[x_1(t) x_2(t)]$$

$$R_{x_1 x_2}(0) = E\left\{ \int_{-\infty}^{t} u_1 \epsilon \sigma_1 e^{-\left(\frac{t-\epsilon}{\tau}\right)} d\epsilon \int_{-\infty}^{t} u_2(\eta) \sigma_2 e^{-\left(\frac{t-\eta}{\tau}\right)} d\eta \right\}$$

$$= \int_{-\infty}^{t} d\epsilon \int_{-\infty}^{t} d\eta \, E[u_1(\epsilon) u_2(\eta)] \sigma_1 \sigma_2 e^{-\frac{2t}{\tau}} e^{-\frac{\epsilon}{\tau}} e^{-\frac{\eta}{\tau}}$$

Now let $u_1$ and $u_2$ have a cross correlation of $\gamma \delta(t)$ ,

191

$$R_{x_1 x_2}(0) = \sigma_1 \sigma_2 e^{-\frac{2t}{\tau}} \gamma \int_{-\infty}^{t} e^{-\frac{2\epsilon}{\tau}} d\epsilon$$

$$= \sigma_1 \sigma_2 \left(\frac{\tau}{2}\right) \gamma \qquad\qquad (B-4)$$

Using (A-3) and (A-4)

$$\gamma = \left(\frac{2}{\tau}\right) \exp(-\Delta\rho/2500 \text{ km})$$

The required $G$ matrix to generate the correlated driving noises $u_1$ and $u_2$ from uncorrelated white noises $\tilde{u}_1$ and $\tilde{u}_2$ can be found from

$$E\left[\begin{pmatrix} u_1 \\ u_2 \end{pmatrix}(u_1 \; u_2)\right] = E\left[G \begin{pmatrix} \tilde{u}_1 \\ \tilde{u}_2 \end{pmatrix}(\tilde{u}_1 \; \tilde{u}_2) \; G^T\right]$$

$$= G \; E\left[\begin{pmatrix} \tilde{u}_1 \\ \tilde{u}_2 \end{pmatrix}(\tilde{u}_1 \; \tilde{u}_2)\right] G^T$$

$$= G G^T$$

Then

$$GG^T = \begin{bmatrix} \sigma_1^2 \left(\frac{2}{\tau}\right) & \sigma_1 \sigma_2 \left(\frac{2}{\tau}\right) \exp\left(-\Delta\rho/2500\right) \\ \sigma_1 \sigma_2 \left(\frac{2}{\tau}\right) \exp\left(-\Delta\rho/2500\right) & \sigma_2^2 \left(\frac{2}{\tau}\right) \end{bmatrix}$$

The extension to four correlated ionospheric delay errors is now straight-forward.

# APPENDIX C

## Glossary of
## Abbreviations and Acronyms


CANOMIS:     Covariance ANalysis Of Multisensor Integrated System - an ORINCON computer program for covariance analysis and Monte Carlo simulation.

ECI:     Earth Centered Inertial - a coordinate frame with origin at the center of the Earth and fixed in inertial space.

EM-log:     Electro Magnetic log - a ship's instrument to determine speed with respect to the water.

GDE:     General Dynamics Electronics - the prime contractor for the NAVSTAR system.

GDOP:     Geometric Dilution Of Precision - a relative measure of satellite constellations.

GPS:     Global Positioning System

NR:     Newton Raphson - a numerical technique for iterative solution of nonlinear equations.

PSD:     Power Spectral Density

RMS:     Root Mean Square - the square root of the average of squares of a set of numbers.

RSS:     Root Sum Square - the square root of the sum of squares of a set of numbers.

TOA:     Time-of-Arrival

WGS:     World Geodetic System